EXPERIMENTAL INVESTIGATION

OF VORTEX TUBE CONCEPTS

by

Jean Camiré

B. A. Sc., Université Laval, 1992

A THESIS SUBMITTED IN PARTIAL FULFILLMENT OF

THE REQUIREMENT FOR THE DEGREE OF

MASTER OF APPLIED SCIENCE

in

THE FACULTY OF GRADUATE STUDIES

Department of Physics

We accept this thesis as conforming
to the required standard

THE UNIVERSITY OF BRITISH COLUMBIA

April 1995

Abstract

The vortex tube is a very simple device which separates a compressed gas into a cold and a hot stream. The compressed gas is injected tangentially into the tube inlet by means of a nozzle. The gas develops a swirling motion in the tube. The gas leaving the tube near the wall will be warmer and that leaving the tube from the center will be cooler. Typically, with compressed air at 3 atm. and 290 K, it is possible to obtain a cold stream of $T_c = 260$ K and a hot stream of $T_h = 330$ K.

The general motivation of this thesis was to clarify the numerous assumptions on the vortex tube effect by the analysis of new measurements. Compared to previous studies, standard measurements of pressures and temperatures were improved by having the sensors very close to the tube. New measurements were obtained with the help of three novel techniques:

i) Velocity profile measurements were done with a special pitot tube.

ii) The vortex tube was tested at inlet pressures below atmospheric.

iii) The spectrum of sound generated in the vortex tube was measured with the help of internally mounted microphones.

The new data were compared to previous models, especially the two-streams model by Ahlborn et al. (1994), where the heating in the vortex tube is attributed to the conversion of kinetic energy into heat and the cooling to the reverse process. Due to the accuracy of the inlet pressure measurements, the new experiments showed unexpected high inlet velocities. In contradiction to Ahlborn's model, where the cold and hot streams have the same amount of energy, the vortex tube effect is explained in this work by an energy separation, in which the cold stream exits the tube with a lower energy than the hot stream.

Table of contents

List of tables

List of figures

1 - Introduction

The vortex tube is a very simple device which separates a compressed gas into a cold and a hot stream. A standard vortex tube is shown in Figure 1.1a. The compressed gas is injected tangentially into the tube inlet by means of a nozzle. The gas develops a swirling motion in the tube. The gas leaving the tube near the wall will be warmer and that leaving the tube from the center will be cooler. Typically, with compressed air at 3 atm. and 290 K, it is possible to obtain a cold stream of T_c = 260 K and a hot stream of T_h = 330 K. All vortex tubes described in the literature have an elevated inlet pressure and exhaust the cold and hot stream at atmospheric pressure.

While the vortex tube shown in Figure 1.1a is the most common, there are also vortex tubes where the fluid exits on one end only. In the configuration of Figure 1.1b, the cold end can be used to extract cold air since the heat exchangers along the tube will extract the heat from the hot stream. However, the vortex tube shown in Figure 1.1c, with only the hot end, cannot be used for commercial applications since the two streams are mixed together at the exhaust. That type of vortex tube was used by scientists to study a simpler flow pattern.

1.1 History

G.J.Ranque (1933) appears to have been the first to observe the vortex tube behavior. R. Hilsch (1946) studied Ranque's observation in more detail. He made a rough optimization of the tube geometry, related the temperature difference to the inlet and outlet pressures and flow rates and evaluated the vortex tube efficiency. However, he did not explain the physical process behind the effect. His final remark was that the efficiency was low compared to standard cooling systems, specially at low inlet pressure. He suggested that the tube could be used for gas separation processes.

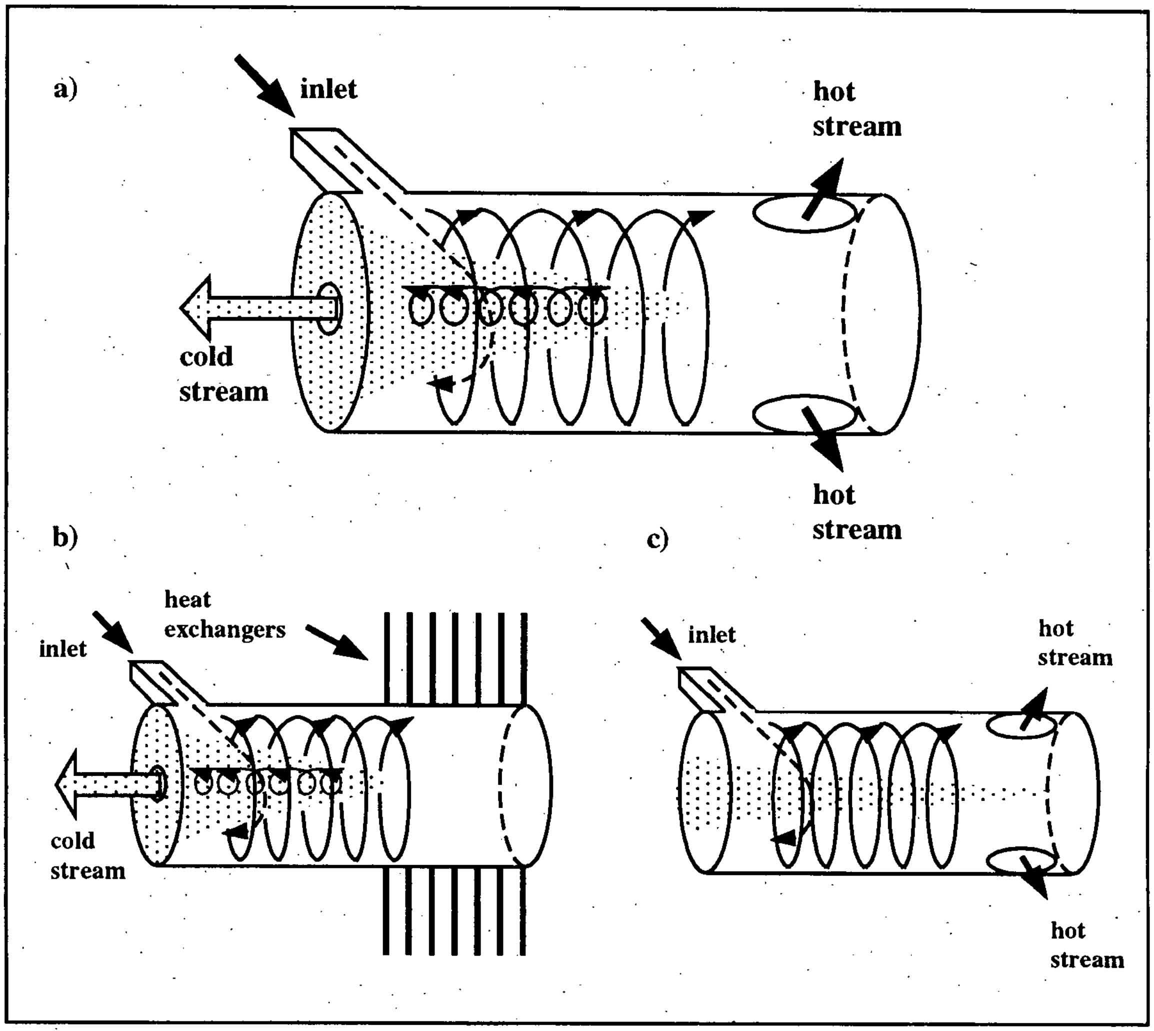

Figure 1.1: Vortex tubes a) standard b) end on cold side only c) end on hot side only. The dotted areas represent the flow that will exit on the cold end.

Hilsch's publication generated considerable interest and since then many papers have appeared in the literature with possible explanations of what is now called the Ranque-Hilsch vortex tube effect. Many trials have been made to present a general formulation for the energy separation process taking place in the tube. However, the complexity of the flow field made the mathematical analysis difficult and inconclusive. The vortex tube flow field is compressible, viscous, and has complicated temperature, pressure and velocity distributions. Furthermore, since the process is assumed to be highly irreversible (Negm et al., 1988), the task of modeling the tube by analytical method is tremendously difficult. Some models were done on the uniform-flow configuration, which is a vortex tube with only the hot end opened. However, the results were not really applicable to the standard configuration. Meanwhile, further experiments were done on the vortex tube. Takahama (1965,1966) did an extensive research on the tube optimization and developed a set of empirical criteria for the vortex tube design. Rough measurements of the pressure, temperature and velocity field within the tube were done (Bruun, 1969, Harnett, 1957, Savino, 1961, Takahama, 1965, 1966) and they have been used to support analytical models ((Deissler and Perlmutter, 1960, Linderstrøm-Lang, 1971).

The most successful models for predicting the temperature separation effect take into account the geometry and also external parameters, such as exit and inlet pressure, temperature and flow rate. There is not yet a model which can predict the effect based on just the entrance conditions and the geometry. In other words, the temperature separation effect has to be assumed in order to be predicted. This is because in most models, the tube is analyzed with thermodynamic relations, where the tube is taken as a control volume, and the entrance and exit conditions are an indication of the fluid state. However, the physical process leading to the temperature separation is not taken into account. In fact, there is a great confusion about the cause of the Ranque-Hilsch effect.

1.2 Applications of the vortex tube

In the past 50 years, many applications for the vortex tube have been proposed. A large amount of research has been done on gas separation applications. The centrifugal acceleration in the vortex tube (10^6 g) is stronger than in any other centrifuges (Fekete, 1986). The tube has been widely used in petroleum industry and in many plant processes (Fekete, 1967, 1970, 1986). The temperature splitting characteristic has been used for cooling applications such as cooling cutting tools and electronic parts. Some others investigated the sound properties of the vortex tube, and found that the tube was emitting a dominant frequency which depended on the inlet velocity (Chanaud, 1963, 1965, Vonnegut, 1954). The tube has also been used as a static temperature probe. The aerodynamic heating experienced by thermometers exposed to high speed flow (e.g. thermometers on airplanes to measure air temperature) can be very nearly eliminated over a wide range of operating conditions by mounting the thermometer in a vortex tube. By adjusting the valve setting, one can compensate the heating by the refrigeration effect and then obtain the true temperature (Vonnegut, 1950). More recently, the centrifugal characteristics were investigated for particulate trapping. In his experiments, Sibbertsen (1990) attached a vortex tube to a Diesel engine exhaust, and found that 80% of the particulates leave the tube in the hot flow, which comprises only 20% of the total mass flow.

1.3 Thesis objectives

There are many speculations about the physics behind the Ranque-Hilsch effect. In his preliminary research, Hilsch attributed the cooling effect to gas expansion and the heating to friction (Hilsch, 1946). Deissler and Perlmutter (1965) postulated that the effect was due to turbulent migration. Kurosaka (1982) assumed that an acoustic streaming was the cause of the effect and was driving heat from cold to hot. He noticed that strong resonant sound waves were present in the tube. By using a tunable cavity instead of a standard straight tube, he was able to stop the temperature splitting by reducing the sound intensity. Despite his remarkable discovery, he has not been able to formulate a clear physical interpretation of the effect. Although sound can produce a flow (which is the definition of acoustic streaming), it is not understood how this flow could carry the heat from cold to hot.

In 1983, Wheatley discovered the thermoacoustic effect, where sound waves are able to perform a full thermodynamic Brayton cycle and carry heat from a cold to a hot reservoir. His discovery led to the design of thermoacoustic refrigerators (Hoffler, 1994), which are still experimental but possess a great potential. Wheatley showed that this effect was existing in many different processes in the nature, from the microscopic to interstellar scale. This effect can be present when strong sound field exists in temperature gradients. It could possibly give an explanation to Kurosaka's discovery. An excellent account of the thermoacoustic phenomenon is given by Swift (1988) and it can be shown that there exist a maximum for the heat transfer from the cold to the hot reservoir if the temperature difference is chosen correctly (Ahlborn and Camiré, 1995).

More recently, Ahlborn et al. (1994) derived a model for the vortex tube which attribute the heating to conversion of kinetic energy into heat and the cooling to the reverse process. The model relates the temperature splitting to the pressure ratios and predicts an upper and lower limit for the temperature separation. It was also predicted from this model that the tube could be working with atmospheric pressure on the inlet and vacuum on the cold and hot side. Unlike previous studies, the model is derived from flow field characteristics in a standard double ended vortex tube (unlike Deissler and Perlmutter, Sibulkin and Linderstrøm-Lang, who used a one-end vortex tube). Although the model has interesting conclusions, further studies have to be done to confirm them.

The absence of a good model restricts the design of new applications to trial and error. The energy separation mechanism and the centrifugal effect could likely be improved by a new geometry or new design. However, without good guidelines, the research of a better design can take years of work. The knowledge of the effect behind the vortex tube has to be improved in order to develop new applications. The flow field has to be characterized by accurate temperature, pressure and velocity measurements. Furthermore, the physical process which lead to the effect has to be understood.

Most of the previous models were using upstream and downstream data taken far from the vortex tube. The vortex tube inlet and outlet conditions were then calculated from these data, assuming isentropic flow and using fluid mechanics equations. Since the vortex tube experiences great variation of pressure and temperature at the inlet and outlets, the calculations can lead to erroneous parameters. In order to develop a good model, it is crucial to measure the inlet and outlet parameters directly.

The general motivation of this work was to clarify the numerous assumptions on vortex tubes by the analysis of new direct measurements. For this purpose a modular vortex tube and a test stand were designed, allowing different precise measurements. The tube would be greatly versatile, allowing rapid changes on the design and many different measurements. Also, it was designed to permit a qualitative investigation of the internal flow field.

The work done in this project can be divided into 3 parts. The first part consisted in the design and building of a fully instrumented vortex tube allowing accurate measurements and flow field studies. Experiments were done to first verify that the vortex tube properties were somehow similar to other commercial tubes.

The second part of this work aimed at confirming predictions from models, especially results from Ahlborn et al (1994). For this purpose, new measurements were obtained with the help of three novel techniques:

i) Velocity profile measurements were done with a special pitot tube. This helped to confirm hypotheses about the flow field.

ii) The vortex tube was tested at low pressure. These measurements are particularly interesting since a low vortex tube could be useful in many applications, e.g. cleaning of Diesel exhaust.

iii) The spectrum of sound generated in the vortex tube was measured with the help of internally mounted microphones. Kurosaka's results have shown that sound must be playing an important role. Unlike his experiments, our measurements were performed in a standard vortex tube, for various flow rates and pressure settings.

The third part of the project consisted in the analysis of the results. The results were analyzed and compared with existing models, with the aim of obtaining new relations between the vortex tube parameters. Attempts were made to clarify physical phenomena in the vortex tube, such as the anomalous heat transfer and the sound wave interactions. Furthermore, some new hypotheses about the energy separation mechanisms have been proposed.

1.4 Thesis outline

The next chapter describes the vortex tube (called UBC VT-01), the instrumentation and the set up designed, built and used for this project. It also explains the guidelines that were used for the design. In chapter 3, the tube properties are presented to show that the tube is indeed working like any other vortex tube described in the literature.

Chapter 4 shows an extensive analysis of the results from experiments. Results are compared to previous models. Emphasis is given to the model by Ahlborn et al. (1994), since it is the most recent one and needs confirmation by further experiments. The analysis methods differ from classic fluid dynamics by the absence of complicated flow field mathematics. Instead, the analysis deals with simple conservation equations that are obtained by combining qualitative flow field studies, fluid dynamics equations and physics principles. The main advantage of this type of analysis is a direct interpretation of the results.

In chapter 5, several possible explanations of the energy separation effect are presented. This chapter deals more with the physics behind the Ranque-Hilsch effect, while the previous chapter was predominantly concerned with fluid dynamics. In the conclusion the results are summarized. Novel applications for vortex tube are presented, as ideas for future research.

The basic calculations, e.g. units conversion, velocity and flow rate calculations, etc., are presented in the appendix. There are also some tips for designing a better vortex tube, based on the experience gained in building and analyzing the vortex tube used in this study.

1.5 Coordinate system and units

Most of the analysis in this thesis will refer to the system of coordinates shown in Figure 1.2. The tube parameters will be defined in the next section where the design is described. In the thesis, the imperial unit system will be used for the drawings and the raw data. This is more practical, since all the drawings and design were done in inches for the ease of machining. Also, during the experiments, the pressure and flow rate data were displayed on the computer screen with the same units as the mechanical gauge and the comparison for calibration purposes was then easier to do. However, all the analysis was done in the metric system.

Appendix A describes the conversion formulas used and the calculations for different parameters.

Throughout the thesis, the terms "velocity", "pressure" and "temperature" will refer to the time-averaged parameters. The analysis presented in this work does not consider time-varying phenomena and consider the vortex tube effect as quasi stationary.

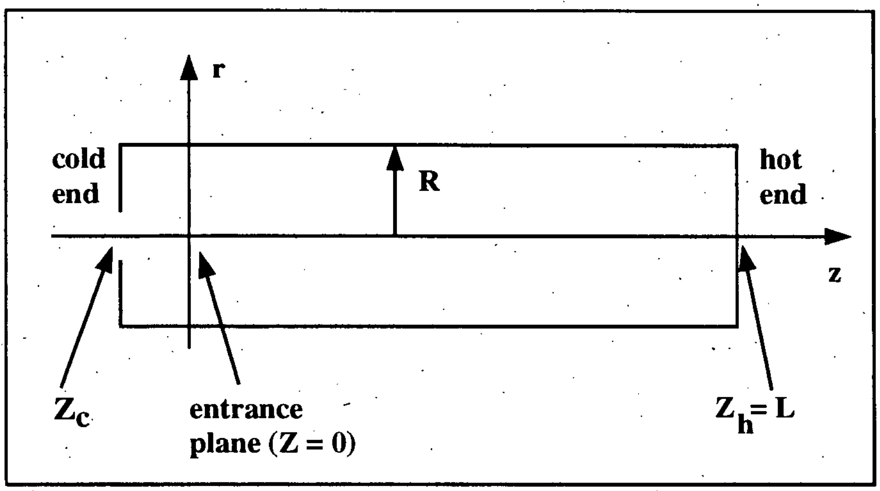

Figure 1.2: System of coordinates

2 - Experimental set up

The very complicated vortex tube flow field (3-D, compressible, viscous) is very difficult to model without the use of experiments. Furthermore, the size of the tube does not allow the insertion of standard pressure or temperature probes without perturbations. Hence the past studies of vortex tubes were trying to relate the energy separation effect to external measurements taken far from the tube.

In this work, several sets of experiments were performed on a vortex tube. The aim of these experiments was to improve the energy separation model by accurate measurements of the entrance and exit conditions within the tube and by a qualitative flow field study. One of the principal guidelines in designing the tube was for it to have modular parts, allowing rapid machining and changes of the principal components: the inlet nozzle, the tube, the hot and cold exit parts. Also, since flow field visualization was desired, the tube was made out of Pyrex. Furthermore, since the vortex tube experiments involved the simultaneous recording of many measurements, all the readings were recorded in real time on a computer. In this chapter, the standard test stand, the tube, the instrumentation and the calibration are described. The standard test stand was used for most of the experiments on the vortex tube. However, some modifications were done for the flow field studies, the sound waves and the low pressure measurements. The set up for these three layouts of experiments is also described.

2.1 Standard vortex tube set up

2.1.1 Test stand overview

In order to study the energy separation in the vortex tube, a tube and a test stand have been designed. Figure 2.1 is a schematic diagram of the test stand. The air coming from a compressor passes through a trap filter for removing water and then into the tube. Mass flow rates were measured on the input and on the cold side. The pressure and temperature were also measured. The measurements were amplified in the amplification unit and recorded in the PC computer via a DT-2805 A/D board. A refrigeration silencer was used on the cold end, where most of the noise was emitted. A valve on the hot end was used to adjust the ratio of flow rates from the cold and hot outlets. To verify occasionally if the computer recordings were right, a set of Bourdon gages and rotameters were also on the stand (not shown in Figure 2.1).

2.1.2 Design of the tube

The vortex tube characteristics are strongly dependent on the design, which has to be chosen properly to get the right flow field. There are a number of parameters that can be varied in designing a tube. The main ones are the length, diameter, nozzle area, cold end area and hot end area. These parameters, together with the cold and hot air ratio and the entrance conditions, will mostly determine the exhaust parameters of the tube, which are the cold end and hot end temperature, pressure and flow rate, and the flow velocity field. Most of the models that describe vortex tube performance require knowledge of the exhaust characteristics of the tube. There is not yet a model that predicts the performance of a tube based only on the input conditions and the geometry of the tube. Therefore, most of the guiding criteria in designing a vortex tube come from empirical relations and experiments. They are presented below.

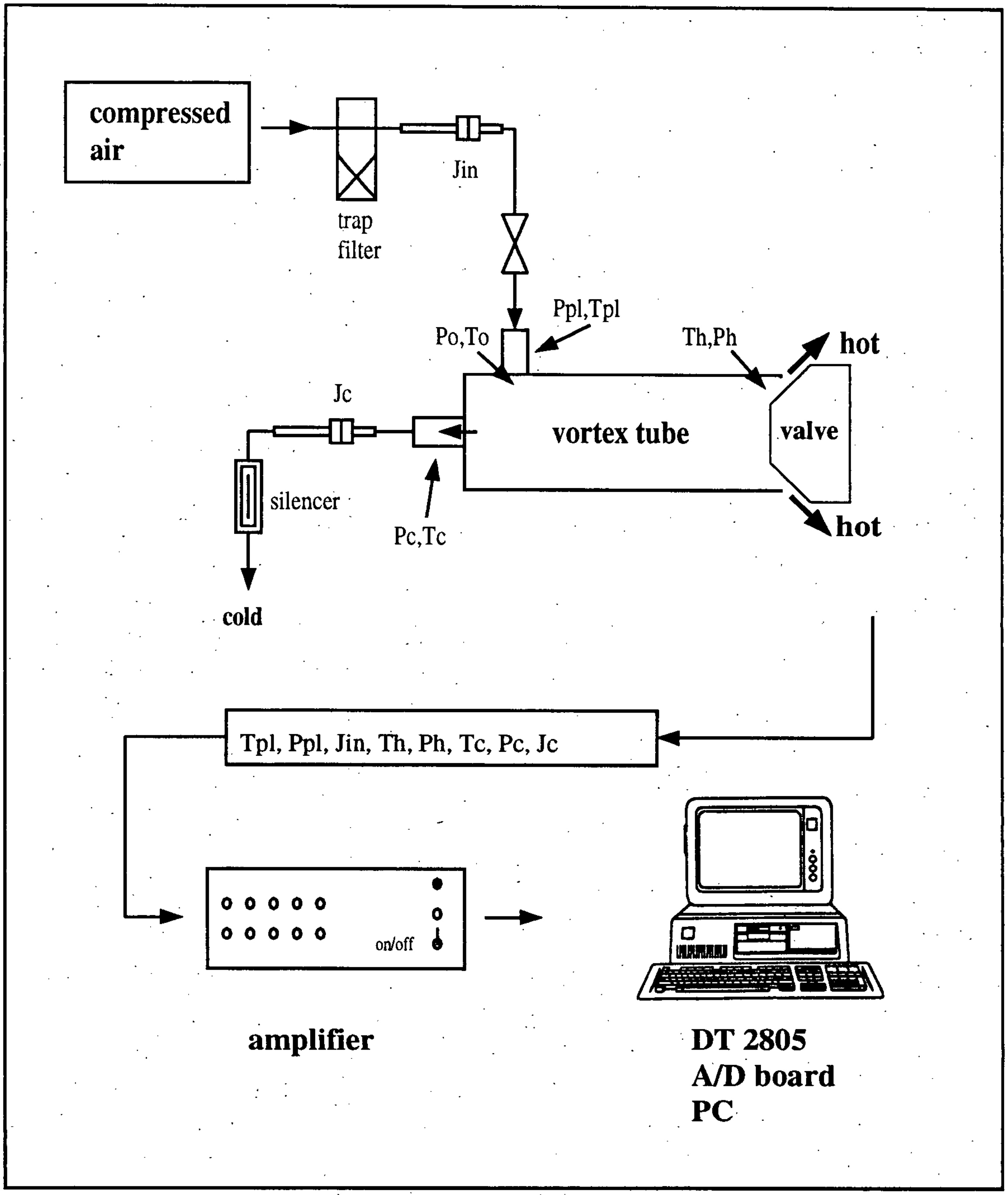

Figure 2.1: Block diagram of the vortex tube test stand showing the tube, the amplifier and the data acquisition system.

Tube length

The flow inside the tube separates into a stream going to the hot side and an inner core (back flow core) going towards the cold side, which is cooled during its motion. If one wants to subtract the hot air from the hot end, the tube needs to be longer than the back flow core, otherwise a mixing of hot and cold gas will be present on the hot outlet. Although Takahama (1965) used a length of 150D for his experiments, most of the vortex tubes researches were done with L >24D. The length chosen for this research was 24D (24 in.).

Tube diameter

Negm et al. (1988) experimented with different tube diameters and compared their performances, i.e. their temperature separation characteristics. It was found that the tube performance increased with an increase of the diameter up to 16mm and then decreased as the diameter was further increased (see Figure 2.2). They associated this phenomena with the Reynolds number Re, which can be interpreted as the ratio of inertial forces to viscous forces. Negm postulated that for small diameter (small Re), the inertial forces which drive the vortex motion are weak and the vortex effect deteriorates. For large diameter (large Re), the inertial forces are large compared to viscous forces (friction forces) which are presumably responsible for the energy separation process and the performance deteriorates again. They found an optimum diameter of 16mm. The tube diameter selected in this thesis was bigger (25.4 mm) for practical reasons: it was planned to insert relatively bulky equipment, such as a pitot tube and microphones, and flow visualization was desired. Furthermore a number of 25.4 mm dia. glass tubes with quick mounting flanges were readily available.

Cold size orifice

In any double ended vortex tube, the back flow diameter is always smaller than $D-2d_n$, since the air enters in the tube from holes having diameter d_n. A very conservative criteria is to set the cold end diameter $d_c < D-2d_n$. In this research, $d_c = 0.4(D - 2d_n) = 8.255$ mm.

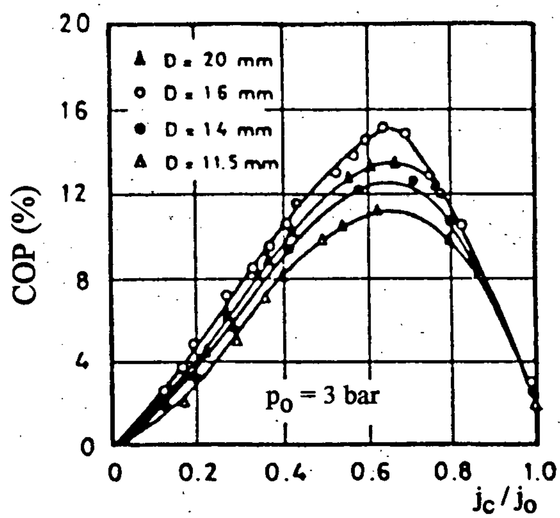

Figure 2.2: Effect of the tube diameter on the temperature separation characteristics (from Negm et al., 1988). COP is a measure of the tube coefficient of performance and is proportional to the temperature difference between the inlet and the cold side.

Nozzle opening

The nozzle is the entrance part of the vortex tube where the fluid is injected tangentially in the tube. It is the most important part of the vortex tube, since its shape and area will determine the vortex characteristics (fluid velocity, vortex shape). Vortex tubes can operate with one or many nozzles. One way to design the nozzle is to look at the entrance velocity requirements: it should be around 100m/s. However, this velocity cannot be calculated easily since it depends not only on the applied pressure and nozzle diameter d_n, but also on the pressure inside the tube. Takahama set up the following criteria: $0.16 < Nd_n^2/D^2 < 0.20$ and $d_n/D < 0.2$, where N is the number of holes in the nozzle. With those two equations, the number of openings in the nozzle can be determined. For example, with a 1 in. tube diameter, the two criteria hold when N = 4. If the nozzle diameter is bigger, the flow velocity is too small. If the area is too small, there is not enough fluid entering to drive the proper vortex shape. Since the vortex tube used in this work had a nozzle ring (see Figure 2.4) which could be replaced easily, these latter criteria have only been used as a general guide and different nozzles were tested. The final nozzle used had 4 holes of 0.1 in. diameter.

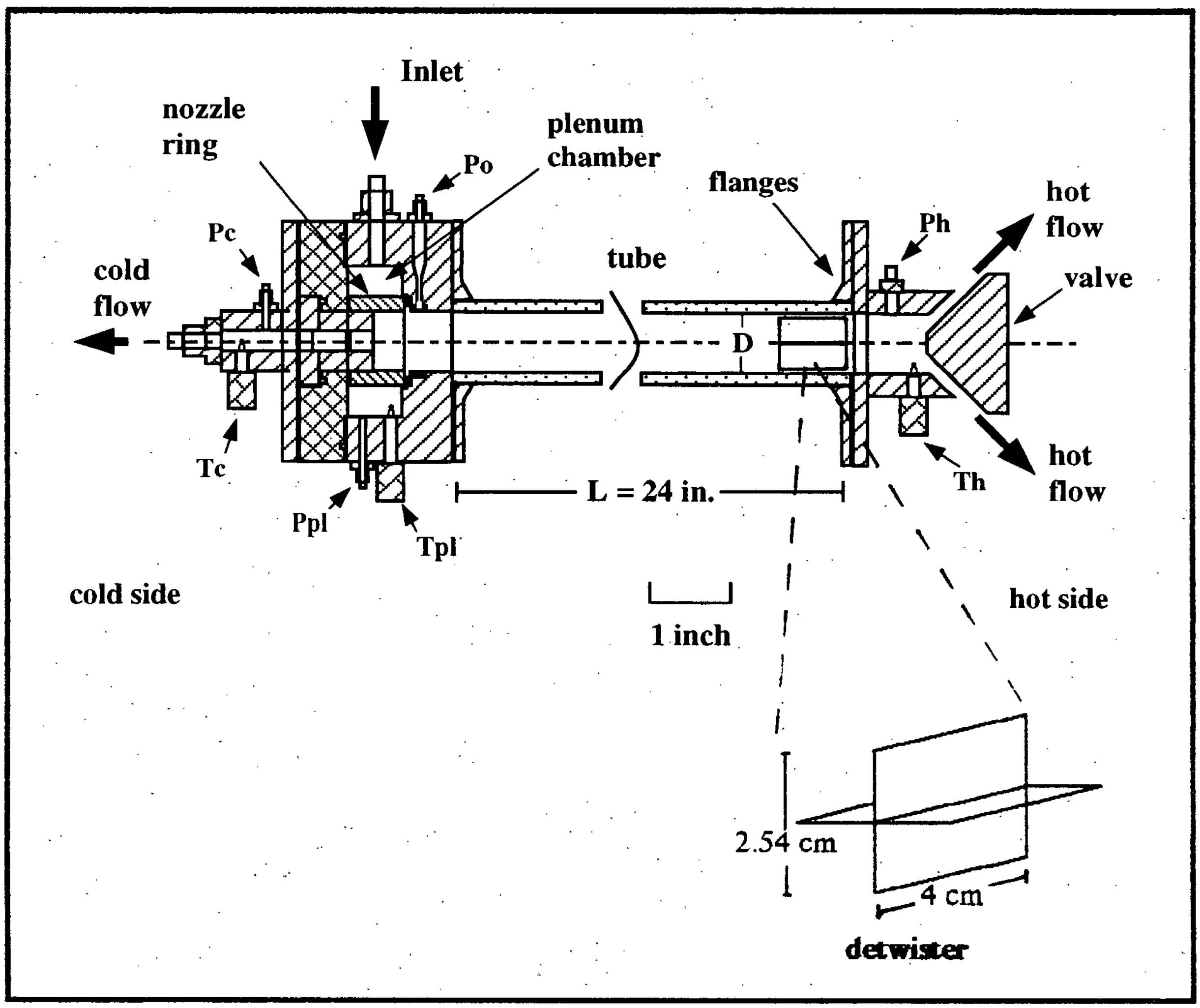

Figure 2.3: Vortex tube VT-01

Figure 2.3 shows a general view of the VT-01. The air is first injected into the plenum chamber, then passes through the nozzle ring. The air enters the tube with a tangential velocity which creates the vortex. The three main parts are the entrance end, the tube, and the hot end.

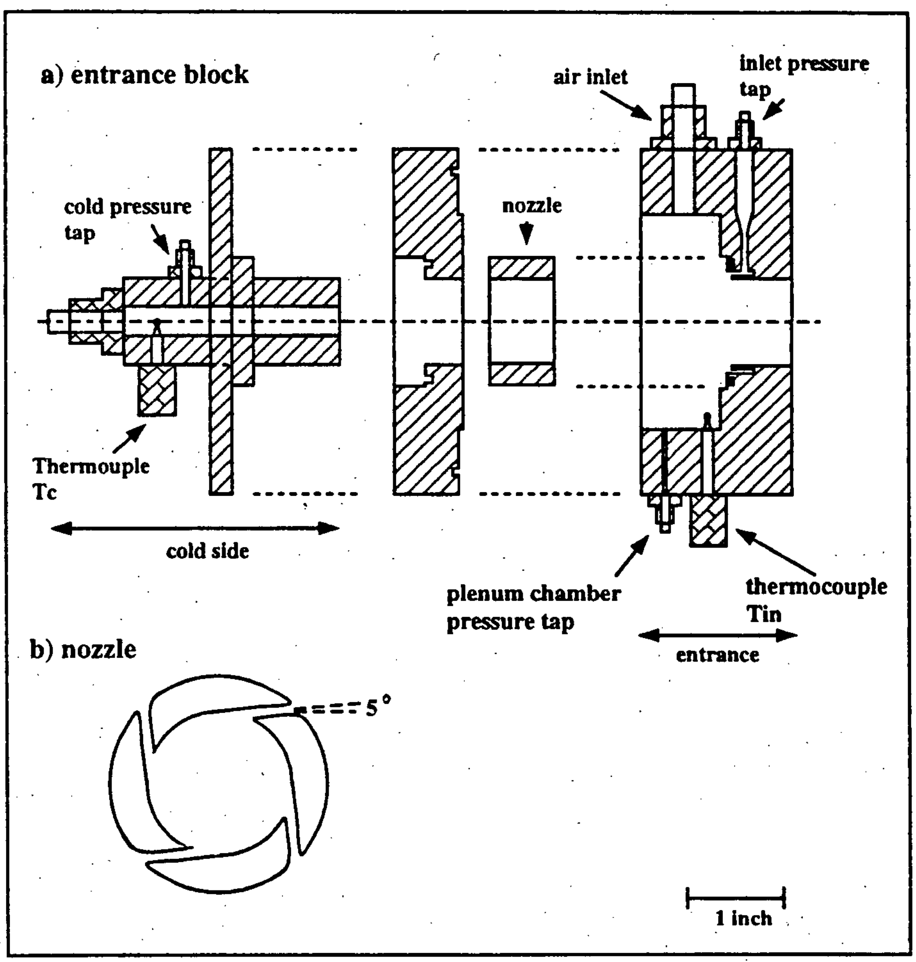

Figure 2.4: a) inlet block, with cold side and entrance parts b) nozzle

The entrance end which includes the cold side outlet is shown in Figure 2.4. The cold outlet diameter can be changed without having to rebuild the whole unit. The distance between the cold orifice and the inlet plane can also be changed by placing some washers between the cold-end unit and the entrance unit.

The plenum chamber pressure p_{pl} and the cold pressure p_c are measured through standard pressure taps having a 13 thou. diameter. The inlet pressure p_o is measured through a circular opening 3 thousands of an inch wide (see Figure 2.5). This circular opening is allowing an accurate measurement of the pressure close to the entrance since it is located at 5mm from the inlet nozzle in the hot side direction.

A pressure tap was also drilled in one of the nozzle inlets in order to calculate accurately the entrance velocity. In that case, the circular pressure tap was blocked with Teflon sealing tape and the pressure from the nozzle was collected in the pressure collector groove. To our knowledge, VT-01 is the first vortex tube having pressure taps at these locations. The temperature is measured in the plenum chamber by inserting the junction of a thermocouple through a Wilson seal (see Figure 2.3).

The second main part, the tube, connects the entrance block and the hot end. It consist of one or more sections of Pyrex tubes with 1 in. inner diameter and 1.5 in. outer diameter. Glass was used because visual flow field observation was desired. These tube sections have o-ring seals at their ends and are attached with flanges (see Figure 2.3).

Near the hot end, a detwister was used to reduce the rotational motion of the fluid at the hot exit (see Figure 2.3). The detwister was an aluminum cross made from two flat plates of 2.54cm x 4 cm with 1.6mm of thickness.

2.1.3 Instrumentation

Temperature sensors

Type J (Iron-Constantan) gage 24 thermocouples were used to measure various temperatures. Since a thermocouple voltage is determined by the temperature difference between its two ends, it is necessary to have a constant and known reference temperature at the end not used to measure temperature, which is usually called the reference junction. An ice bath was used for this purpose (Figure 2.6). The thermocouples were inserted in the tube through Wilson vacuum seals. Each thermocouples had one of their junctions in the ice bath, as shown in Figure 2.6. According to Benedict (1984), it is the most accurate circuit to measure temperatures with thermocouples.

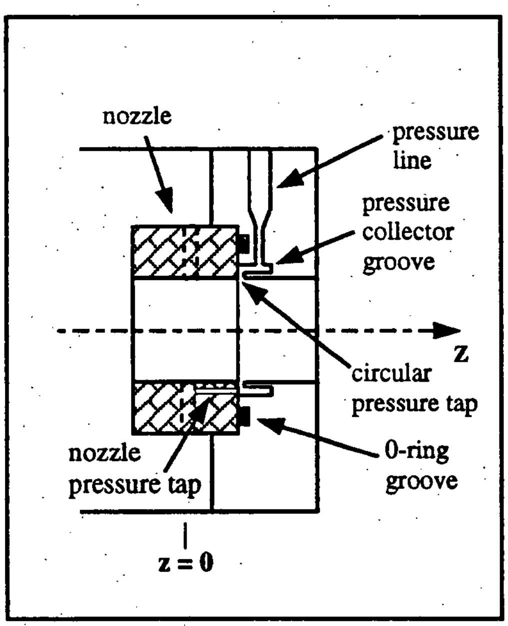

Figure 2.5: Inlet pressure measurement. When the nozzle pressure tap was used, the circular pressure tap was blocked and vice versa.

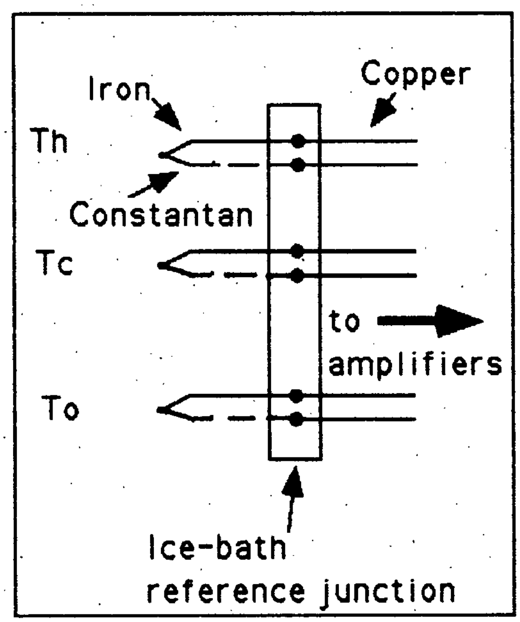

Figure 2.6: Thermocouple arrangement

Pressure measurements

Pressure taps were drilled with 13 thou. diameter drill bit. Care was taken to have the tap perpendicular to the surface and to remove any burrs. Polyflow 1/4in. tubing was used for the pressure lines. All the pressure measurements were done with diaphragm-type differential pressure transducers with a linearity better than 1%. Table 2.1 shows the various transducers used.

Parameter	Transducer label	range (psig)	type of transducer
j_o	Motorola MPX	30	differential, with arbitrary pressure
j_c	Motorola MPX	30	differential, with arbitrary pressure
p_o	Omega PX 136	60	differential, with ambient pressure
p_c	Omega PX 136	15	differential, with ambient pressure
p_h	Motorola MPX	30	differential, with ambient pressure

Table 2.1: Pressure transducers specifications. Arbitrary means the diaphragm can be connected to arbitrary pressures on both sides. Ambient means only one side of the diaphragm can be connected, the other being at ambient pressure.

Flowmeters

Two orifice flowmeters were designed to measure the mass flow rate. In those meters, the pressure is measured in front and behind an orifice. The pressure drop through the orifice is expected to be a monotonic function of the mass flow rate. With conservation of mass, one can get the flow rate on the three sides with two flowmeters. The flowmeter is shown in Figure 2.7. An entrance length of 20 times the inner diameter was used in order to get a fully developed flow (Benedict, 1984). Four pressure taps of 13 thou. diameter were collecting air into a groove, where a pressure line was connected. The design allowed the orifice plate to be changed if a different flow sensitivity was desired.

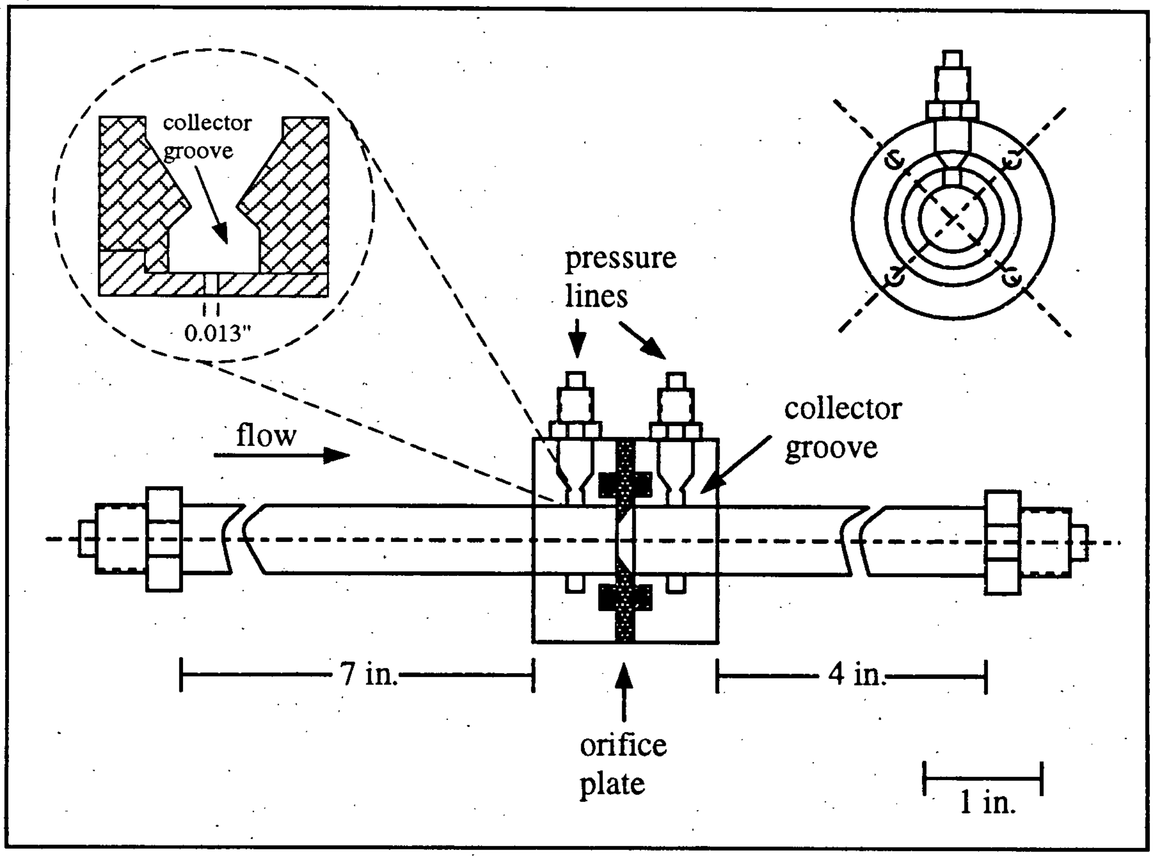

Figure 2.7: Orifice flowmeter

Signal processing unit

The signal processing unit contains the pressure transducers, the amplifiers for all the sensors and a power supply (Figure 2.8). Figure 2.8c shows the electronic circuit used for each amplifier. The amplifiers have two variable resistors allowing a gain of 1 to 10 and a variable offset of +/- 15 Volts. A PowerOne +/-15 V power supply powered the electronics. Two regulators provide the correct voltage to the transducers. 1μF capacitors were used for filtering the output of the pressure transducers in order to remove signal noise.

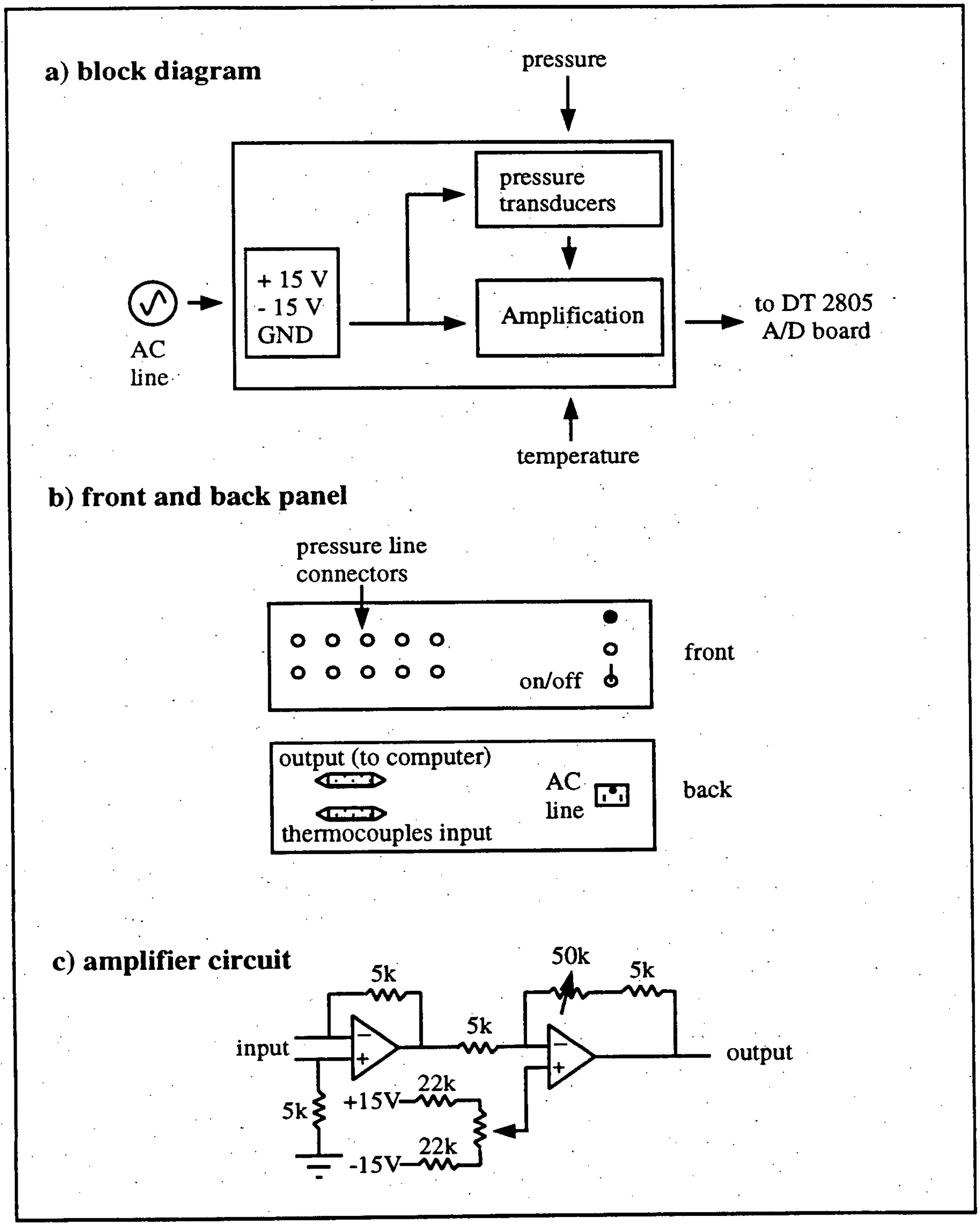

Figure 2.8: Signal processing unit

Data acquisition

Data were recorded from the signal processing unit on an XT computer via a DT-2805 12-bit A/D card. The board allowed programmable gain of 1,10,100,500 and a input range of ±10V. 8 differential channels were available. A computer program was written to operate the board. The program allowed real-time recording of the measurements on the screen, averaging of the data, selection of the gain and included a user control to save the desired measurements. The program listing is shown in appendix D.

2.1.4 Calibration

As described earlier, numerical values recorded by the computer were intended to be proportional to the input voltage signals supplied to the A-D converter, which in turn are related to actual physical parameters by the amplifier gain and sensitivity. Thus, in order to interpret the data, this entire measurement chain had to be calibrated, as described in the following sections. The amplifiers gain and offset were selected by some quick measurements of the limit of the parameter range to be measured. It was hoped that the amplifier signal would cover the range ±10V of the board to give a good resolution. As discussed below, the final accuracy of the measurements depends on the instrumentation accuracy and also how the measurements are taken.

Pressure sensors

The pressure sensors were calibrated with a Bourdon pressure gage. 5 sets of 5 to 10 pressures covering the range were taken. A typical pressure calibration curve is shown in Figure 2.9a. Even if the resolution of the gage was 0.1 psi, the uncertainty of pressure measurements could be greater. Pressure taps are supposed to measure the true static pressure. However, if the tap is not exactly perpendicular to the surface, some component of the dynamic pressure can be included in the measurement. With this factor and with the calibration curves, the accuracy of the pressure measurements is assumed to be better than 0.2 psi.

Flowmeters

The flowmeters were calibrated with a commercially calibrated rotameter. The pressure drop across the flowmeter orifice was measured for various mass flow rates. The flowmeter response was not linear, as expected. A curve fitting algorithm was used to determine the flow-voltage relation. A typical flow calibration curve with curve fitting is shown in Figure 2.9b. For large flow rate, the slope of the signal increases. Therefore, the flow rate accuracy was varying. From Figure 2.9b it can be seen that a reasonable estimate for accuracy is +/-0.5 SCFM, providing the flow is larger than 4 SCFM. Since most of the interesting features in the vortex tube occur when the flow rate is larger than 5 SCFM ($\sim j_c/j_o > 0.1$ for $p_{plenum} =$ 20 psig), the flowmeters were allowing accurate measurements. The resolution could have been better if the reference instrument (rotameter) had been better.

Even if the pressure drop through an orifice will mostly depend on the mass flow rate (Benedict, 1984), it will also vary with the inlet pressure. However, in the calibration described above the orifice flowmeter was calibrated by varying the mass flow rate (which was implicitly varying the inlet pressure) but not by varying specifically the inlet pressure. To check if the calibration relations were valid for the different inlet pressures used in the vortex tube, the orifice flowmeter measurements were regularly verified by rotameters measurements during the vortex tube experiments. Also, when varying the flow rate ratios the value j_c/j_o were always ranging between 0 and 1, which also demonstrate that the calibration was valid.

Temperature sensors

The thermocouples and amplifier units were calibrated by placing them in a water beaker and reading the water temperature with a 0.1°C resolution thermometer. The water temperature was varied from 0 to 60°C on a hot plate, and was stirred to allow uniform temperature on thermocouples and thermometer. The thermocouple reading had an accuracy of +/- 0.1 °C. A temperature calibration curve is shown in Figure 2.9c.

The measuring junctions of the thermocouples were placed directly into the flow at the locations shown in Figure 2.3. If all the fluid would come to rest at the thermocouple surface one would measure the stagnation (total) fluid temperature $T_t = T + u^2/2c_p$ where T is the true temperature, u is the fluid velocity and c_p is the specific heat at constant pressure. In reality, the probe measures a temperature slightly smaller than T_t and a correction factor has to be considered (see appendix A). For fluid velocities of about 40m/s and room temperature, the difference between the total and static temperature is less than 0.8 °C. Since the highest flow velocity at the thermocouples locations was approximately 40 m/s, the thermocouples resolution was expected to be better than 1 °C. The complete calculations for determining the real temperature from the measurements are presented in Appendix A.

Due to the small thermocouples cross section, the effect of thermal conductivity along the thermocouple wires is assumed to be negligible. To check this assumption a test was done were the part of the cold end thermocouple outside the vortex tube was submerged into boiling water and then removed from it. No variation in the measured temperature was noticed.

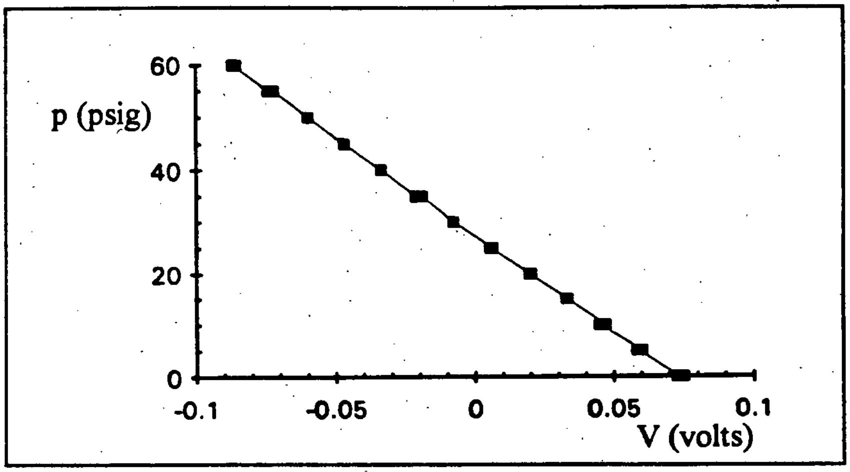

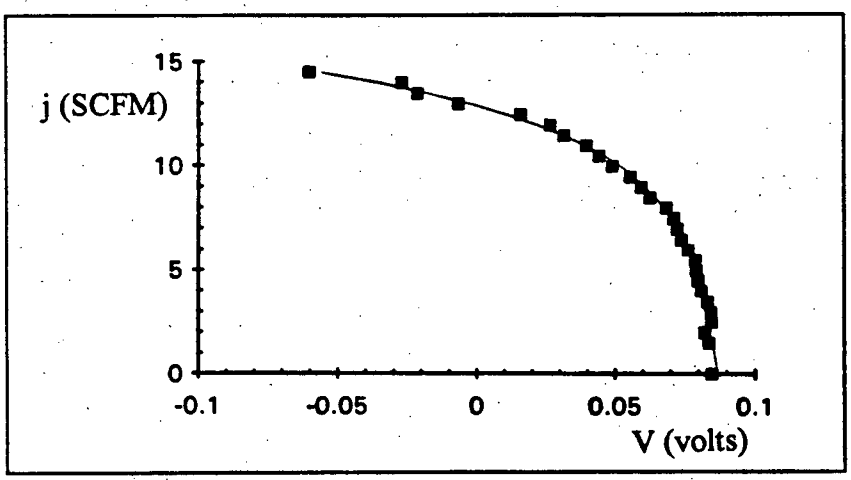

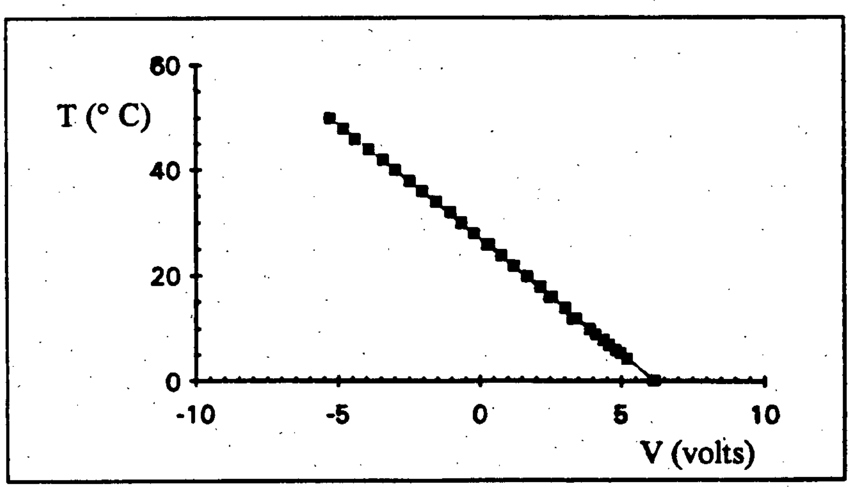

Figure 2.9: calibration curve for a) pressure, b) flow rate and c) temperature

The equipment described to this point represents standard technologies which have been employed in many studies in this field. The following three sections of this chapter describe novel techniques which, to our knowledge, have not been used in vortex tube research. With the novel technique used to measure inlet pressure (described in page 17), they constitute the original experimental contribution of this thesis to the study of the physics of vortex tubes.

2.2 Flow field studies

Little is known about internal flow field in vortex tubes. The time-averaged velocities in the vortex tube have axial, tangential and radial components. As discussed in the introduction, the present work considers time-averaged velocities and pressures, and the terms "velocity" and "pressure" will describe "time-averaged" velocities and pressures throughout the thesis. Even if a small radial flow has to be present to drive the fluid from the inlet (located at the periphery of the tube) to the center of the tube, the radial component is usually assumed to be negligible compared to the two other components. The amplitude and the orientation of the velocity vector varies with the location, the inlet conditions and the hot outlet valve setting.

If one insert a pitot tube having a relatively slow time response (>10 ms), time-averaged pressures will be measured. If pressures are measured in this field with a pitot tube that can axially rotate on itself, the direction at which the maximum pressure is measured will be the velocity vector angle and the pressure amplitude will correspond to the sum of the static pressure and the dynamic pressure (see Figure 2.10). Since measurements of the velocity angle give the direction of the flow at a point it is then possible to estimate the velocity profile by moving the sensor to different locations. One must know the local temperature and pressure in order to determine the velocities from the stagnation pressure. However, even in the absence of any knowledge of local pressure and temperature, the angle at which the stagnation pressure peaks gives valuable information about the direction of the local flow velocities. For that reason a miniature pitot tube was built by a summer student, Mr. Stuart Groves.

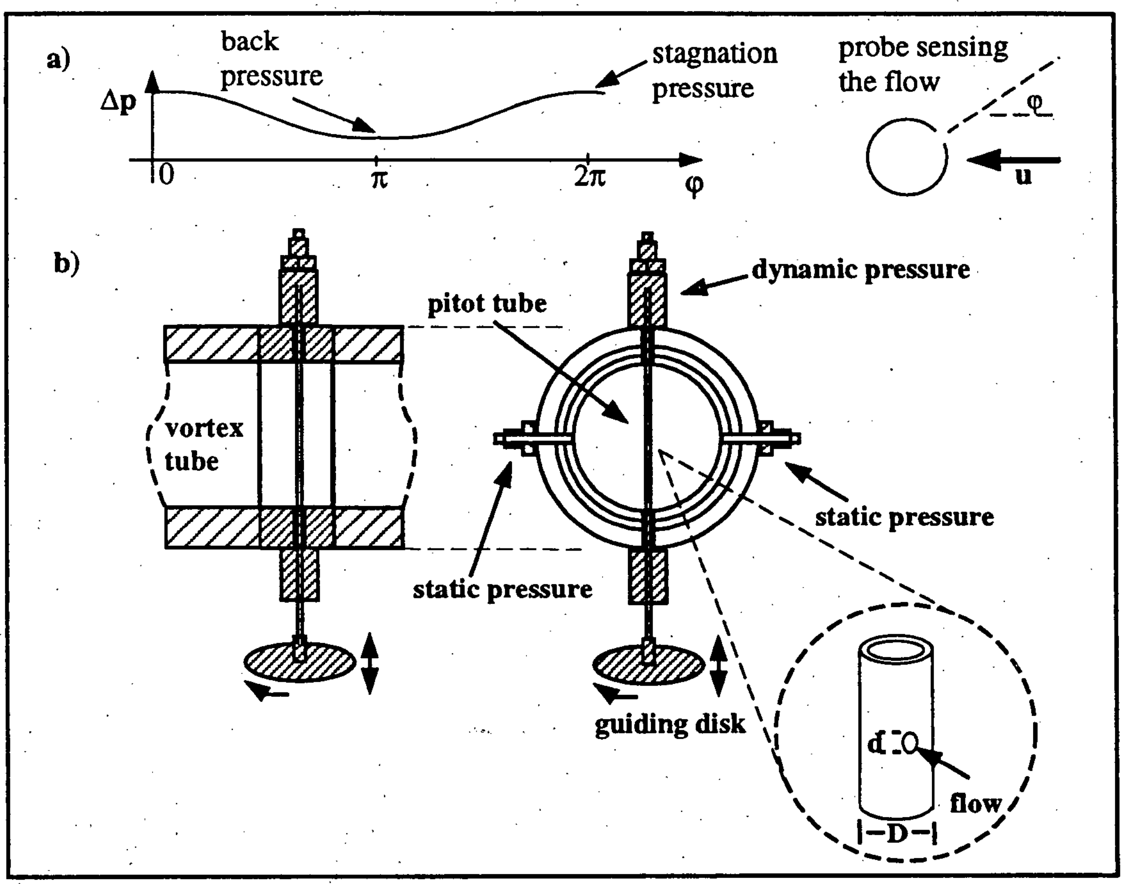

Figure 2.10: a) Pressure measured by a pitot tube in a flow field for various angles b) Pitot tube used for flow field measurements

The special pitot tube is shown in Figure 2.10b. The pitot tube allowed measurements of the difference between the dynamic pressure at different locations along a line crossing the center of the vortex tube and the static pressure measured at the tube wall. The pitot tube is attached to a ring of 1 inch inner diameter so that it can be attached to the vortex tube. The pressure taps are connected to the type of pressure transducers used for pressure measurements in the standard VT-01 (see section 2.1.3). A complete description of the experimental set up and experiments on flow field Stuart Groves's project report (1994). Although all the information needed to understand the experiments is summarized in this thesis.

2.3 Low pressure vortex tube measurements

All previous work on vortex tubes were done at above atmospheric pressures. However, previous studies by Ahlborn et al. (1994) predicted that vortex tubes should operate even below atmospheric pressures. In order to test this hypothesis, a set of experiments was performed in which air was sucked through the tube rather than pushed through. The set up is shown in Figure 2.11. A vacuum pump (Kinney KS-27, 27 CFM capacity) was connected to the cold and hot side of the tube. The standard tube was slightly modified by a different valve on the hot side since the former one was incompatible with the vacuum coupling. The vortex tube inlet was open to atmospheric pressure. The vacuum pump was connected to the vortex tube by a 1 in. diameter copper pipe on the hot side and by a 0.5 in. diameter Polyflow tubing on the cold side. The vacuum pump cycle was producing pressure pulses in the vortex tube that could be seen on the pressure Bourdon gauges. With the use of an air buffer volume of 0.02 m^3 between the vortex tube and the pump, the pulses were no longer detectable.

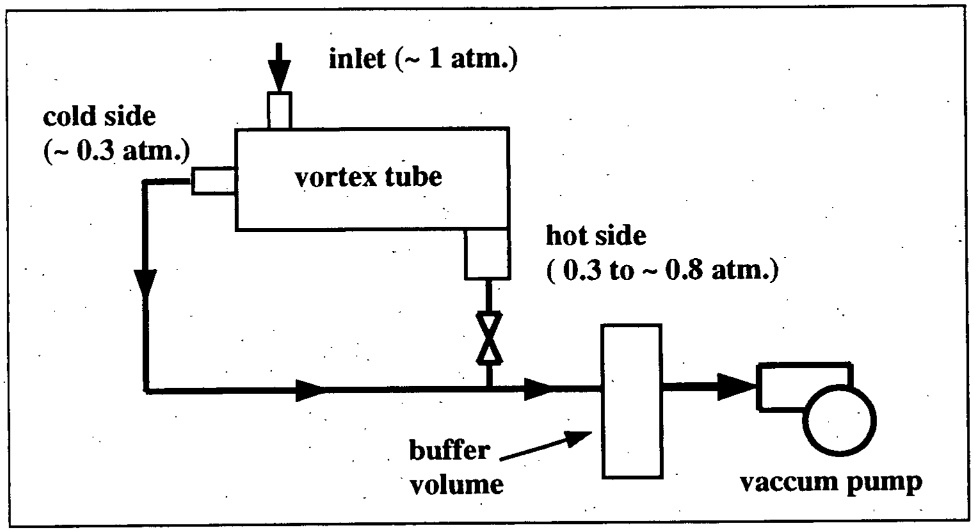

Figure 2.11: Suction vortex tube set up

2.4 Acoustics studies

One of the recent theories of vortex tubes by Kurosaka proposes that sound waves play an important role in the Ranque-Hilsch effect. However no acoustic measurements in standard vortex tubes have been reported in the literature. For that reason a miniature microphone was assembled during a summer research project by Mr. William Neil. This microphone was used to obtain vortex tube sound spectra for several flow rate and pressure settings.

Figure 2.12 shows the set up used for the sound waves measurements. A condenser microphone (Electret MC 1306 condenser cartridge) was attached to the valve of the standard vortex tube. The microphone signal was analyzed by an FFT spectrum analyzer (HP 3582A). The frequency spectra were then recorded using an X-Y recorder (HP 7046B).

The microphone was calibrated for various frequencies and intensity levels. Since no manufacturer data were available for the frequency response of the condenser cartridge, the microphone's response was evaluated by changing the frequency of a sound source with an assumed constant intensity of about 50 dB. The sensitivity of the microphone was significantly increasing above 10 kHz. Therefore in the spectral features the high frequencies appear to have more weight. Due to the absence of a reference sound source with known intensity and variable frequency, the microphone's response is not known well enough to allow quantitative spectrum analysis. While the absolute intensity of the signals may be in doubt these measurements should give a reasonably accurate account of the sound frequencies present in the vortex tube.

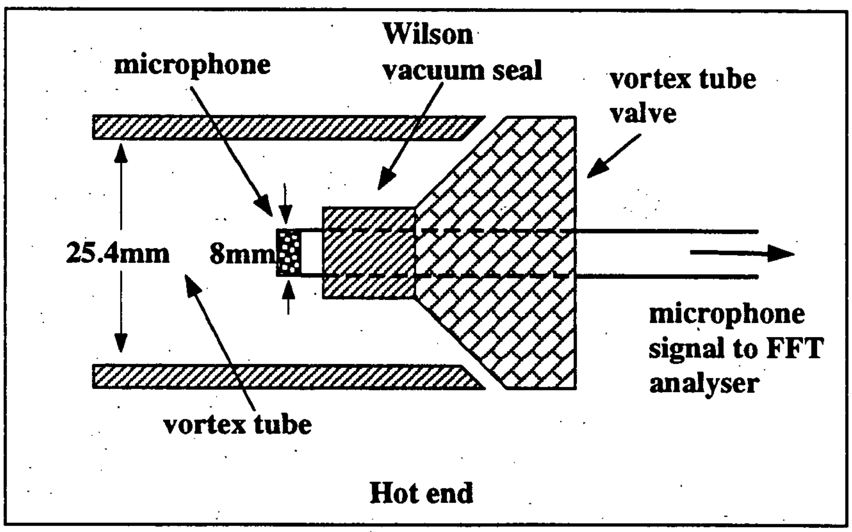

Figure 2.12: Sound measurements set up

3 - Experimental results

The main objective of this thesis is to shed new light on the vortex tube effect through new analysis of data obtained by standard and novel methods. This section presents the properties of the UBC VT-01 when used with compressed air (standard vortex tube) and also used with vacuum. The sound field and velocity measurements are also presented.

The main property of a vortex tube is its temperature splitting characteristics. Before analyzing data taken on the new tube and comparing them with results obtained in other research, one has to know if the tube performs like any other vortex tube, i.e. if the temperature splitting properties are similar. For each type of experiments, a brief description of the experimental method is presented.

3.1 Standard Vortex tube experiments

Experimental method

The aim of these experiments was to try the vortex tube with many settings, from low pressure to high pressure and by changing the flow rate ratios on the cold and hot sides. The easiest way to obtain different settings was to fix the plenum chamber pressure at the inlet, and to record data for different flow rate ratios. A constant inlet pressure could be easily obtained by using a pressure regulator on the inlet. Given the inlet temperature and pressure and for a specific valve setting, the inlet flow rate j_o, the pressures p_c and p_h and the temperatures T_c and T_h are then determined in a unique way for a specific vortex tube. Therefore, the tube can be completely characterized by changing three parameters: T_o, p_o and the valve setting on the hot end. In these experiments, the inlet gas temperature upstream of the vortex tube where the flow velocity is negligibly small was kept constant, since there was no facility to change the temperature of a high speed gas flow. The gas inlet temperature was a fairly constant value of 293K. An air trap filter was used to reduce moisture in the gas.

Table 3.1 shows the parameters that were recorded on each setting at the locations shown in Figure 2.2. As explained previously, the static temperatures measured were very close to the total temperatures since the fluid velocities were not high at the probe locations. On most of the settings p_o was measured with the circular pressure tap (Figure 2.5). However, it was found that the pressure was varying greatly in the entrance and using the inlet pressure from the nozzle tap was more appropriate (see appendix A). A time recording was also taken and was used in some tests to look at the thermocouple time response. It was found that this response can be very slow, especially on the hot side for a valve setting where j_c is large compare to j_h. In this situation the air velocity in the hot end was low and its temperature was too high. A longer equilibration time was required until the thermocouple had acquired the same temperature as the hot gas stream. The thermocouple response has not been studied extensively but typically a waiting time of approximately 20-30 sec. was necessary for the sensor to stabilize.

Temperatures	T_{nl}, T_c, T_h
Pressures	p_{nl}, p_o , p_h, p_c
Flow rates	j_o, j_c
time	t

Table 3.1: Parameters recorded for each standard vortex tube experiments

Before a set of experiments, the instrumentation calibration was checked. The instrumentation box was turned on at least 15 minutes before the tests to let the power supply and transducers warm up and stabilize. The flow rates reading from computer were compared to the reading on the rotameters. The pressure values were compared to values on the Bourdon gauges. Finally the thermocouples were placed into an ice and water mixture and the readings were compared to a thermometer. The thermocouples locations were verified and it was also checked if there was any leakage on the tube connections. The tube was then insulated by wrapping 1/2 in. polyethylene foam sheets around it.

For each setting, about 10 data points were recorded. Each point was an average of 25 measurements taken by the computer. For each different inlet pressures, 8 to 12 flow ratios were tried. The same settings were recorded on three different runs to check the repeatability of the measurements. This way, about 300 points were recorded for each different inlet pressure.

Data have been taken for the following inlet pressures: 10, 20, 30, 40 psig. Due to the air system capacity, (the compressor of the physics department has a 80 gallons tank, which is relatively small, and a maximum pressure of 150 psig) it is not possible to operate the vortex tube for a sufficient amount of time at pressure higher than 40 psig (the air system pressure drops from 150 psig to 40 psig within 1 minute). Furthermore, the hot end temperatures could not be recorded properly on the set at 40 psig since there was not enough time for the thermocouple voltage to stabilize. At lower pressures, e.g. 30 psig, the vortex tube can be operated for at least 3 minutes and the hot side thermocouple attains constant readings within 2 minutes.

Results

The heating and cooling is shown for different inlet pressures as function of the mass flow ratio j_c/j_o in Figure 3.1. It should be noted that the temperature splitting is quite reproducible. The temperatures plotted are the total temperatures, which are defined by

$$T_t = T + u^2 / 2c_p \tag{3.1}$$

where u is the fluid velocity and c_p is the specific heat at constant pressure. The total temperature concept is fully described in appendix A. In previous work where high entrance velocities were considered (>100 m/s), total temperature was used while in models with low velocities, there is no difference made between total and static temperatures since they are almost the same. Results shown in chapter 4 will prove the use of total temperature to be adequate. Since at the thermocouples locations the velocities were always smaller than 40 m/s, the total temperature difference is similar to the temperature difference. In Figure 3.2, an average of the data is presented. Each point is an average of about 10 points. The curves shapes are similar to other vortex tube data (e.g. Stephan et al., 1983). The hot gas temperature rises steadily with increasing j_c/j_o, with a maximum hot temperature difference for a ratio of about 0.8, and decreases for higher flow rate ratios. A maximum cold temperature difference is obtained for a flow rate ratio of 0.3 to 0.45. In the middle range of flow rate ratios, the temperature difference between the hot and cold side is nearly constant for a specific inlet pressure. For a specific flow rate ratio, the temperature splitting increases by increasing the inlet pressure. The temperature difference values on the cold side are similar to Stephan's data, but on the hot side Stephan was getting a larger difference. However, he used a different vortex tube having the optimum diameter for temperature separation.

Overall, this graph shows that the vortex tube UBC VT-01 has the characteristics of a normal vortex tube. This averaged set of data will be used for further analysis in the next chapters.

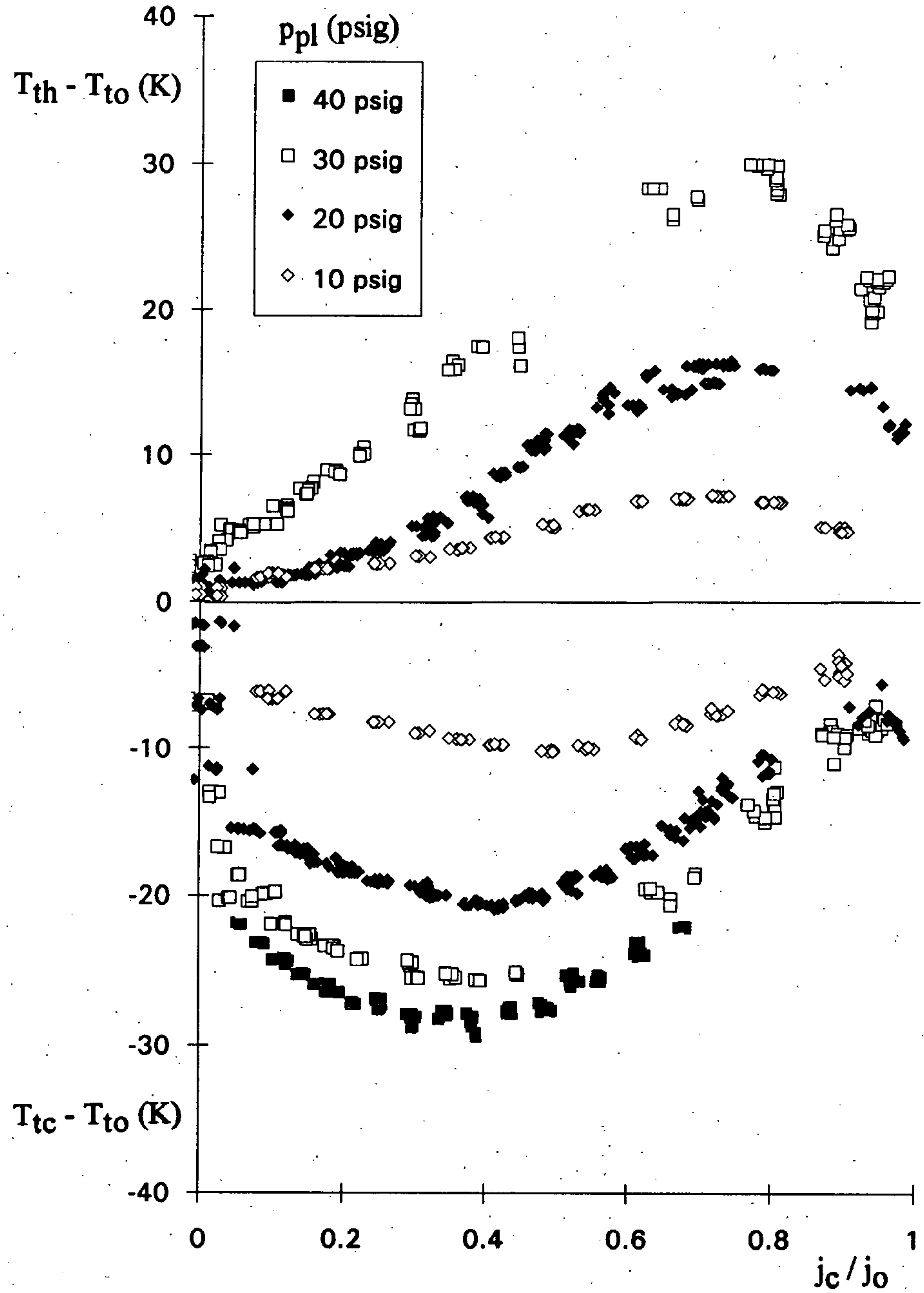

Figure 3.1: Total temperature separation for the vortex tube UBC VT-01: raw data

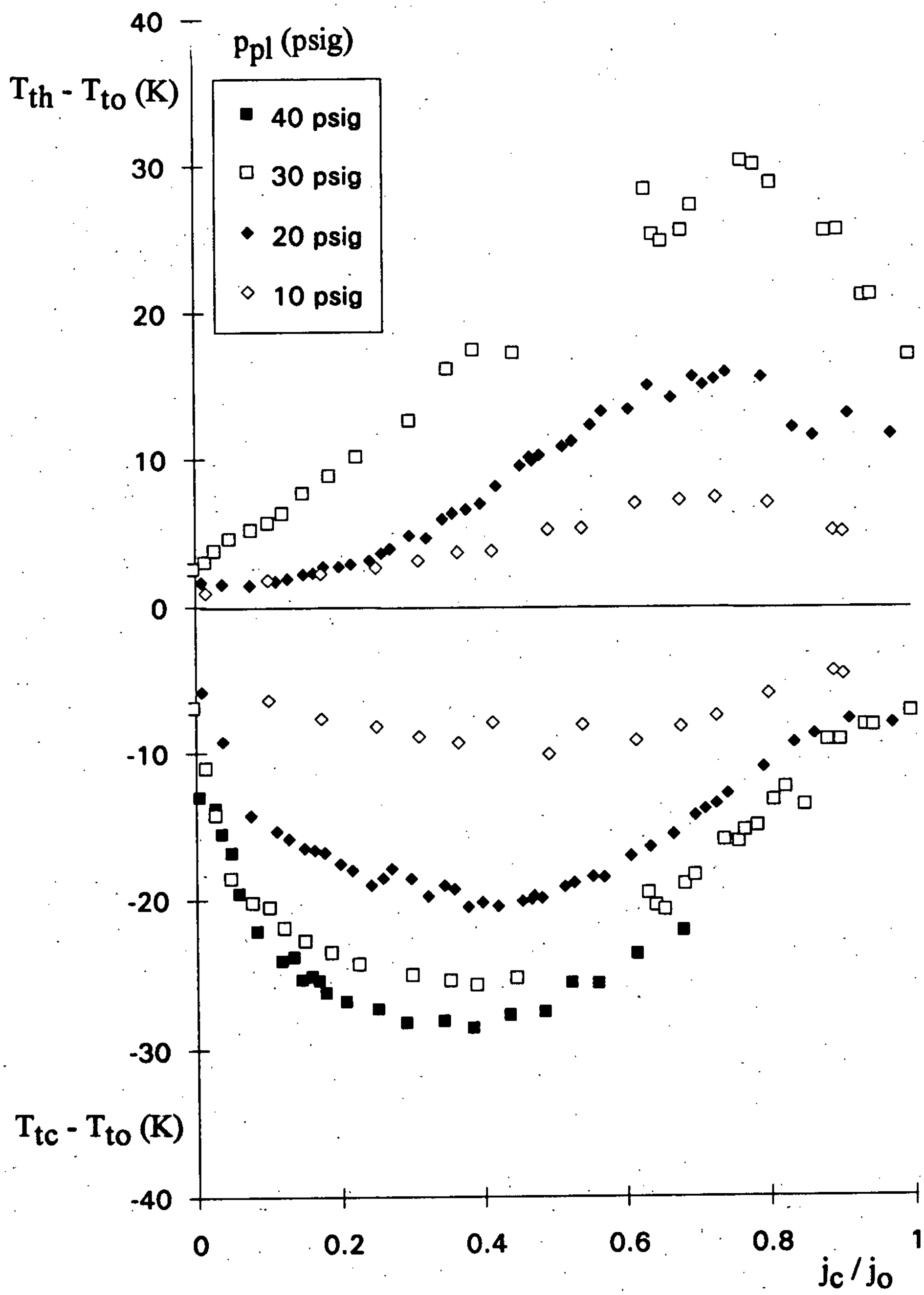

Figure 3.2: Total temperature separation for the vortex tube UBC VT-01: averaged data

3.2 Low pressure vortex tube experiments

In order to test the hypothesis that vortex tube could operate at below atmospheric pressure, a set of experiments was performed in which air was sucked through the tube rather than pushed through. To our knowledge, low pressure vortex tubes have never been tested.

Experimental method

The methods for vacuum and standard vortex tube measurements were similar. The main difference was that the pressure data were recorded by hand for the vacuum, since the pressure transducers used in this work were not made for vacuum measurements. The diaphragm in the pressure transducers could have been damaged if used with vacuum since it would have been moving in the wrong direction. Simple checks of the flowmeter measurements with rotameter measurements showed that the flowmeter calibration was still valid. The air entering the flowmeter before the vortex tube was at atmospheric pressure. The tube plenum chamber pressure was slightly fluctuating between 91 to 94 kPa while the hot and cold end pressure varied from 33 to 67 and 33 to 58 kPa respectively by changing the valve setting.

The results are presented in Figure 3.3. To our knowledge, it is the first time that temperature splitting has been observed for a vortex tube working below atmospheric pressure.

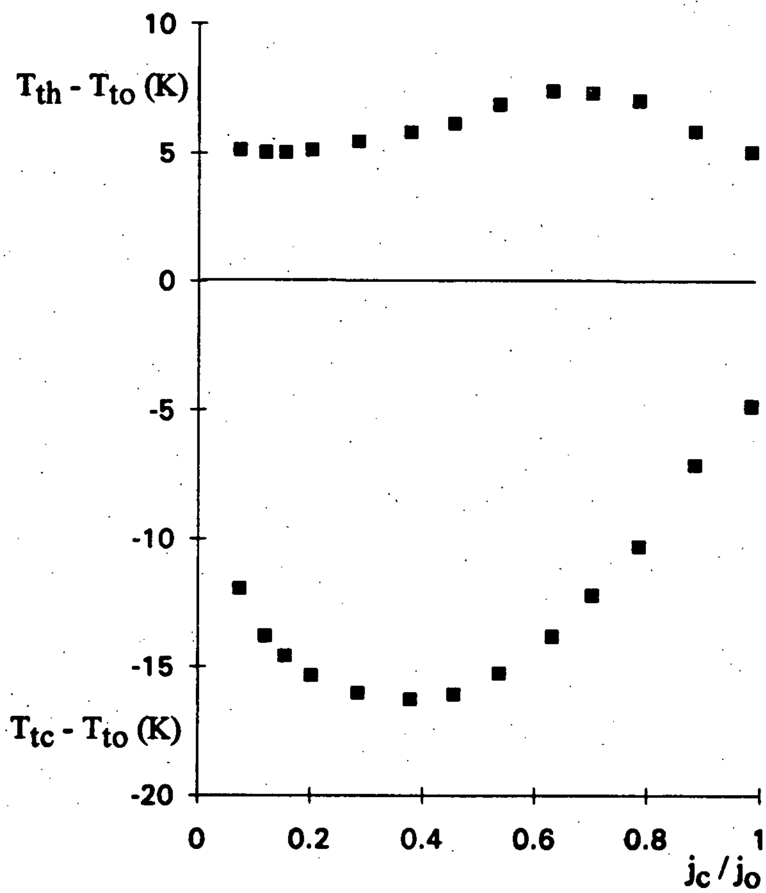

Figure 3.3: Total temperature separation for the suction vortex tube

3.3 Velocity field measurements

The internal vortex tube flow field was studied with the help of the miniature pitot tube. The velocity vector angle and the total pressure amplitude were measured in the plane z = 33 cm, which correspond to the location L/2. It should be pointed out again that the velocity, pressure and temperature discussed in the thesis are "time-averaged" values, which means small scale fluctuations from turbulence were not taken into account in the analysis.

In order to understand the results that are presented, it is useful to have a qualitative description of the flow field. The flow models in Figure 3.4 shows some important features of the flow field. First, the angle measured by the pitot tube is the angle between the z axis and the maximum velocity vector. Knowing this angle, the velocity can be divided into an axial and tangential component (the radial component is assumed negligible). An angle greater than 90° means the gas flows in axial direction towards the cold side, while angle smaller than 90° means the gas flows towards the hot exit. θ = 180° means the flow is purely axial and flows towards the cold exit. On the other hand, θ = 0° would mean a purely axial flow towards the hot end. Finally, θ = 90° means the flow is purely rotational. The vortex tube flow field will be extensively described in the next chapter, where the data measured by the pitot tube will be analyzed and the magnitude of the axial and tangential velocities will be estimated.

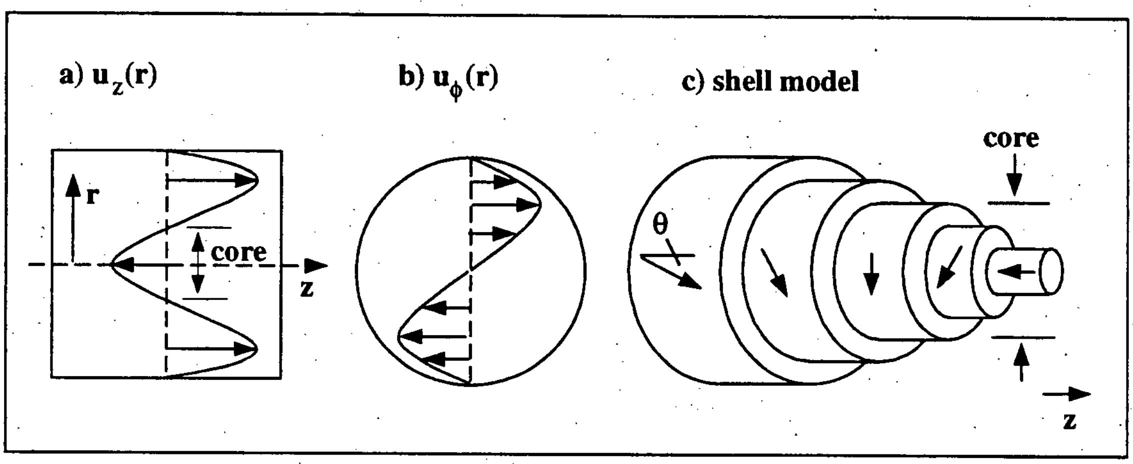

Figure 3.4: Vortex tube flow field: a)axial plane b)cross section c)shell model

The measurements were done at p_{pl} = 20 psig for 5 different valve settings: j_c/j_o = 0, 0.2, 0.4, 0.6, 0.8. For each setting, the measurements locations were r = 4, 8, 12, 16 and 20 mm. The maximum dynamic pressure was found for each location by rotating the pitot tube. The results are shown in Figure 3.5. The width of the cold core can be estimated by looking at the intersection between the velocity plots and the 90° boundary. In order to verify if the pitot tube was not affecting significantly the flow, we operated the vortex tube with and without the pitot tube for the same operating conditions. The temperature separation was similar in both experiments.

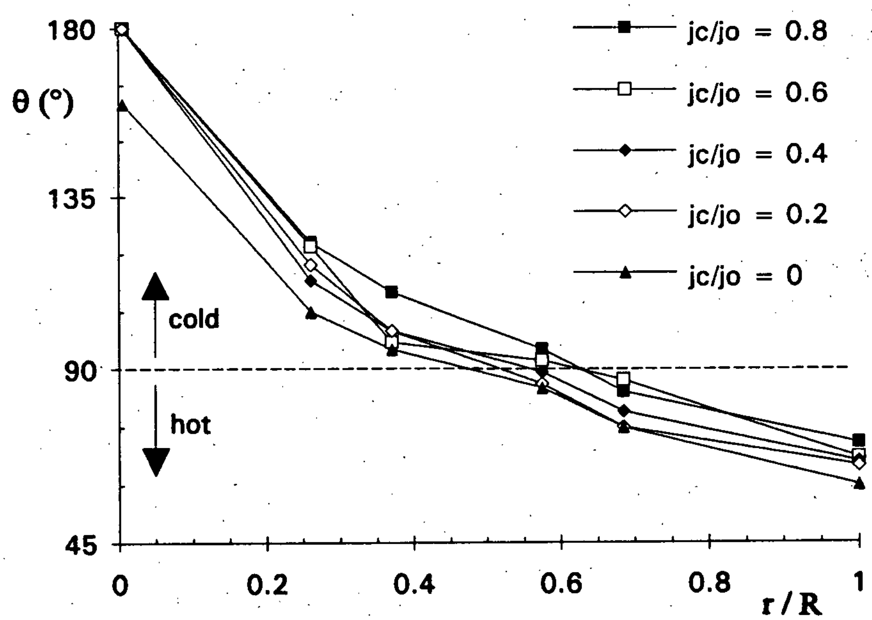

Figure 3.5: Velocity vector angle and total pressure at z = 33 cm (L/2) and p_{pl} = 20 psig for different valve setting (0° means the velocity vector is along the z axis)

3.4 Sound wave measurements

In an attempt to clarify the importance of sound in vortex tubes, sound spectra were measured with the microphone located close to the hot exit at 20 and 30 psig for flow rate ratio of 0, 0.2, 0.4, 0.6, 0.8 and 1. All the spectra are presented in a project report by William R. Neill (1994), who helped taking the measurements. Here, the main spectrum features are presented.

Figure 3.6 shows a typical sound spectrum recorded. A large peak is present around 17 kHz. However, the microphone has much higher sensitivity at this range of frequency. Therefore the energy in this section of the spectrum (from 10kHz to 25kHz) represents in fact a much smaller fraction of the total energy.

The peak at 2.2 kHz is probably caused by the fluid rotation. The frequency can be described by $f = u_o/(2\pi R^*)$ where R^* would be close to the tube radius. This sound is probably produced at the inlet of the tube, as proposed by Chanaud (1963) and by Kurosaka (1982). This frequency is related to the tangential rotation (see Figure 3.7a). Also, a smaller peak is present at f = 1.1 kHz, which strangely correspond to the half of the tangential rotation frequency. So far, no explanation of this "half rotation frequency" was obtained. The three small fluctuations between 5kHz and 10 kHz could be seen as harmonics of the tangential rotation frequency.

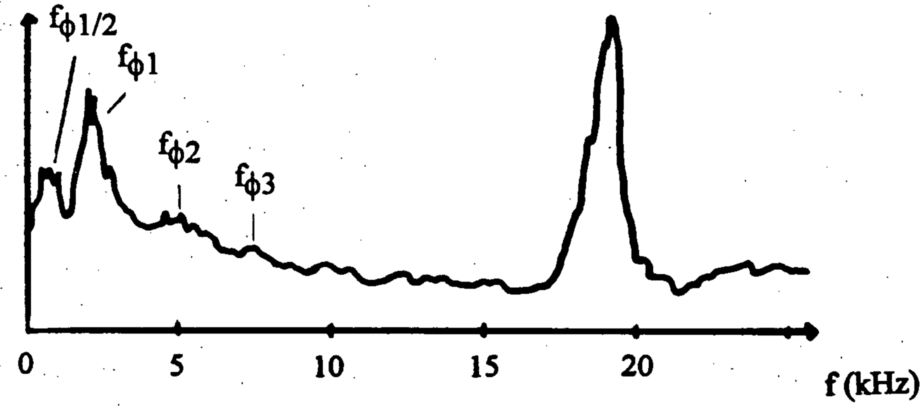

Figure 3.6: Typical sound spectrum from vortex tube (p_{pl} = 20 psig; j_c/j_o = 0.95).

Looking in the 0-5 kHz range in Figure 3.8, the two big peaks below 5 kHz appear to be composed of several peaks spaced by 250 Hz. These peaks could result from axial resonances where f_n = na / 2L where L is the length of the vortex tube. These axial resonances are similar to the one present in a two-open end pipe, as shown in Figure 3.7b.

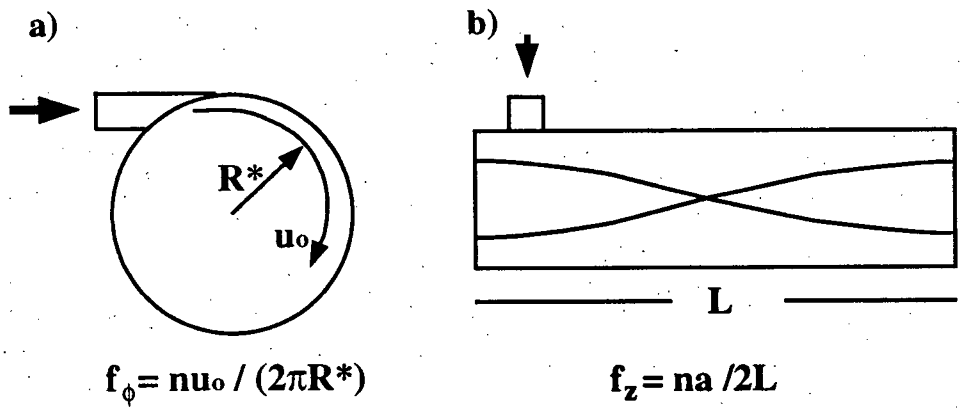

Figure 3.7: Sound standing waves production by a) tangential rotation b)node and antinode of fundamental mode of axial motion

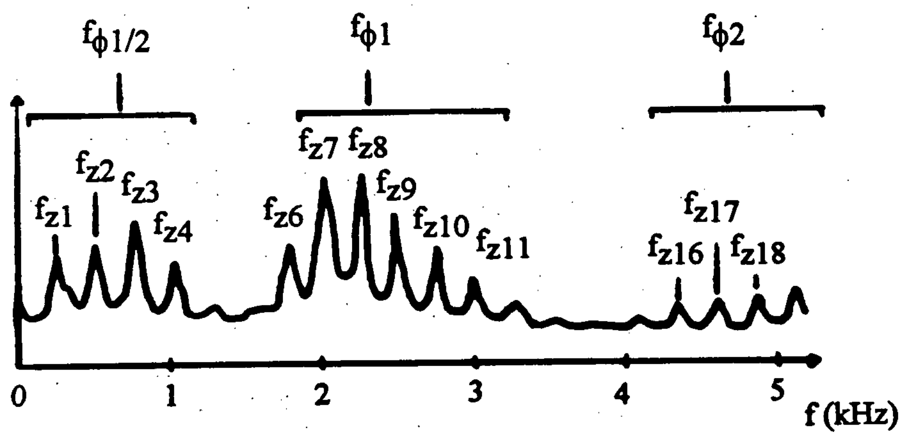

Figure 3.8: Sound spectrum of Figure 3.6 in a smaller frequency range (0 to 5 kHz) (p_{pl} = 20 psig; j_c/j_o = 0.95).

To obtain a very rough measure of the sound intensities for different flow rate ratios, the area under the spectra for various flow rate ratios were measured and related to the total sound intensity. In Figure 3.9, the intensity is plotted versus the flow rate ratio. The decrease at high flow rate ratio could possibly be explained by the fact that less fluid is coming out by the hot end. Therefore the microphone receives a lower intensity. It should be pointed out again that no instrumentation for calibrating the microphone accurately was available and therefore these measurements only give a first qualitative account of the sound fields in the vortex tube.

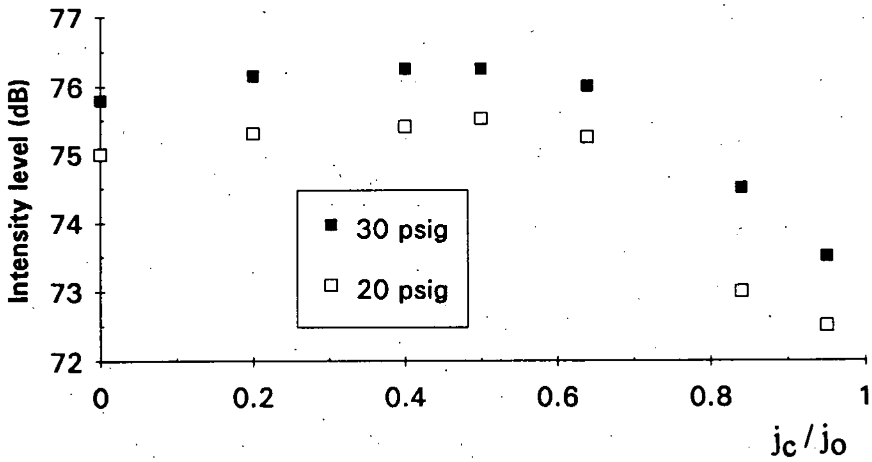

Figure 3.9: Sound intensity in the vortex tube (p_{pl} = 20 psig).

The experimental data presented in this chapter provide the basis of analysis to test previous models of the vortex tube and provide new insight into the working of the strange device. In the next sections, these data are analyzed and compared to results from previous models, especially the model from Ahlborn et al. (1994).

4 - Analysis

The previous chapter contained all the description of the method of measurements and all the measurements taken in this work for analysing the vortex tube. In this chapter, these measurements will be analysed in order to confirm predictions from Ahlborn's model (1994). Most of the derived equations are from Ahlborn's model, and they are checked against the new measurements. But first, it will be discussed how this model compares to the previous ones and how it can be useful to understand the vortex tube effect.

Throughout the years, many attempts have been made to understand the physical mechanisms that are responsible for the heating and cooling effects in vortex tubes, and to derive simplified analytical vortex tube models. Most of the models were trying to solve the Navier Stokes equations by making some assumptions on the flow field, and by using the thermodynamics relations after. For example, Sibulkin (1962) assumed low entrance velocities (Mach number much less than 1), Deissler (1960) assumed the tangential velocity to be independent of the axial position in the tube. These hypothesis were contradicted by subsequent experiments. It is believed in the present work that the entrance velocity can go up to Mach one (to be explained later in the thesis). Also, many researchers were modelling the uniflow type vortex tube, with the cold end closed (Deissler, 1960, Kurosaka, 1982, Linderstrøm-Lang, 1971, Savino, 1961). This configuration is fairly different from the standard vortex tube since all fluid elements move in the same axial direction. None of these models were able to properly explain the energy separation effect in standard vortex tube. The Navier Stokes equations are just too complex and too many assumptions have to be made to solve them.

Some other researchers developed empirical relations by using dimensional analysis. Stephan (1983) developed a set of dimensionless numbers from the entrance conditions, the tube geometry and the gas properties and by the use of the Buckingham-π theorem, fitted a function that predicted the temperature splitting from the flow rate ratio and the inlet pressure. However, it is not obvious that this relation holds for a different vortex tube. Furthermore, dimensional analysis gives very little insight into the physics of the energy separation process.

More recently, the interest has shifted to simpler analytical models, where part of the Navier Stokes equations were combined with experimental evidences to develop relations for some part of the flow inside the vortex tube. For example, Eckert (1986) attributed the fluid heating to viscous dissipation and the cooling effect to the superposition of a solid-body rotation and a channel flow. Ahlborn et al. (1994) developed a model in which heating is attributed to the conversion of kinetic energy and cooling to the reverse process. Radial dynamics, axial dynamics and energy balance were first considered separately to yield three independent relations. These were then combined to give limits of the temperature splitting in vortex tubes. This type of analysis has several advantages. First, this leads to simple physical interpretation. Also, the mathematical relations can be easily tested. Finally, possible non agreement with measurements can be easily traced to errors with assumptions, possibly leading to new insight into unexpected physical phenomena. Since this approach has several advantages, it will be used in this thesis.

In this chapter, the basic flow structure described from results of previous and new experiments will first be presented. This will help to understand the fluid motion in the vortex tube. Secondly, the simple fluid dynamics relations from Ahlborn's model will be derived and checked against experiments. An energy balance will then be done, since it is the third equation of Ahlborn's model and it can also be used to verify if the measurements were right. The main results of the model, i.e. the limits of temperature separation will also be verified against the new measurements. In chapter 5, emphasis will be given to possible explanations of vortex tube effect.

4.1 Flow structure

The vortex tube flow field can be characterized by two different flow components: the flow that will exit on the hot side (hot flow annulus), located near the tube wall and near the hot side, and the flow that will exit on the cold side (cold flow core), located in the center of the tube (see Figure 4.1). The cold flow core comprises all the fluid which presently or will eventually exit on the cold side. For example, near the nozzle, there are some fluid elements that initially go towards the hot side, but will reverse their motion and will finally leave on the cold side. These elements are part of the cold flow core. The center of the cold flow core consists of the fluid elements with negative axial velocity: the back flow core.

Between the two flows, a separatrix surface separates the flow going towards the cold and hot sides. The separatrix intercepts the z-axis at the stagnation point. The radial velocity can drive the fluid elements through the stagnation surface (see Figure 4.1), such that fluid elements enter the back flow core on all its surface. The stagnation surface is expected to be subject to strong shear stresses, since the latter are proportional to velocity gradients.

When most of the gas goes towards the cold side, the stagnation point should be located closer to the hot side since the cold gas flow rate is larger than that of the hot gas. Conversely, when most of the gas goes towards the hot side, the stagnation point should move closer to the cold side. These were confirmed by the velocity profile measurements (to be described later in the chapter). The stagnation point can also be seen as the farthest location to which fluid elements of the cold flow core component will advance before they turn back.

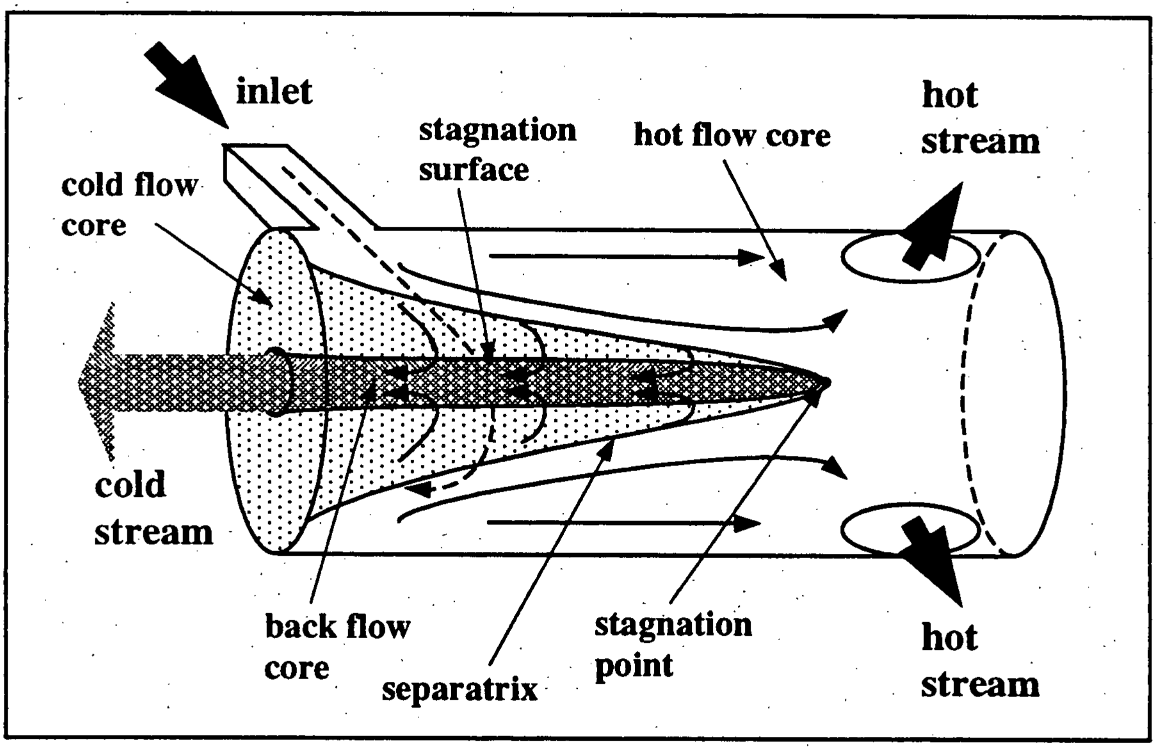

Figure 4.1: Scheme of the vortex tube, showing the hot flow core, back flow core and cold flow core

4.1.1 Velocity profiles

In this section, the velocity profile inside the vortex tube will be described qualitatively and quantitatively. An estimate of the velocity magnitude in a cross section of the tube will de derived and will be used later in the thesis to analyse the vortex tube.

In the earlier vortex tube models (Hilsch, 1947, Knoernschid, 1948) a Rankine vortex was assumed to exist in the entrance plane. A Rankine vortex is a free vortex coupled with a forced-type vortex in the center (see Figure 4.2) The free vortex is for instance produced if one spins a cylindrical rod on the z axis. A forced vortex is generated if one rotates a cylindrical vessel filled with a fluid. The free vortex is internally forced while the forced vortex is externally forced. The velocity profiles can be represented by the following equations:

forced vortex	$u_\phi(r)\big\|_{z=0} = u_o(r/r^*)$	$r < r^*$	(4.1)
free vortex	$u_\phi(r)\big\|_{z=0} = u_o(r^*/r)$	$r > r^*$	(4.2)

where r^* is the radius of a known reference point. In the case of a Rankine vortex r^* is the radius separating the free and forced vortex. This representation is not completely true for a vortex inside a stationary tube since it does not include a thin boundary layer were the velocity approaches the no-slip condition ($u_\phi = 0$) at the tube surface. Hilsch and Knoernschid assumed that a free vortex was present in the hot stream of the vortex tube while the cold core was more like a forced-type vortex. This process was then causing friction and heating the outer fluid. However, in all pressure and velocity profile measurements in the entrance plane the free vortex was never observed. On the contrary, the tangentially injected cold fluid acts like a spinning wall, and that should encourage forced vortex flow. In addition to this external friction, Kurosaka (1982) demonstrated that acoustic plane except for a very thin boundary layer near the wall where the velocity has to drop down to respect the no slip condition (see Figure 4.2d).

This assumption of a forced vortex can be adequate for the uniflow-type vortex tube, but probably not for the standard one. In the standard vortex tube, there is a region in the entrance plane that separates fluid elements moving in different axial directions where friction and shear stresses cannot be neglected. This region is part of the stagnation surface and is not present in the uniflow configuration. In this thesis, the forced-type velocity profile is then assumed in the entrance plane for the flow having positive axial velocities (going toward the hot end). Experiments will have to be used to estimate the velocity profile in the back flow core (see Figure 4.2e).

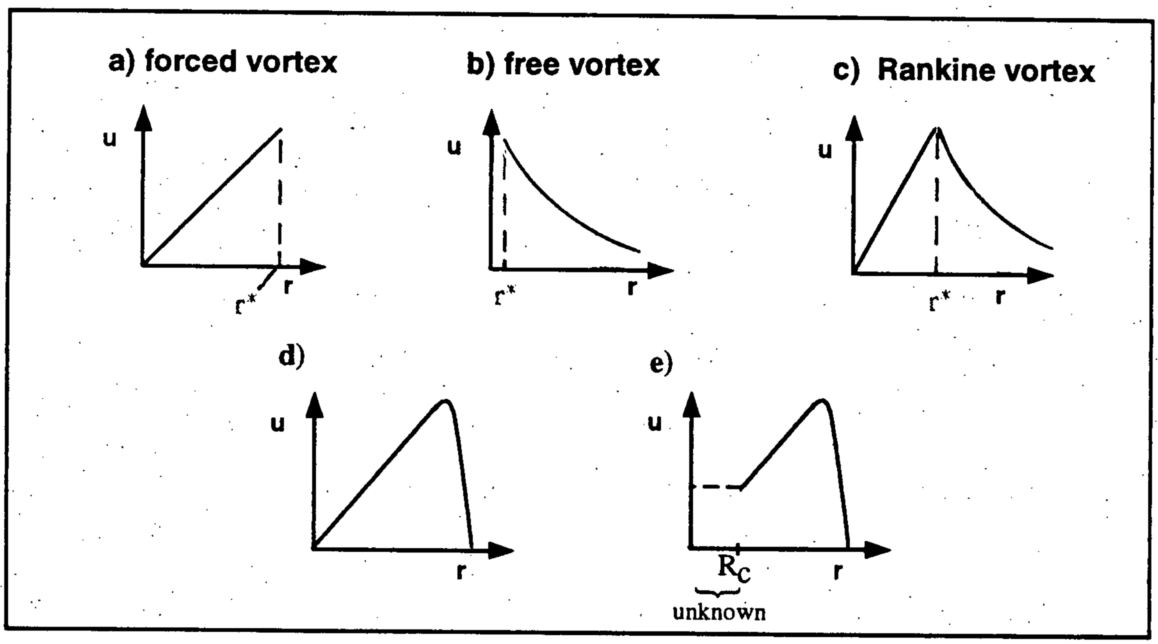

Figure 4.2: Vortex flows near entrance plane: a) free vortex b) forced vortex c) Rankine vortex d) Uniflow vortex tube profile e) Double ended vortex tube profile

The assumptions of a forced vortex is probably not true for cross section closer to the hot side. It is generally assumed that the vortex loses its strength while moving in the z direction. This is mainly due to friction from walls. The motion is no longer purely rotational since the axial velocity becomes more important compare to the tangential velocity. In this thesis, the flow is assumed to be completely axial at the hot end. This was helped in the present experiments by a detwister placed close to the hot end (see Figure 2.3). The detwister was used to stop the vortex motion at the hot end. The use of a detwister did not change the vortex tube characteristics but allowed us to neglect the tangential velocity at the hot end. Also, since the hot side area A_h is much bigger than the cold end and nozzle areas, the velocity there must be substantially smaller than that at the cold end:

$$u_h << u_o \tag{4.3}$$

There is also some confusion about the magnitude of the entrance velocity. Some researchers have proposed supersonic velocities, while some others thought the maximum velocity to be around 200 m/s. The work presented in this work shows that the pressure varies greatly near the entrance and a pressure measurement far from the inlet can lead to quite erroneous assumptions about the entrance flow velocities (see appendix A). The inlet velocities calculated from the present experiments were ranged to 311 m/s.

Internal velocity measurements with the pitot tube

Velocity direction measurements were done to investigate assumptions about the flow structure. As explained in section 2.2, the pitot tube measured the pressure difference between the static pressure at the tube walls and the maximum total pressure in a cross section at any selected radius.

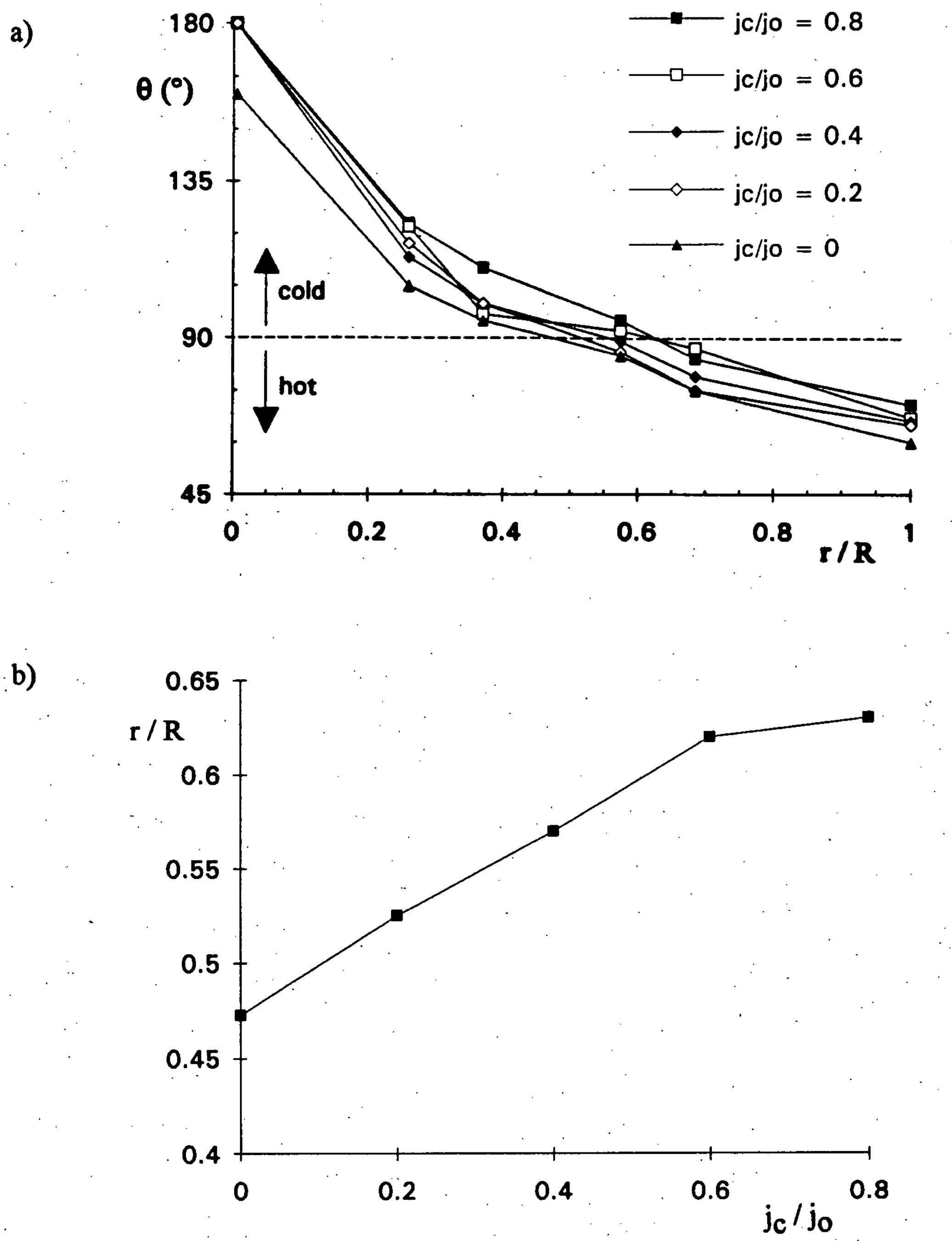

Figure 4.3: a) Angle between maximum velocity vector and z-axis **b)** Width of the back flow core (z = 33 cm (L/2), p_{pl} = 20 psig)

The measurements were taken along a cross section located in the middle of the tube (z = 33 cm or L/2). The angle, θ, between the z-axis and the maximum velocity vector was also determined and recorded. It should be noted that for $\theta < 90°$, the flow is towards the hot end, while for $\theta > 90°$, the axial flow goes in the cold exit direction. Hence for $\theta = 90°$ the flow is purely rotational, i.e. $u_Z = 0$, so that the radial distance where $\theta = 90°$ marks the radial distance of the stagnation surface (back flow core). In Figure 4.3b, the width of the back flow core is shown. When the flow rate ratio increases, the width increases, as expected. Figure 4.3a shows the angle as a function of the location for various flow rate ratios. The fact that the back flow core is existing even when $j_C/j_O = 0$ (cold end closed) is really surprising. This would mean that an axial rotating motion is present even when no fluid exits at the cold end (refer to Figure 3.4 or 4.1 for qualitative flow field description). Measurements for all flow rate ratios j_C/j_O show a back flow core, even for $j_C/j_O = 0$. This implies that the stagnation point in the vortex tube was always in the half of the tube closer to the hot end. However, it should be acknowledged that the pressure readings at the center of the tube at $j_C/j_O = 0$ seemed to fluctuate, making the determination of the direction θ somewhat unreliable, and possibly suggesting that the position of the stagnation point is unstable under that condition.

The pitot tube measurements can be used to obtain a radial velocity profile as follow:
Introducing the total pressure $p_{total} = p + 1/2(\rho u^2)$ and using the gas law $\rho = p/(RT)$, the measured pressure difference can be expressed as

$$\begin{aligned} \Delta p(r) &= p_{total}(r) - p_{wall} \\ \Delta p(r) &= p(r)\left(1 + \frac{u^2(r)}{2RT(r)}\right) - p_{wall} \end{aligned} \tag{4.4}$$

where $u^2 = u_z^2 + u_\phi^2 + u_r^2 = u_z^2 + u_\phi^2$ since u_r^2 is considered negligible compare to u_z^2 and u_ϕ^2. Knowing u(r) and the flow direction angle θ, $u_z(r)$ and $u_\phi(r)$ can be obtained by

$$u_z(r) = u(r)\cos(\theta) = \left[2RT\left(\left(\frac{\Delta p(r) + p_{wall}}{p(r)}\right) - 1\right)\right]^{1/2} \cos(\theta) \tag{4.5}$$

$$u_\phi(r) = u(r)\sin(\theta) = \left[2RT\left(\left(\frac{\Delta p(r) + p_{wall}}{p(r)}\right) - 1\right)\right]^{1/2} \sin(\theta) \tag{4.6}$$

where θ is defined as the angle between the maximum velocity vector and the z-axis. For θ = 0°, $u_\phi(r) = 0$ and $u_z(r) = u(r)$ since $u_r(r)$ is assumed to be negligible. Therefore, it is possible to obtain the velocity profile if p_{wall}, p(r) and T(r) are known. Due to the size of static pressure and temperature probes, the radial pressure and temperature profiles would have been difficult to measure with simple techniques and therefore they have to be estimated. It was assumed that the variation of the static pressure along the wall is linear, as well as the variation of the pressure along the z axis at r = 0. As a first guess, the pressure is modelled as a linear function of r^2 (this will be explained later in the section) and is confined between p_{wall} and p_{axis}. A linear decrease of temperature was assumed, with T_{max} = 283 K and T_{min} = 263 K. With these assumptions, we get, for Z = L/2,

$$p_{wall} = (p_h + p_o)/2 \tag{4.7}$$

$$p(r) = \left[\left(\frac{r}{R}\right)^2 \left(\frac{p_o - p_c}{2}\right)\right] + \left(\frac{p_h + p_c}{2}\right) \tag{4.8}$$

$$T(r) = 20\left(\frac{r}{R}\right) + 263 \tag{4.9}$$

With these interpolated values for pressure and temperature one obtains the tangential velocity profile u_ϕ (r) as shown in Figure 4.4. It should be noted that the similarities in the velocity profile for different flow rate ratios might be due to the above estimate of the pressure field used for the calculations of velocity profiles. Since in reality, the pressure field will probably change for different flow rate ratios, the velocity profile could be fairly different than those shown.

It would be interesting to investigate how accurate these profiles are. The most inaccurate estimate is T(r). However, its uncertainty is typically ΔT = +/- 10 K over 263 K for the temperature, so that $\Delta T/T$ is about 4%, and the temperature profile does not have a strong effect on the velocities. The velocities will be more sensitive to the estimate on p_{wall} but the latter is believed to be resonably accurate. By using very conservative value of pressure limit (not the most realistic, however), i.e. $p_{wall} = (0.8p_o+p_h)/2$, the velocity was dropping from 120 m/s to 105 m/s. Therefore, an approximate uncertainty of 25% is estimated for the velocity profiles.

In Figure 4.4, the maximum tangential velocity is not at the tube walls. In fact, the tangential velocity reaches a maximum near the stagnation area and then decreases when it approaches the center of the tube. This confirms the hypothesis of the forced vortex degradation: due to friction at the wall, the vortex cannot keep the same tangential velocity and a Rankine vortex appears. However, it seems that the tangential velocity at low radius is larger than in the entrance plane. In the entrance plane, with an initial velocity of 250 m/s, the velocity at r/R = 0.3 would be 75 m/s with a forced vortex while the velocity appears to be around 120 m/s. As in Ahlborn's model (1994), this can be explained by two phenomena opposing each others; the conservation of angular momentum, which tends to increase the tangential velocity when the radius of rotation decreases and the shear forces which tend to make the whole fluid core rotate as a solid body. Since the fluid elements located in the center of the tube (at L/2) travelled on a smoother path with less shear forces than the elements in the entrance plane, they were able to conserve a bigger part of their kinetic energy. Therefore, for small radius, fluid elements at z = L/2 can have higher tangential velocity that those in the entrance plane.

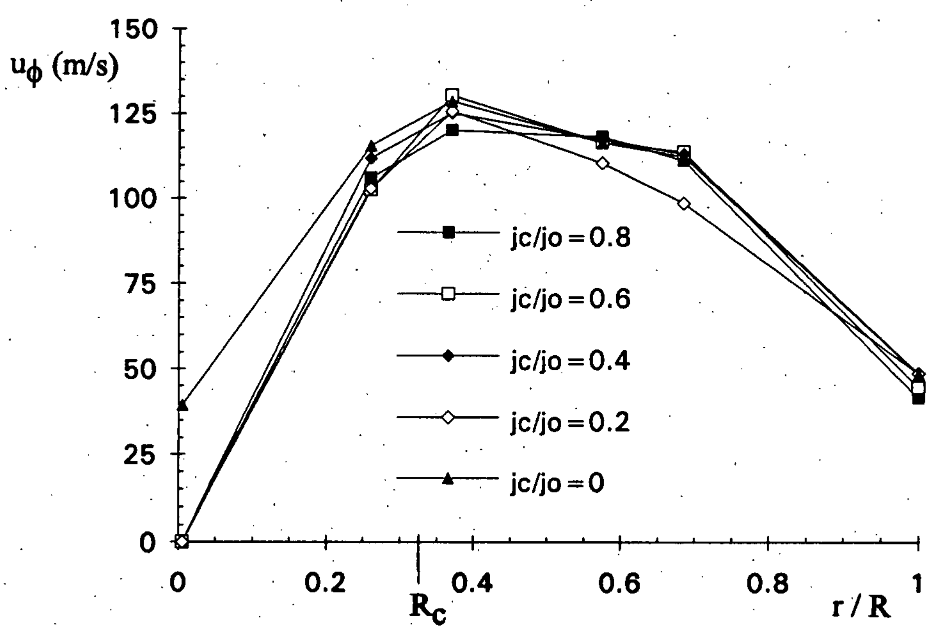

Figure 4.4: Tangential velocity profile (z = 33 cm (L/2), p_{pl} = 20 psig). The estimated uncertainty on velocity magnitude is 25%.

Figure 4.5 shows the axial velocity profile (refer to Figure 3.4 or 4.1 for flow field qualitative description). Here the presence of the back flow core is also obvious. The core is even present for j_c/j_o = 0. The presence of a very high axial velocity around the centerline is intriguing. This high velocity was not expected, particularly for $j_c/j_o = 0$. There is no doubt that a back flow exists even with no flow through the cold end, since the flow angle was measured directly. However, the calculations performed to obtain the axial velocity required assumptions on the pressure profile, and they might not be very accurate. Using a different pressure profile could yield to a decrease in the calculated magnitude of the axial velocity. Therefore, the presence of the back flow is beyond any doubts, but its magnitude is somewhat uncertain. Due to the assumptions on pressure and temperature profiles, an uncertainty of at least 25% is again expected for the axial velocity magnitude.

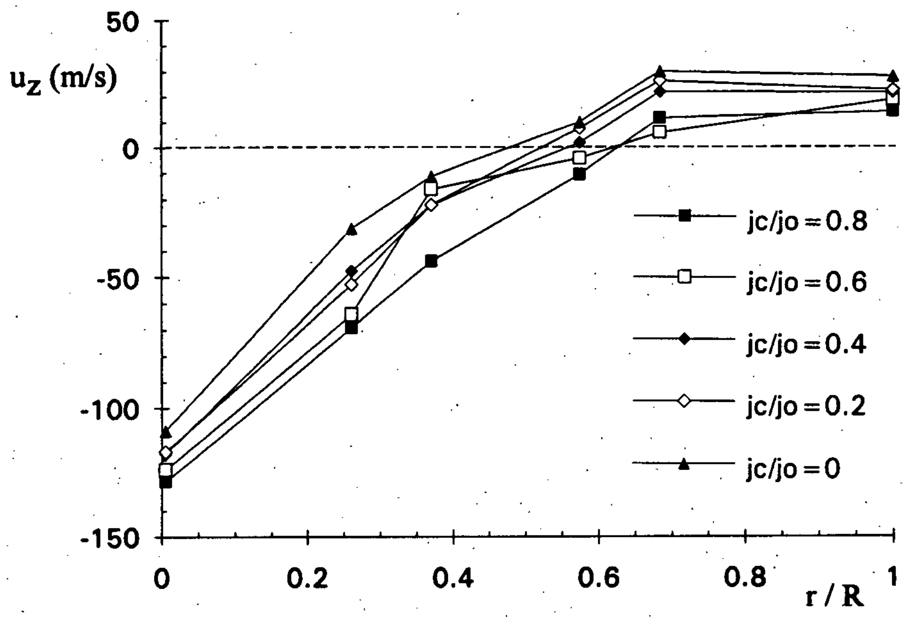

Figure 4.5: Axial velocity profile (z = 33 cm, p_{in} = 20 psig). The estimated uncertainty on velocity magnitude is 25%.

4.1.2 Pressure profile

The assumed pressure profile in the vortex tube is shown in Figure 4.6. For a given cross section, the pressure is a linear function of r^2 (to be proved later in the chapter). Since the radial pressure profile is linked to the velocity profile, the pressure gradient is very strong in the entrance plane and slowly decreases to become almost constant at the hot end. The axial pressure profile is expected to drive the axial fluid velocity. According to this assumption, the pressure on the tube walls must decrease from the inlet plane to the hot end. On the centerline, the pressure has a maximum at the stagnation point, and minimums on the hot and cold ends.

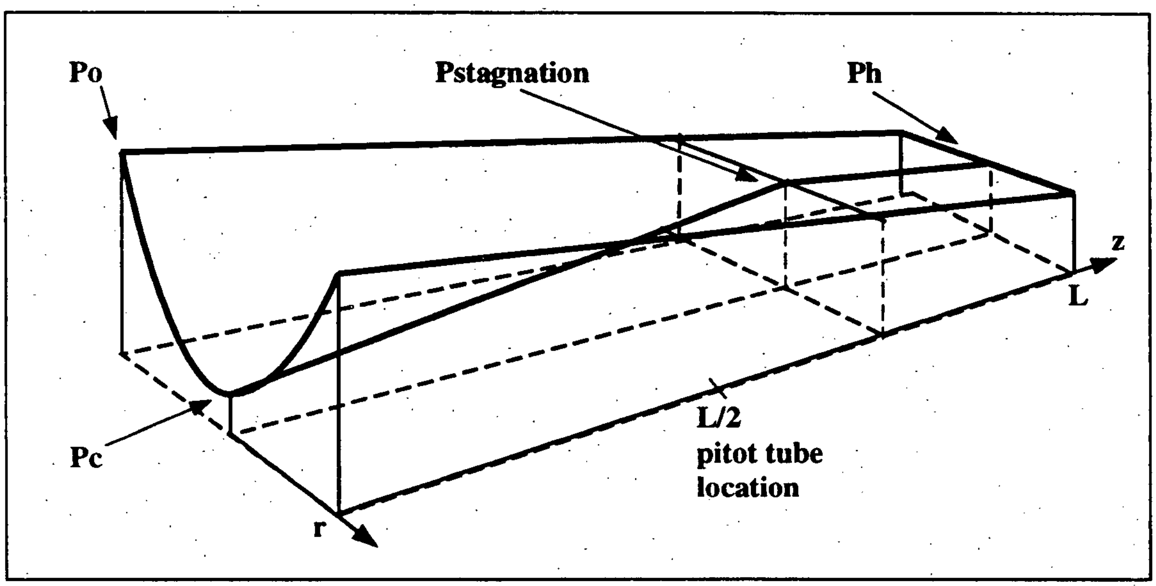

Figure 4.6: Pressure profile in the vortex tube

4.2 Flow analysis

With the flow structure described previously in mind, it is now possible to analyse the vortex tube. The following equations in chapter 4 and their derivation are based on Ahlborn's model (1994). In his model, Ahlborn developed three independent equations, i.e. radial dynamics, axial dynamics and energy balance. These equations were combined to obtain limits of temperature separation for the vortex tube. In the following sections in chapter 4, the model is checked against the new measurements.

Assumptions

Before starting to derive equations of Ahlborn's model, it is useful to summarize the assumptions used in his work. We assume a quasi stationary flow and neglect turbulence effects. The radial velocity u_r is then assumed to be small compare to u_z and u_ϕ. Viscous forces are assumed to be confined close to the stagnation surface and are neglected elsewhere. Therefore Euler equations (Navier Stokes equations without viscous terms) can be used in the analysis.

4.2.1 Radial dynamics

The radial dynamics can be described by the radial component of Euler equations written in cylindrical coordinates (Munson et al., 1990):

$$\rho u_r \frac{\partial u_r}{\partial r} + \rho u_z \frac{\partial u_r}{\partial z} - \frac{\rho u_\phi^2}{r} + \frac{\partial p}{\partial r} = 0 \tag{4.10}$$

It can be assumed that u_r is negligible compared to u_ϕ. The equation is then reduced to

$$\frac{\partial p}{\partial r} = \frac{\rho u_\phi^2}{r} \tag{4.11}$$

By assuming a forced-vortex velocity profile $u = u_o(r/R)$ it is possible to integrate the equation (4.11) and obtain the pressure profile. Inlet and cold pressure measurements can then be related to the inlet velocity. The pressures were measured at the inlet ($r = R$) and on the cold side ($r = R_c$). By integrating (4.11), we obtain:

$$p_o - p_c\big|_{z=0} = \frac{\rho' u_o^2}{2}\left(1 - \frac{R_c^2}{R^2}\right) \tag{4.12}$$

where $\rho' = \frac{1}{\pi R^2}\int_{R_c}^{R} \rho 2\pi r dr$ is an area-averaged density, which gives greater weight to the density at larger radii, so that $\rho' \approx \rho_o$. It is assumed that the pressure at $r = R_c$ (cold end radius) in the entrance plane is p_c. This should be reasonable since the cold end is very close to the entrance plane. Equation (4.12) can be expressed in a more useful form, by employing the Mach number relations:

$$u_o^2 = (M_o a_o)^2 = M_o^2 \gamma p_o / \rho_o \tag{4.13}$$

where a_o is the inlet speed of sound, M_o the inlet Mach number and γ is the specific heat ratio, and by defining a new dimensionless parameter

$$X = \frac{p_o - p_c}{p_o} \tag{4.14}$$

to obtain

$$X = \frac{p_o - p_c}{p_o} = \frac{\gamma}{2} M_o^2 \left(1 - \frac{R_c^2}{R^2}\right) \tag{4.15}$$

Since the Mach number and the parameter X can be directly calculated from the measurements, equation (4.15) can be checked against experiments. Figure 4.7a is a draft of M_o^2 vs. X and the line represents equation (4.15). With $R_c = 0.325$in. and $R = 1$in., which are the cold end radius and the tube radius of the vortex tube used in this experiments, equation (4.15) leads to $M_o^2 = 1.6(X)$.

It can be seen from Figure 4.7a that equation (4.15) is not fully confirmed by the new measurements. For each sets of plenum chamber pressures p_{pl}, the data approach the line $M_o^2 = 1.6(X)$ for the lowest Mach number of the set. The inlet Mach number has then some dependence on the parameter X. For a specific p_{pl}, the lowest Mach number will occur when $j_c/j_o = 1$, since in this situation the valve on the hot side is fully closed and the vortex tube offers more restriction to the flow. Similarly, the highest Mach number for a specific p_{pl} occurs when $j_c/j_o = 0$. From Figure 4.7a and the above discussion, we can therefore suspect that M_o will not only depend on X but also on the flow rate ratio j_c/j_o. By plotting M_o^2 / X vs. j_c / j_o in Figure 4.7b, we can see that all the data fall on the same line. This leads to the following empirical relation:

$$M_o^2 = X(2.55 - 1.26(j_c/j_o)) = 1.29X(1 + 0.98(j_h/j_o)) \tag{4.16}$$

Equation (4.16) describes adequately the relation between entrance velocity, pressures and flow rate ratio for the vortex tube used in the present experiments. Since equation (4.16) is an empirical relation, it would probably not hold for a different vortex tube. However, since the flow configuration is strongly dependent on the flow rate, it is probably true that for any vortex tubes the Mach number M_o will depend on both the parameter X and the flow rate ratio j_c/j_o. The formulation of a general equation valid for any vortex tube would probably require a full 3-D dynamics of the problem.

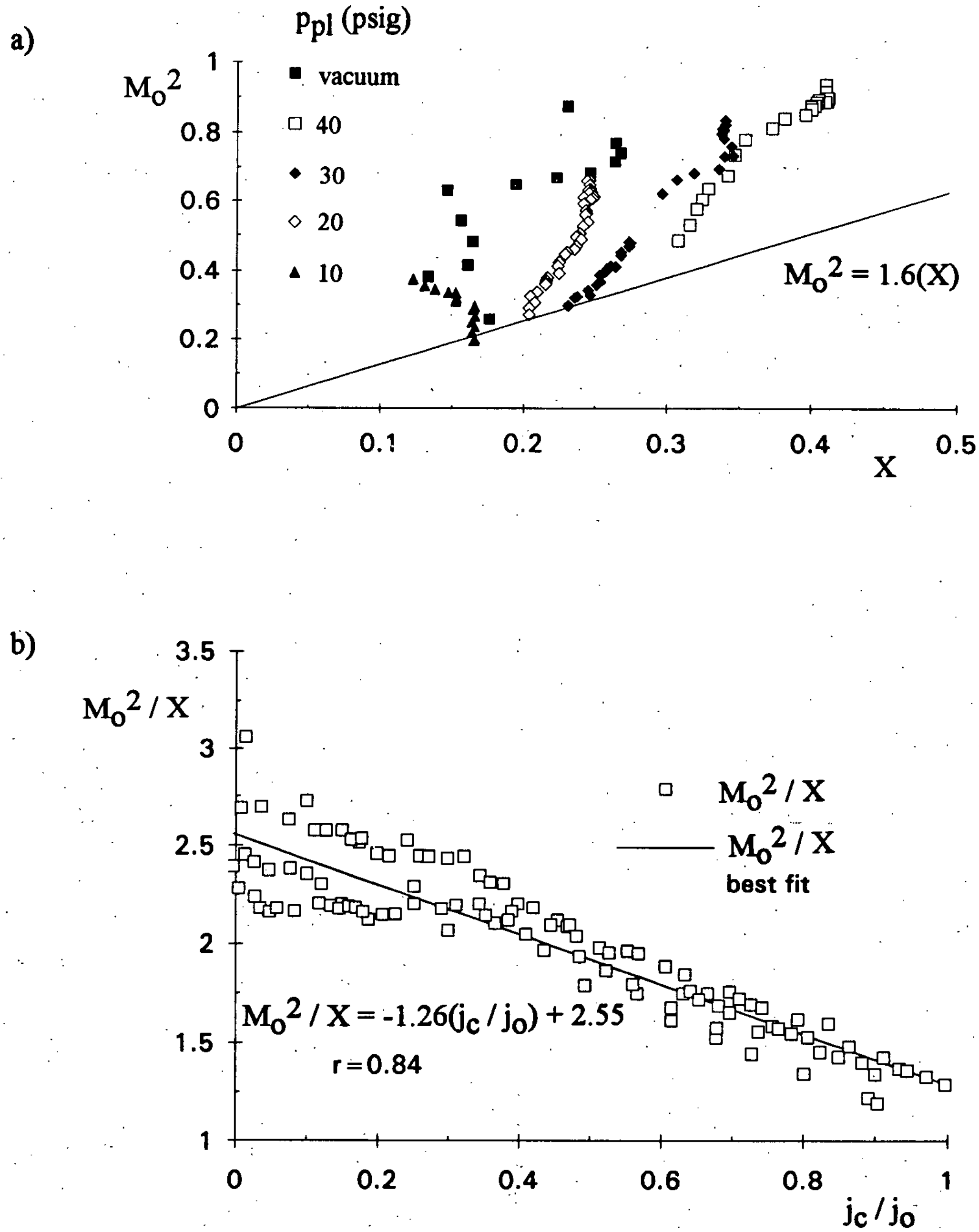

Figure 4.7: Radial dynamic a) M_o^2 vs. X b) M_o^2/X vs j_c/j_o with fitting function

According to equation (4.16) and Figure 4.7a, it seems possible to obtain supersonic velocities ($M_o > 1$) by increasing the parameter X or the plenum pressure p_{pl}. However, it is unlikely that supersonic velocities can be achieved in a vortex tube. Even if supersonic velocities were present, they would be restricted to a small volume around the entrance plane, as explained by Ahlborn et al. (1994). If a supersonic flow of gas was directed at the curved walls of the vortex tube, a sequence of oblique shocks would form. Behind this entrance discontinuity the speed would go down to subsonic values. In this case the radial dynamics in the entrance plane would be different and the present analysis would not hold. Indeed, in all the experiments the inlet velocity never exceeded Mach one. The tube would have to be tested at higher pressures to confirm the absence of supersonic velocities in vortex tubes. However, since supersonic velocities at the inlet would certainly require much higher pressures, this analysis is valid for most of the vortex tube operating conditions.

4.2.2 Axial dynamics

Ahlborn et al. (1994) assumed the velocity u_{cz} to be governed by the axial pressure drop $p_h - p_c$. Assuming a negligible velocity on the hot end, an incompressible gas and neglecting viscous forces, the Bernoulli equation can be written:

$$p_h - p_c = \frac{1}{2}\rho_c u_{cz}^2 = \frac{p_c}{2RT_c} u_{cz}^2 \tag{4.17}$$

Where R is the gas constant. The velocity can be related to the Mach number by the following relation:

$$u^2 = a^2 M^2 = \gamma RTM^2 \tag{4.18}$$

where γ is the specific heat ratio. Combing (4.18) into (4.17), we obtain

$$\frac{p_h}{p_c} = 1 + \frac{\gamma}{2} M_{cz}^2 \tag{4.19}$$

Since the cold flow Mach number M_{cz} as well as p_c and p_h have been measured, equation (4.19) can be checked against experiments. The relation is shown in Figure 4.8. The ratio of hot and cold pressure is 5 to 20% larger than the one predicted by equation (4.19). A too small escape velocity could imply that viscous forces cannot be neglected and that one should rather use the full Navier Stokes equation than the Bernoulli approximation.

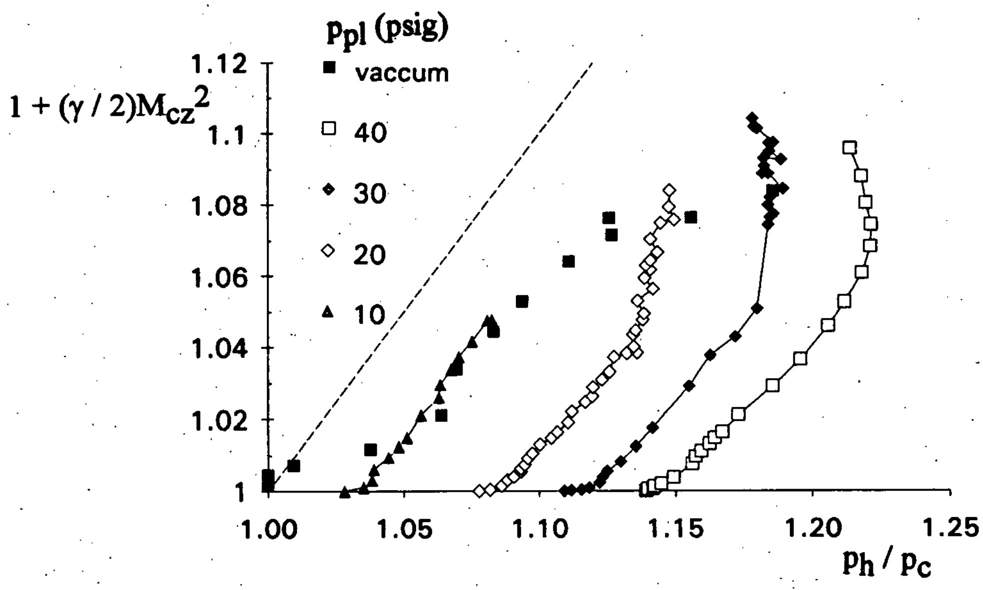

Figure 4.8: Axial dynamics relation. The straight line is the equation $p_h/p_c = 1 + (\gamma / 2)M_{cz}^2$.

4.3 Energy balance

In Ahlborn's model (1994), the radial and axial dynamics relations described above were combined with the energy balance equations to obtain the limits of temperature separation. In this section, the energy balance equations will be derived. They will also be used to check if any form of energy was gained or lost by the vortex tube. The limits of temperature separation will be derived in section 4.4.

The vortex tube can be considered as a system where the air is entering by the inlet and leaving by the cold and hot side (see Figure 4.9). One can look at the total energy balance, i.e. consider the whole tube as a control volume. The system could exchange heat Q_{out} with the outside through the tube walls. Energy Q_h in the form of heat or work can be exchanged between the hot annulus and the cold core. This internal heat exchange Q_h need not be considered for the total energy balance. Since the fluid separates in two streams with the stagnation area between them, the energy balance can also be made for each branch. In that case, the energy balance is made separately and the internal heat exchange Q_h between the two streams must be considered. In this section, the total energy balance and the balance for each branch will be analyzed.

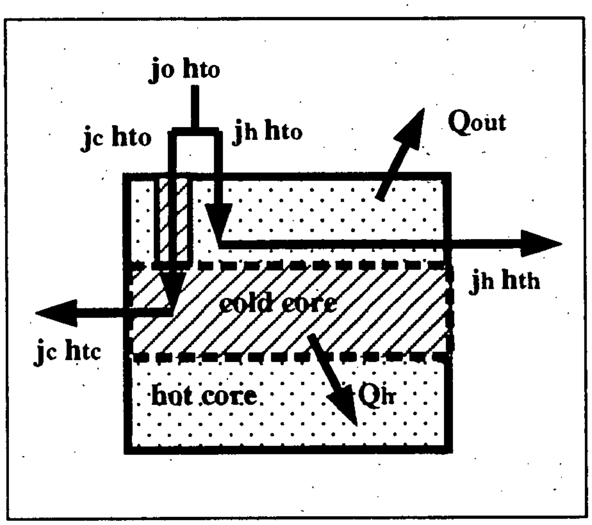

Figure 4.9: Control volume for energy balance. In the total energy balance, Q_h is not considered since it does not exit the control volume.

4.3.1 Total energy balance

By conservation of energy;

$$\text{Energy}_o = \text{Energy}_c + \text{Energy}_h + E_{out} \tag{4.20}$$

Where E_{out} is the energy that could be exchanged with the outside. E_{out} is positive if the heat is leaving the tube. For an open system (with a net flow rate through the system), it is more convenient to write a power equation

$$j_o(h_{to}) = j_c(h_{tc}) + j_h(h_{th}) + Q_{out} \tag{4.21}$$

where $h_t = h + u^2/2$ is the total enthalpy, h is the enthalpy and Q_{out} is the rate of energy losses in Watts. The energy in the vortex tube can be written as internal (related to the enthalpy h_o, h_h and h_c) and kinetic (velocity terms). Eq. (4.21) then becomes

$$j_o(h_o + u_o^2/2) = j_c(h_c + u_c^2/2) + j_h(h_h) + Q_{out} \tag{4.22}$$

where u_h was neglected since the experiments showed $u_h << u_o$ and $u_h << u_c$. The enthalpy can be related to the specific heat at constant pressure c_p and to the temperature T by

$$h = c_p T \tag{4.23}$$

By inserting (4.23) into (4.22) we get

$$j_o(c_p T_o + \frac{1}{2}u_o^2) = j_c(c_p T_c + \frac{1}{2}u_c^2) + j_h c_p T_h + Q_{out} \tag{4.24}$$

where $u_c^2 = u_{c\phi}^2 + u_{cz}^2$. All the parameters in this formula are known from the measurements except u_c and Q_{out}. From j_c, one can obtain u_{cz} but not u_c since the tangential component $u_{c\phi}$ is not known. However, by using the results from the velocity field measurements presented in section 4.1, it is possible to estimate $u_{c\phi}$.

Estimation of $u_{c\phi}$

In Figure 4.10, it is expected that fluid elements #1 which travelled far from the cold side and then went back will have conserved a bigger part of their angular momentum compared to the fluid element #2 which went directly on the cold side since they travelled on region with smaller pressure gradients and then smaller shear forces. Once these elements reach the tube center line, they can just be accelerated axially but cannot gain angular momentum. They can conserve or lose their angular momentum, depending on the strength of shear forces. By looking back at Figure 4.4, we can estimate the maximum tangential velocity in the back flow core near $R_C/R \approx 0.3$ at the location $z = L/2$ to be around 120 m/s. The average velocity in the back flow core at L/2 will give greater weight to velocity at larger radii and therefore the average velocity will be approximately 100 m/s. Since the back flow radius at the location $z = L/2$ is larger than the cold end radius, this tangential velocity could slightly increase. On the other hand it could decrease due to shear forces exerted between $z = L/2$ and $z = 0$. In the absence of a better knowledge, it is assumed in this work to be the same. This velocity was for an inlet velocity of 250 m/s. Therefore we assumed that

$$u_{c\phi} \approx 0.4u_o \tag{4.25}$$

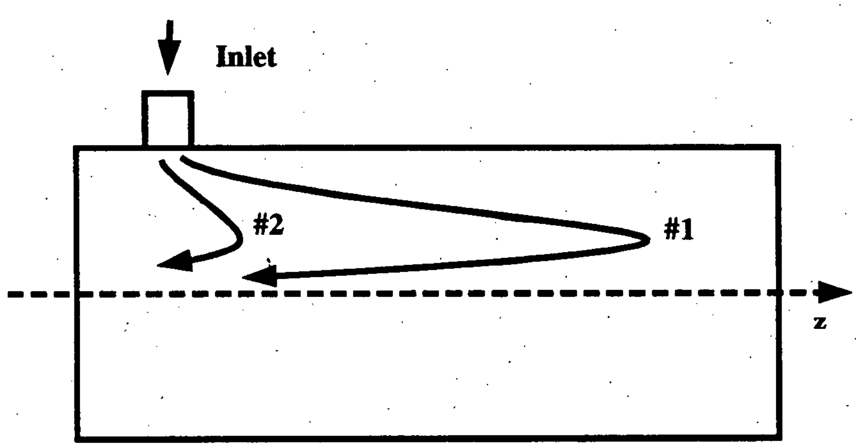

Figure 4.10: Fluid elements having different path in the vortex tube.

Net heat loss

With the assumption on the cold end velocity, the energy balance equation (4.24) contains only one unknown, namely Q_{out}. A value for Q_{out} can be calculated for any set of measured data. This has been done for all measured points and the results are given in Figure 4.11, where the net heat loss Q_{out} is plotted versus the flow rate ratio. For the standard vortex tube, Q_{out} increases with the inlet pressure. This is expected, since with an increase in the inlet pressure, the temperature gradients, the fluid velocity and the friction effects increase. The Q_{out} values for the low pressure vortex tube are similar to the standard vortex tube losses at 10 psig of operating pressure. This is reasonable since the temperature difference for the two operating conditions were similar.

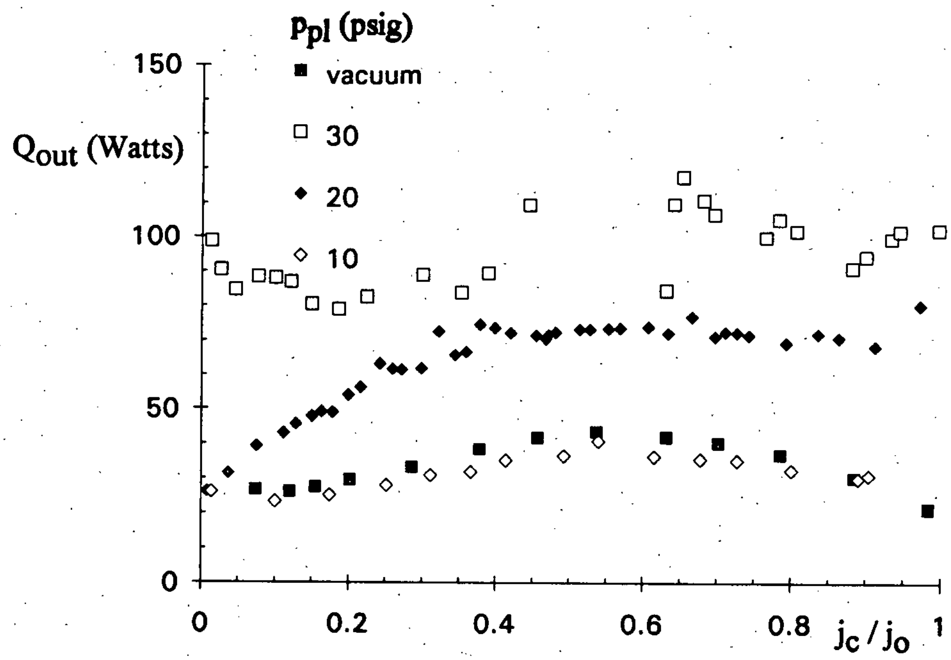

Figure 4.11: Heat exchanged by the tube walls versus the flow rate ratio. Heat going from the tube to the outside is considered positive.

The maximum value for Q_{out} is around 100 Watts. To check if this amount of heat can be exchanged with the surroundings, a simple heat transfer analysis was done (see appendix B). It was concluded that a temperature difference between the outside an the inside of the tube of no more than 1K could lead to 100 Watts of heat transferred. Therefore, even with the tube insulated, this transfer is possible.

It would be interesting to know what portion of the inlet energy the heat transferred by the walls represents. For a data point in the highest range of heat loss, with $p_{pl} = 30$ psig and $j_o = 0.012$ kg/s, Q_{out} is around 90 Watts (see Figure 4.11). The rate of inlet energy $j_o c_p T_{to} = j_o(c_p + (u_o^2)/2) = 3.5$ kW. Therefore Q_{out} is approximately 2.6% of the total inlet rate of energy. A comparison with the amount of inlet kinetic energy is more meaningful since most of the energy variation in the vortex tube are the order of magnitude of the kinetic energy. With $j_o = 0.012$ kg/s and $u_o = 292$ m/s, $j_o(u_o^2)/2 = 511.6$ W. Therefore Q_{out} is about 18% of the inlet kinetic energy.

Q_{out} depends on the assumptions concerning the velocity at the cold end. Therefore it is interesting to know how precise the heat transfer calculations are. In the calculations, $u_c = 0.4u_o$ was assumed. If instead the values $u_c = 0.6u_o$, $u_o = 292$ m/s and $j_o = 0.012$ kg/s had been taken, the change in the rate of kinetic energy would be $j_o((0.6u_o)^2 - (0.4u_o)^2)/2 = 102.3$ W which is about 3% of the total energy flow rate of 3.5kW but is 20% of the kinetic energy of the inlet flow 511.6 W. Therefore a slight change in the velocity calculations could change significantly the calculated heat loss. However the results presented in the next chapter on the efficiency of the vortex tube will show that the cold end velocity assumptions seems to be adequate.

4.3.2 Energy balance of the hot and cold core

As discussed previously, the fluid inside the vortex tube can be separated into two streams: the cold core and the hot shell. Since these two components are separated by the separatrix surface as indicated in Figure 4.1, it is interesting to do their energy balance separately and to see how much energy can be transferred from one core to the other.

In this analysis, the control volumes shown in Figure 4.9 are used. It is assumed that the fluid is separated into two streams right after the inlet. By analyzing the control volume we can write the two following equations:

(cold branch) $$j_c h_{to} = j_c h_{tc} + Q_h \tag{4.26}$$

(hot branch) $$j_h h_{to} = j_h h_{th} - Q_h + Q_{out} \tag{4.27}$$

These two equations can be rewritten in terms of the measured parameters:

(cold branch) $$j_c(c_p T_o + \frac{1}{2}u_o^2) = j_c(c_p T_c + \frac{1}{2}u_c^2) + Q_h \tag{4.28}$$

(hot branch) $$j_h(c_p T_o + \frac{1}{2}u_o^2) = j_h(c_p T_h) - Q_h + Q_{out} \tag{4.29}$$

Since Q_{out} is known from the previous calculations it is now possible to analyse the internal exchange of energy and to determine in particular the exchange of energy between each flow components. A plot of Q_h vs. j_c/j_o is shown in Figure 4.12. It should be noted that Q_h is always positive, which means that heat goes from the cold to the hot core. Q_h increases with increase in plenum pressure. Also, Q_h seems to be dependent of the flow rate ratio the same way the total temperature difference (T_{th} - T_{to}) is. It is interesting to note from equations (4.28) and (4.29) that $Q_h/(j_c c_p)$ is equal to the total temperature difference on the cold side while $Q_h/(j_h c_p)$ would be equal to the total temperature difference on the hot side if no heat was lost by the tube walls ($Q_{out} = 0$).

The internal heat transfer Q_h cannot be explained by the conversion of kinetic energy into heat and it certainly goes against the direction of regular thermal conduction where heat only flows from hot to cold. In the next chapter we will speculate on possible physical mechanisms that could be responsible for this strong flow of thermal energy.

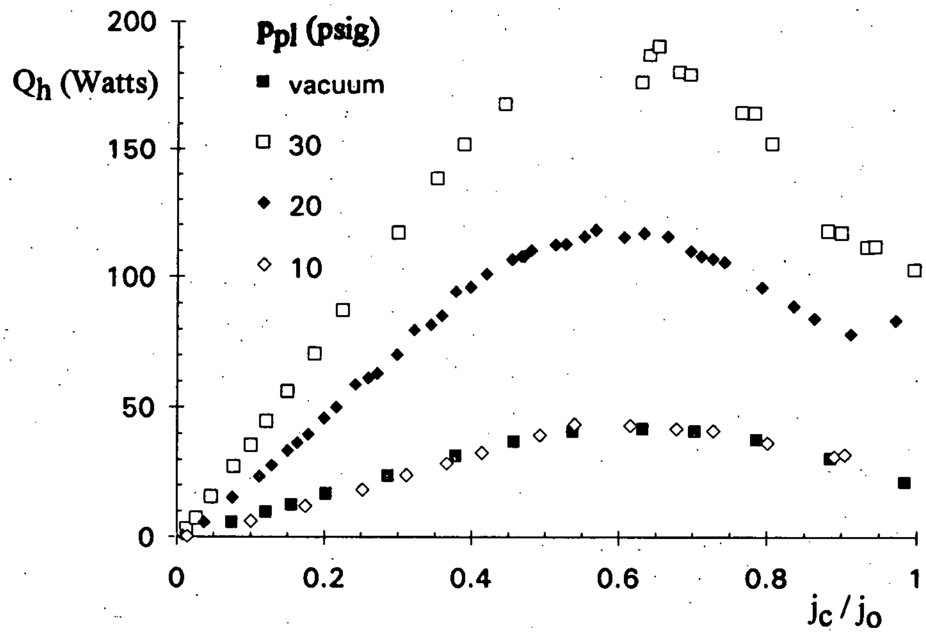

Figure 4.12: Heat exchanged between cold core and hot core. Heat going from the cold to the hot core is considered positive.

4.4 Limits of temperature separation in a vortex tube

Ahlborn et al. (1994) concluded that the heating and cooling in a vortex tube could be explained by conversion of kinetic energy into heat and by the reverse process respectively. From this concept one can derive relations predicting limits for the temperature separation in vortex tube which are based on the energy balance of each branches and the radial and axial dynamics relations discussed previously in the chapter.

Limit of temperature separation T_h - T_o

In Ahlborn's model (1994), the limit of temperature separation $T_h - T_o$ in the hot component was found by demanding the heat flux terms in equation 4.29 to be always positive ($-Q_h + Q_{out} > 0$). The following relations for the specific heat ratio and the kinetic energy terms were used:

$$c_p = \frac{\gamma R}{\gamma - 1} \tag{4.30}$$

$$\frac{u^2}{2} = \frac{a^2 M^2}{2} = \frac{\gamma R T M^2}{2} \tag{4.31}$$

where R is the gas constant. Then equation (4.29) leads to:

$$T_h - T_o \leq T_o\,((\gamma - 1)/2)\,M_o^2 \tag{4.32}$$

By combining (4.32) with the radial dynamic relation (4.15) and neglecting the term R_c^2/R^2 in (4.15), a temperature limit can be given for the hot flow component:

$$\frac{T_h - T_o}{T_o} \leq \left(\frac{\gamma - 1}{\gamma}\right)\frac{p_o - p_c}{p_o} = \left(\frac{\gamma - 1}{\gamma}\right)X \tag{4.33}$$

In Figure 4.13, the temperature separation from experiments and the limiting relation (4.33) are plotted. Almost all the data are exceeding the limit. As shown in section 4.2.1, the axial dynamics relation (4.15) is incorrect. An empirical relation (equation 4.16) including the flow rate ratio was found to be much more realistic. However, the major reason why the limits of temperature separation cannot hold is the assumption that heat transfer must always go from the hot to the cold component. By looking at Figures 4.10 and 4.11, one can see a large operation range where Q_h is larger than Q_{out}, so $(-Q_h + Q_{out} < 0)$. Therefore the inequality in equation (4.33) is not true anymore. Also, by assuming a completely insulated tube, Q_{out} would be negligible and the total heat transfer would always be from the cold to the hot component. It can then be concluded that the limit of temperature separation should not be strictly valid. It should be pointed out that in these experiments the ratio $(T_h - T_o)/T_o$ is much larger than in the experiments underlying Ahlborn's analysis. This comes about not because T_h is larger in the experiments reported here, but because T_o is smaller. In the present work, T_o was calculated from accurate measurements of the inlet pressure, while in the previous measurements T_o was assumed to be the room temperature.

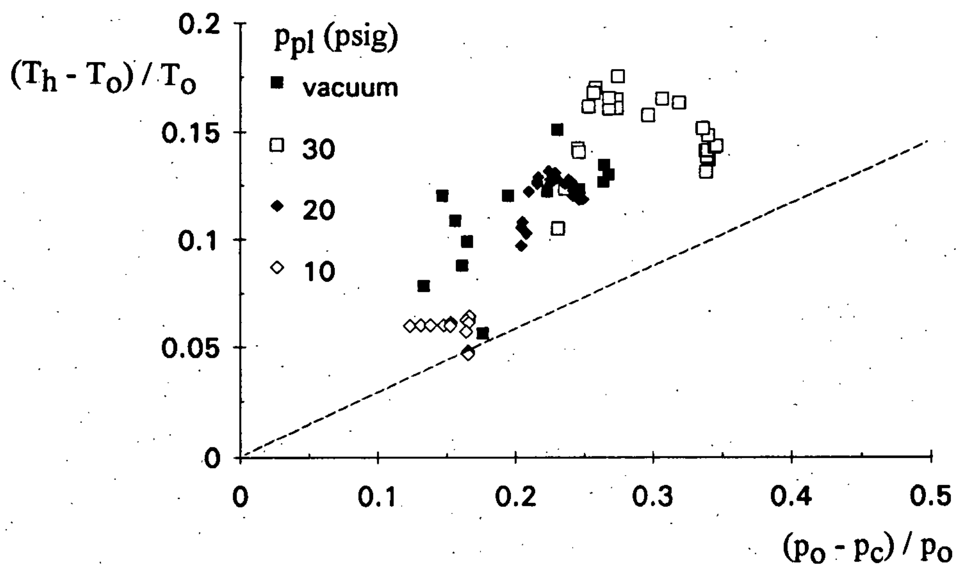

Figure 4.13: Limit of temperature separation $(T_h - T_o) / T_o$ in a vortex tube

Limit of temperature separation T_c - T_o

In Ahlborn's model (1994), a limit of temperature in the cold component was obtained by combining the energy balance (4.28) with axial dynamics relation (4.18). In the absence of a better knowledge, the tangential velocity $u_{c\phi}$ was assumed to be equal to u_o, such that

$$M_{cz}^2 = M_c^2 - M_{c\phi}^2 = M_c^2 - M_o^2 \tag{4.34}$$

Combining (4.28), (4.18) and (4.34), the following equation was obtained

$$\frac{T_o - T_c}{T_o} \leq \left(\frac{\gamma - 1}{\gamma}\right)\frac{p_h - p_c}{p_c} \tag{4.35}$$

This limit was considered to be an approximation due to the number of assumptions. The relation is plotted in Figure 4.14 with the new measurements. Again, there is a significant number of data points which violate the limit.

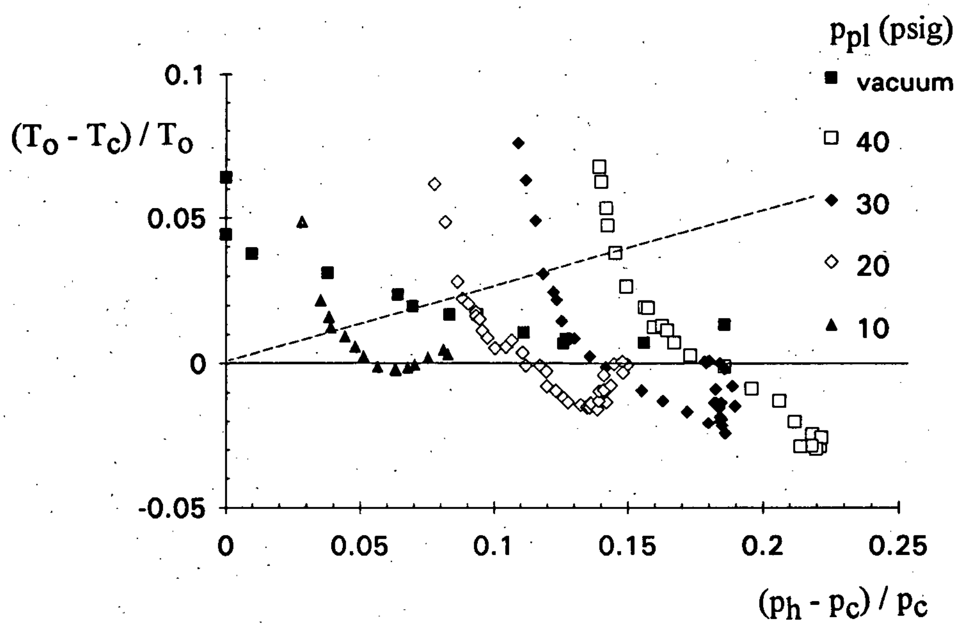

Figure 4.14: Limits of temperature $(T_o - T_c) / T_o$ in a vortex tube. The dashed line is the temperature limit predicted by eq. (4.35). All measured points should lie below the line.

Contribution of kinetic energy at the inlet

It would now be interesting to find the main reason why the new measurements disagree with the temperature limits predicted by Ahlborn's model. It was first noted that the dynamical equations of momentum balance in radial and axial directions (equation 4.15 and 4.19 respectively) do not quite agree with the new measurements. This might be reason enough to render the energy balance incorrect. However it is believed that these discrepancies are not the main cause of disagreement between the new measurements and Ahlborn's model. It will now be shown that the principal reason of discrepancy is the contribution of kinetic energy at the inlet.

In Ahlborn's model, the inlet temperature was assumed to be the room temperature (T_o = 293K) and the maximum inlet velocity u_o was considered to be around 100 m/s. By looking at the total temperature equation, we get:

$T_{to} = T_o + ((u_o)^2) / 2c_p = T_o + ((100 m/s)^2) / (2007 kJ/Kg K) = T_o + 5 K$

Again, T_{to} is called the total temperature at the inlet and is a measure of the total inlet energy, which is composed of a kinetic energy term represented by $(u_o)^2) / 2c_p$ and an internal energy term represented by the static temperature. For this range of kinetic energy the distinction between total and static temperature is not great since the kinematic component is only a small fraction of the total temperature (5/293 K =1.7%). Therefore there is no need to make a distinction between total and static temperature. Then the assumption T_o = 293K is adequate. However, in the present experiments the inlet velocities were reading values up to 311 m/s, which yields a kinematic component to the total temperature of about 48 K. Since the air in the plenum chamber had a low velocity and ambient temperature and the flow through the nozzle was considered to be adiabatic, the air temperature in the nozzle had to drop while the velocity was increasing.

Measurements of the inlet pressure and estimates of the heat transfer through the nozzle ring led to the conclusion that the heat transfer through the inlet nozzle must be negligible. Therefore the temperature could decrease considerably in the inlet nozzle. The magnitude of this heat transfer inside the nozzle was estimated as follows:

We assumed a temperature difference of 40K between the plenum chamber and the coldest part inside the nozzle, and estimated the heat flux through the nozzle. A net heat flux of about 1 Watt was obtained (see appendix B). In reality the maximum temperature difference between the outside and the inside of the nozzle measured in the present experiments was only 20K so the real heat flux should be below 1 Watt. This amount of heat flux is negligible compared to the convection flux of heat $j_o h_{to} \approx 1\text{kW}$ going through the nozzle. A heat flux of 1 Watt would correspond to an increase of temperature of about 1K. It can also be argued that the fluid going through the nozzle didn't have enough time to exchange energy with the nozzle walls, since the average traveling time through the nozzle was around 10^{-5} seconds. Furthermore, this decrease of temperature is consistent with the new pressure measurements in the throat of the nozzle (pressure and temperature are closely linked in high speed flow) and with the assumption of a maximum inlet velocity corresponding to Mach 1. If the temperature in the nozzle had been higher, the velocity in this work would have exceeded Mach 1. Therefore it can be concluded that the flow through the nozzle must be considered nearly adiabatic, so that a large decrease of temperature could be present.

In this work the inlet temperature was considered to be much lower than in Ahlborn's model (around 270 K compared to 290 K). With a lower inlet temperature, the ratios $(T_0-T_c)/T_0$ and $(T_h-T_0)/T_0$ are bigger than in Ahlborn's work. Due to the accurate pressure measurements close to the inlet, the present results are believed to be right. This difference in the inlet temperature is due to the underestimation of the inlet velocity in Ahlborn's model.

Temperature separation versus total temperature separation

In Ahlborn's model, the heating is attributed to the conversion of kinetic energy into heat and the cooling to the reverse process. This can be easily seen in equation (4.32), where the temperature difference T_h - T_0 is related to the square of the Mach number M_0^2. The cooling effect was attributed to an increase of kinetic energy on the cold side, which produced a decrease in temperature. The hot shell and the cold core of the vortex tube were supposed to act independently and no form of heat or energy needed to be exchanged between them. As a result, the heat exchange Q_h was neglected in equation (4.28) to obtain the limit of temperature separation $(T_0 - T_c)$.

However, the new measurements have shown (see Figure 4.12) that a net heat flow from the cold to the hot side is present. With this heat exchange, the fluid in the cold core exits the tube with a lower energy than the fluid on the hot side. The vortex tube effect therefore produce an energy separation between the two branch of the flow instead of a temperature conversion in each branch. Since the energy of the fluid is fully described by its total temperature, we can say that the vortex tube effect (or Ranque-Hilsch effect) is in fact a total temperature separation or energy separation, and cannot be fully explained by the local conversion of kinetic energy into heat.

This concludes the verifications of the relations from Ahlborn's model. The new work reported in this chapter revealed that a heat flow going from the cold core to the hot shell is present in the vortex tube. It was also found that the limits of temperature separation predicted by Ahlborn were exceeded by the new measurements. This discrepancy was attributed to the fact that the inlet temperature derived from the new measurements of inlet pressure was much lower than in the data used by Ahlborn. Similarly, the new measurements led to a difference in the calculated inlet velocities between this work and data from Ahlborn et al. (1994). In Ahlborn's work, the inlet velocity was underestimated. The vortex tube effect was finally described as a total temperature separation (or energy separation) instead of a system that changes kinetic energy into thermal energy (static temperature separation). Again, it should be clear that the terms energy separation and total temperature separation are similar and describe the same phenomena. In the next chapter, explanations of the energy separation will be presented.

5 - Energy separation mechanisms

As shown in the energy balance of the previous section, there is a net energy separation in the vortex tube. It was also shown that a certain amount of heat was transferred from the cold core to the outer hot flow. This energy flux is quite unusual since normal thermal conduction would go in the opposite direction, namely from the hot to the cold regime. However, the vortex tube is not the only device which separates the energy of a fluid flow. By comparison to other flow fields, we can obtain a better understanding of the Ranque-Hilsch vortex tube effect. In this chapter, different flows with an energy separation will be described. A simple model which can help to understand how heat could be transferred from the cold core to the hot shell is also presented. Using this model, an approximate limit of total temperature separation will be derived. Again, it should be clear from the previous chapter that the terms energy separation and total temperature separation are similar and describe the same phenomena. Finally, some comments about energy separation by sound waves will be made.

5.1 Different flows having an energy separation

In the steady flow of a fluid without viscosity and thermal conductivity there is obviously no possibility for an energy transfer from one stream to another since the pressure forces can deliver no work and no heat can be transferred by conduction. Consequently, the total energy or total temperature remains essentially constant if initially constant. However, when viscosity and heat conduction are present, heat can be transferred even when there is no energy flow through the system. This effect will now be described by first looking at a purely axial laminar flow (Poiseuille flow), then by considering a purely rotational flow and third by a combination of an axial and a rotational flow.

Laminar flow in a tube: Poiseuille flow

The total temperature distribution for a laminar fluid flow in a circular tube (see Figure 5.1a) with adiabatic walls may be obtained by the solution of the energy equation (Harnett and Eckert, 1957):

$$\rho c_p u \frac{\partial T}{\partial z} = \frac{k}{r}\frac{\partial}{\partial r}\left(r\frac{\partial T}{\partial r}\right) + \mu\left(\frac{\partial^2 u}{\partial r^2}\right) \tag{5.1}$$

where c_p is the specific heat at constant pressure, k is the thermal conductivity, μ is the viscosity, all assumed to be independent of the temperature and $u = (u_Z, u_r, u_\phi)$. This equation assumes the axial velocity to be constant along z (z is the tube axis). The term on the left side correspond to the change of internal energy. The first term on the right side correspond to energy transfer by thermal conduction, while the last one is the viscous dissipation per unit of volume. If the gradient of velocity is constant (as in a forced vortex), the second term on the right side is zero.

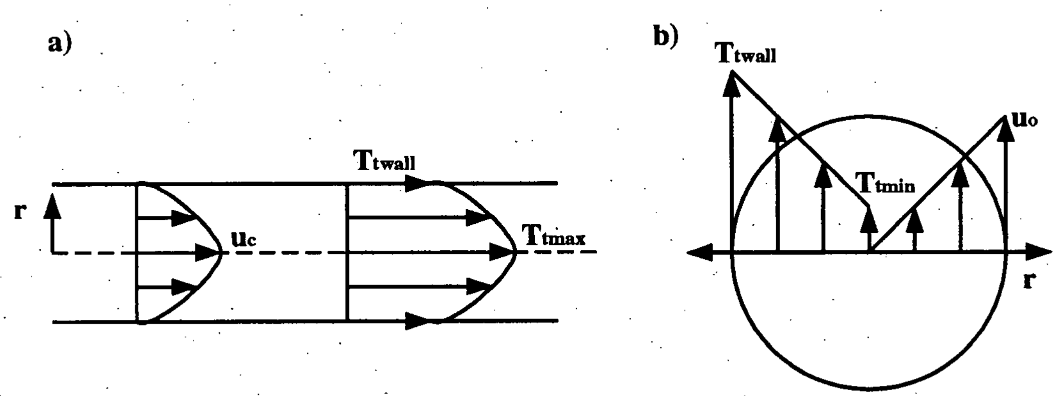

Figure 5.1: a) Poiseuille flow; b) solid-body rotation

If the velocity profile is known, equation (5.1) is reduced to a function T(r). For a purely axial laminar flow (Poiseuille flow), equation (5.1) can be solved assuming a parabolic velocity distribution:

$$u_z(r) = u_c(1 - (r/R)^2) \tag{5.2}$$

where u_c is the axial velocity at r = 0 and R is the radius at the tube walls. The results can be given in terms of the center axial velocity u_c (Harnett and Eckert, 1957):

$$\frac{T_t - T_{twall}}{u_c^2/2c_p} = (1 - Pr)\left[1 - (r/R)^2\right]^2 \tag{5.3}$$

where $Pr = \mu c_p/k$ is the Prandtl number. The total temperature T_t is defined in equation (3.1). For Pr = 1, the total temperature is constant across the tube. For air, Pr = 0.7, and the total temperature in the center of the tube is then higher than on the tube walls. This result implies that energy dissipated by viscosity is mainly transported to the tube walls where presumably no heat sink (in form of heat conduction to the walls) exists. Therefore a laminar axial flow in a tube can have a total temperature separation (or energy separation), where the total temperature in the center of the tube will be higher than on the tube walls.

Solid-body rotation

A simple example of a rotating flow having energy separation is the laminar solid-body rotation (see Figure 5.1b). A solid-body rotation is the motion of a forced vortex and is expressed by $u(r) = u_o(r / R)$.

A solid-body motion has no shearing stresses, since du/dr is constant. Also, if no variation in the axial direction is assumed, equation (5.1) becomes:

$$\frac{\partial}{\partial r}\left(r\frac{\partial T}{\partial r}\right)=0 \tag{5.4}$$

By imposing the following boundary conditions:

$$\begin{aligned} T &= T_{wall} && \text{at } r = R \\ \partial T/\partial r &= 0 && \text{at } r = 0 \end{aligned} \tag{5.5}$$

it is found that $T = T_{wall}$ everywhere in the flow. Since there is no static temperature gradient in the flow, no heat can flow across the walls. The resulting total temperature separation can be written as

$$\frac{T_{twall}-T_t}{u_o^2/2c_p}=1-(r/R)^2 \tag{5.6}$$

The total temperature separation (or energy separation) will then be dependent of the inlet velocity. Also, the energy separation is independent of the Prandtl number. Here, the lowest total temperature is in the center of the flow ($r = 0$), as in the vortex tube.

Comparison to the vortex tube: Poiseuille flow with rotation superimposed

Harnett and Eckert (1957) studied the superposition of the two flows presented previously. The final solution of their analysis was the following temperature distribution:

$$\frac{T_t-T_{twall}}{u_c^2/2c_p}=\left[1-\Pr\left[1-\left(r/R\right)^2\right]^2-\left(u_o/u_c\right)^2\left[1-\left(r/R\right)^2\right]\right] \tag{5.7}$$

Again u_o represents the maximum tangential velocity and u_c represents the maximum axial velocity. As for the solid-body rotation, an increase in the inlet tangential velocity u_o will cause a greater energy separation where the minimum total temperature is in the center. However, due to the axial motion, which creates a high total temperature in the center, the axial component of velocity u_c prevents this separation from ever reaching the value obtainable with a pure solid-body rotation.

This simple model has some interesting correspondences with the vortex tube, where the flow has rotational and axial velocity components. As in the vortex tube, an increase in the inlet velocity will increase the total temperature separation. Also, the solid body rotation has similarities with the forced vortex located in the entrance plane of the vortex tube. Furthermore, the lowest total temperature is at $r = 0$ in both situations. However, these equations represent laminar flow while the vortex tube is expected to have some turbulence (Harnett and Eckert, 1957). Using the solid-body rotation model with a turbulent vortex, Harnett and Eckert (1957) developed the following relation for the maximum total temperature difference in a turbulent solid-body rotation :

$$\frac{T_{twall} - T_t}{u_o^2/2c_p} = 2 \tag{5.8}$$

This relation could be seen as the limit of cold temperature difference in the vortex tube, since it is believed that any motion degrading the solid-body rotation will decrease the energy separation. In chapter 4, it was assumed that the inlet velocity could not go higher than Mach 1. With a total inlet temperature of 295 K, the required velocity for Mach 1 is about 315 m/s and the static temperature at the inlet would drop to 246 K (using equation 3.1). The maximum total temperature separation from equation (5.8) would then be 99 K.

Since a total separation of 99 K was never obtained in vortex tube experiments, it is interesting to ask if the solid-body rotation represents adequately the vortex tube flow. In a real vortex tube, the axial motion is bi-directional, i.e. there is a flow near the axis streaming towards the cold end and an annulus of flow going towards the hot end. Furthermore, the pure solid-body rotation is only present in the entrance plane and becomes a Rankine type vortex closer to the hot side.

Above all, the presence of a solid-body rotation seems to contradict the energy conservation principle, since there is no process by which the heat taken from the cold core can be transferred to the hot core. Considering an hypothetical vortex tube with a solid-body rotation everywhere, the total temperature at the walls would be close to the inlet total temperature and the energy separation would be given by equation (5.8). However, if the center of the tube loses energy, the outer flow needs to increase its total temperature to satisfy the conservation of energy. If the solid-body motion was obtained by rotating the tube walls and if there was no tangential flow through the tube, then the total temperature at the walls could increase so that the conservation of energy would be satisfied. However, in the entrance plane of the vortex tube the total temperature at the walls has to match the inlet total temperature. The solid-body rotation model would then lead to a cooling in the center but no heating in the outer fluid. This violates the conservation of energy principle. We can therefore state that the solid-body rotation model cannot be used to model adequately the vortex tube.

However, these model considerations lead to several interesting conclusions:

1 The solid-body rotation model shows the importance of the vortex structure on the energy separation.

2 Since the solid-body rotation is initiated by the inlet flow, the inlet nozzle becomes an important part of the apparatus (refer to Figure 2.4).

3 The presence of a quasi solid-body rotation is one cause of the vortex tube effect.

4 The axial fluid motion would tend to decrease the vortex tube effect.

5.2 Paddle wheel model

The solid-body rotation model described in the previous section illustrated the importance of high inlet velocities for energy separation. However the pure solid-body rotation differs considerably from the vortex tube flow structure described previously in the thesis. It would be interesting to develop a model with two separate streams (the cold core and the hot shell) that could mutually exchange heat and thereby produce an energy separation. Such a model will be presented in this section.

The following model should help to understand the energy separation process. As shown in chapter 4, the flow coming from the inlet going to the cold end of the vortex tube will experience a pressure drop. The expansion (or pressure drop) in the cold core can be compared to the expansion in a turbine, as shown in Figure 5.2a. The turbine, representing the cold core process, generates rotational mechanical energy out of a swirling flow as well as out of axial motion. This mechanical energy is in the form of work but could also represent the heat exchange Q_h flowing from the cold core to the hot shell as calculated in section 4.3. This work can be transmitted by a shaft to a paddle wheel which can dissipate the received energy into heat. The paddle wheel represents the process in the hot shell. The mechanical connection between the turbine and the paddle wheel, i.e. the shaft, would represent the fluid volume between the two streams in the vortex tube: the separatrix. In a real vortex tube, viscosity would provide the coupling between the turbine and the paddle wheel. This friction coupling between the two flow components would generate an additional amount of heat, which could partly flow back into the cold core by thermal conduction. Therefore the energy separation process pictured by the turbine-paddle wheel model would somehow overestimate the vortex tube capability to move energy from the cold to the hot stream.

In the paddle wheel model, the turbine will generate some work W. Since only the ratio j_c/j_o of the total fluid will contribute to work in the turbine, the work done will be described by

$$W = j_c\,(h_{to} - h_{tc}) = (j_c / c_p)(T_{to} - T_{tc}) \qquad (5.9)$$

This work is then converted into heat by the paddle wheel. Since equation (5.9) is identical to equation (4.25), except for the parameter Q_h now replaced by W, what was assumed to be a heat transfer in section (4.3.2) can be identified here to be the work done by the cold core on the hot shell.

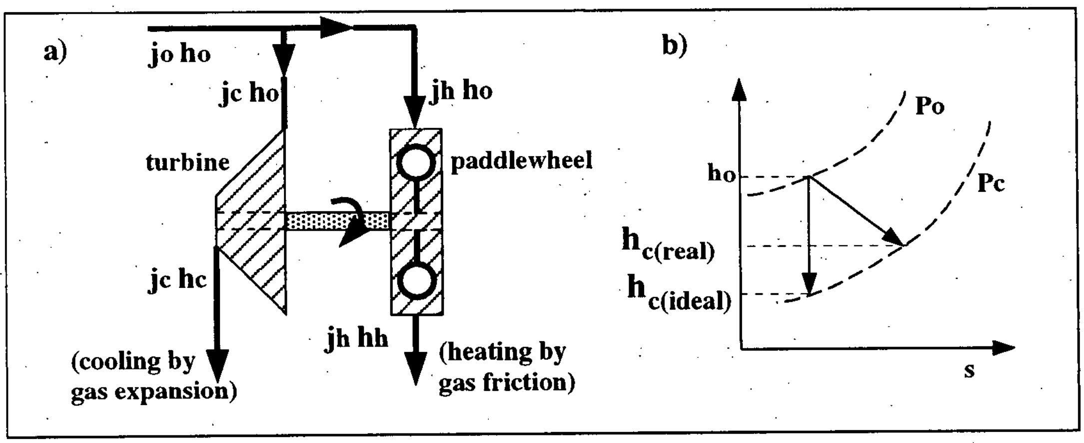

Figure 5.2: a)the paddle wheel model; b)the turbine expansion

The expansion process in the paddle wheel model is pictured in Figure 5.2b. Due to irreversibilities, the vortex tube (or turbine) expansion differs from an ideal process where the entropy s would be constant. The entropy of the cold gas s_c will then be larger than the entropy of the inlet gas s_o. According to the paddle wheel model and Figure 5.2b, it can now be inferred that a minimum total temperature would be obtained on the cold side of the vortex tube when the expansion process would approach an ideal process. Since processes in turbines are often characterized by their efficiency, it will be interesting to find an efficiency for the vortex tube process and then try to obtain a limit of total temperature separation.

5.2.1 Vortex tube efficiency

An ideal turbine expansion would be isentropic and the cold temperature obtained by the process could be expressed by the standard equation for isentropic expansion (Munson et al., 1990):

$$T_c\big|_{\text{isentropic}} = T_o(p_c/p_o)^{(\gamma-1)/\gamma} \tag{5.10}$$

where γ is the specific heat ratio. Since we are dealing with high speed flow, we can assign to the vortex tube expansion a turbine energy efficiency η_{turb} (Munson et al., 1990) that will include kinetic terms and that can be defined by

η_{turb} = (energy exchanged per unit of mass) / (maximum expansion work per unit of mass)

η_{turb} can also be described by the following equation (Munson et al., 1990):

$$\eta_{turb} = \frac{h_{to} - h_{tc}}{h_{to} - h_{tc(ideal)}} = \left(T_{to} - T_{tc}\right) \Bigg/ \left[T_o\left[1 - \left(\frac{p_c}{p_o}\right)^{\gamma-1/\gamma}\right] + \frac{u_o^2}{2c_p} - \frac{u_c^2}{2c_p}\right] \tag{5.11}$$

The right hand side of equation (5.11) contains parameters which were experimentally determined. Therefore equation (5.11) can be used to calculate η_{turb} for each operation point. This is done in Figure 5.3a. As expected, the efficiency is always smaller than 1. The turbine efficiency has a maximum at j_c/j_o = 0.5. The maximum efficiency occurs approximately when the total temperature separation on the cold side is a maximum. In the total temperature separation curves presented in chapter 3 (Figure 3.1, Figure 3.2), the minimums T_{tc} - T_{to} shift slightly toward $j_c/j_o = 1$ with a decrease in inlet pressure. However, the maximum efficiency location in Figure 5.3a seems to be independent of the inlet pressure. It should also be noted that η_{turb} appears to have a finite value for $j_c / j_o = 0$.

The turbine energy efficiency η_{turb} can be used to describe the expansion in the cold core but does not describe the efficiency of the vortex tube for cooling gases. In order to obtain the efficiency of cooling a gas flow, the flow rate ratio j_c/j_o has to be taken into account. A vortex tube cooling power efficiency η_c (Hilsch, 1948) is then defined by

$$\eta_c = \left(\frac{j_c}{j_o}\right)\eta_{turb} = (j_c/j_o)(T_{to} - T_{tc}) \Bigg/ \left[T_o\left[1-\left(\frac{p_c}{p_o}\right)^{\gamma-1/\gamma}\right] + \frac{u_o^2}{2c_p} - \frac{u_c^2}{2c_p}\right] \tag{5.12}$$

and takes into account the amount of fluid coming out of the cold side. Again, all quantities on the right hand side of equation (5.12) were measured in the present work. The cooling efficiency is presented in Figure 5.3b. Compare to the turbine energy efficiency η_{turb} in Figure 5.3a, the maximum of this curve is shifted to larger flow rate ratios and η_c is zero for $j_c/j_o = 0$. It is interesting to note from Figure 5.3b that the best range of operation for using the vortex tube as a cooling device would not be when the minimum temperature is obtained, since then only little cold gas comes out of the tube, but rather for $j_c/j_o \approx 2/3$ where plenty of cold gas flow through the tube (albeit a moderate temperature increase).

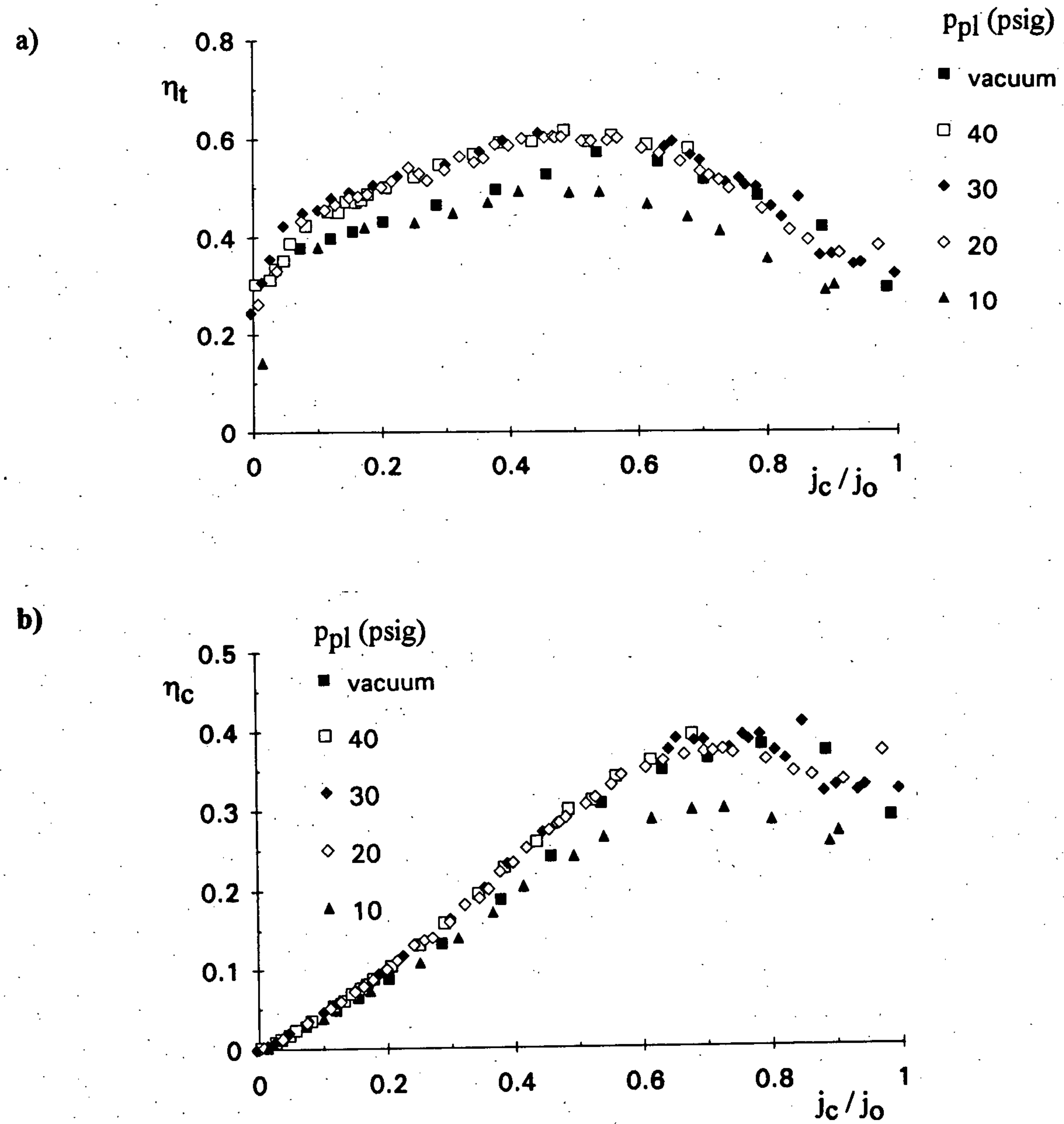

Figure 5.3: a) turbine energy efficiency; b) cooling power efficiency

5.2.2 New limits of total temperature separation

The paddle wheel model described above attributed the cooling effect in the vortex tube to an expansion from the inlet to the cold end. By combining the corrected radial dynamics equation (4.16) with the efficiency equation (5.11), it is possible to obtain new limits of total temperature separation. To this end, we first have to find out what the efficiency η_{turb} will be for the process giving the maximum total temperature separation. At first sight, the maximum cooling effect should occur if the expansion in the cold core was isentropic. Then, the turbine energy efficiency would be $\eta_{turb} = 1$. However, one has to take into account what makes the energy separation happen. As explained in the beginning of the chapter, viscosity and heat conduction have to be present to get a total temperature separation. When $\eta_{turb} = 1$, the process is supposed to be isentropic, which means no heat transfer or friction can occur. Under these conditions, no energy separation can be present. Therefore the maximum cooling effect of an ideal vortex tube could not be at an energy efficiency $\eta_{turb} = 1$.

This distinction between operation at maximum efficiency and at maximum power transfer (or energy transfer) is present in many thermodynamic cycles. For example, heat engines with external heat sources generally have an efficiency η_{mp} at which the power output is maximized. η_{mp} is always smaller than the Carnot efficiency $\eta_{Car} = 1 - T_c/T_h$ because a fraction δT of the temperature difference is used to drive the heat into and out the engine through the process of thermal conduction. The energy transferred per cycle by conduction increases with δT, however only the remaining temperature difference $T_h - T_c - \delta T$ is available to generate work. Since the work which is produced cannot exceed the amount of energy which can be transferred by conduction a maximum power exists at which the efficiency has the value $\eta_{mp} = 1\text{-}(T_h - T_c)^{1/2}$ (Curzon and Ahlborn, 1975, also Novikov, I.I., 1958). In the example presented above, the amount of work that can be generated is limited by the temperature difference. In the vortex tube, the work is generated by the expansion. This work has to be transferred by friction, which is an irreversible process. Therefore, an increase in the work produced will increase the irreversibilities and thereby decrease the efficiency. The maximum efficiency occurs when no work is generated. In the vortex tube, the efficiency η_{turb} will be maximum when there is no fluid motion.

In Figure 5.3a, the efficiency η_{turb} seems to be independent of the inlet pressure. If this efficiency is constant over a large range of inlet pressures, then the maximum efficiency in Figure 5.3a could be the maximum operating efficiency in a vortex tube. At $j_c/j_o = 0.4$, $\eta_{turb} = 0.6$, which seems to be the maximum efficiency. Using this value into equation (5.11), we obtain

$$T_{to} - T_{tc}\Big|_{max} = (0.6)\left[T_o\left[1-(p_c/p_o)^{(\gamma-1)/\gamma}\right] + u_o^2/2c_p - u_c^2/2c_p\right] \tag{5.13}$$

As in chapter 4, we can assume the maximum possible inlet velocity to be the sound speed ($M_o = 1$). From equation (4.16), we can then obtain the maximum pressure ratio:

$$(p_c/p_o)\Big|_{min} = 1 - X_{max} = 1 - M_o^2/(2.55 - 1.26(j_c/j_o)) = 1 - 1/(2.55 - 1.26(0.4)) \approx 0.5 \tag{5.14}$$

In equation (5.13) we can neglect u_c^2 since using equation (4.24) $u_c^2 \approx (0.16)u_o^2 < u_o$. Using this approximation, combining (5.14) and (5.13), using (4.30) and (4.31) for the Mach number relations and taking $\gamma = 1.4$ for air, we obtain

$$\left.\frac{T_{to} - T_{tc}}{T_o}\right|_{max} \approx (0.6)\left[1-(0.5)^{(\gamma-1)/\gamma} + M_o^2(\gamma-1)/2\right] \approx (0.6)\left[1-(0.5)^{0.286} + (0.4)/2\right] \approx 0.23 \tag{5.15}$$

The last equation gives a limit of total temperature separation for the vortex tube used in the present work. Since empirical relations have been used to obtain the limit, it could possibly not be valid for other vortex tubes.

It would now be interesting to estimate what range of total temperature separation can be obtained with this limit. With an inlet total temperature of 290 K and M_o=1, T_o would go down to about 250 K. Entering this value into (5.15), one finds $(T_{to} - T_{tc})_{max}$ = 57 K. To our knowledge, there is no data in the literature exceeding this limit. The maximum total temperature found in the literature was 47 K by Negm (1988).

The same procedure can be used to derive a limit of total temperature for the hot end T_{th} - T_{to}. On the hot side, the maximum total temperature difference is found at about $j_c/j_o \approx 0.8$ (see Figure 3.2). In Figure 5.3a, the turbine efficiency at this flow rate ratio is $\eta_{turb} \approx 0.5$. In an optimized vortex tube, we can again assume the maximum inlet Mach number to be 1. With these values, the pressure ratio in equation (5.14), will then become $(p_c/p_o)_{min} \approx 0.65$. Using equation (5.15), with the last assumptions, we obtain

$$\left(\frac{T_{to} - T_{tc}}{T_o}\right)_{j_c/j_o=0.8} = 0.5\left(1-(0.65)^{0.286} + M_o^2(\gamma-1)/2\right) \approx 0.16 \qquad (5.16)$$

The last equation gives the total temperature separation $(T_{to} - T_{tc})$ when $(T_{th} - T_{to})$ is optimized. The energy balance equations (4.28) and (4.29) can be used to relate the two total temperature separations if an optimized vortex tube is assumed to have no heat conduction through the walls (Q_{out} = 0). Then, combining (4.28) and (4.29) we obtain

$$T_{th} - T_{to} = (j_c/j_h)[T_{to} - T_{tc}] = \frac{j_c/j_o}{1-(j_c/j_o)}[T_{to} - T_{tc}] \qquad (5.17)$$

The estimates from equation (5.16) can now be used into (5.17) to obtain the total temperature separation on the hot end $(T_{th} - T_{to})$:

$$\left.\frac{T_{th} - T_{to}}{T_o}\right|_{max} = \left[\frac{j_c/j_o}{1-(j_c/j_o)}\left(\frac{T_{to} - T_{tc}}{T_o}\right)\right]_{j_c/j_o=0.8} \approx \frac{0.8}{0.2}(0.16) \approx 0.64 \qquad (5.18)$$

With an inlet total temperature of 290 K and M_o=1, T_o would go down to about 250 K and therefore $(T_{th} - T_{to})_{max}$ = 158 K. For the same inlet condition, the limit predicts a higher energy separation for the hot end than for the cold end, which does not seem to respect the energy conservation principle. However the limit for the hot end is reached when only 20% of the inlet gas exits by the hot end (j_c/j_o = 0.8) while the limit on the cold end is reached when 60% of the gas exits by the cold end (j_c/j_o= 0.6). This difference in the amount of fluid cooled or heated explains the difference in total temperature separation for the two limits.

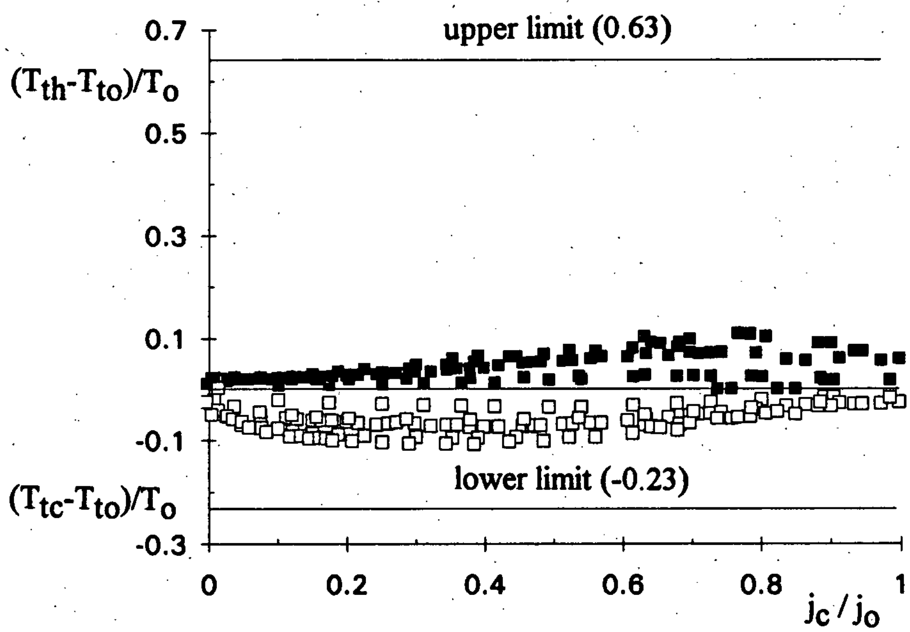

Figure 5.4: New limits of total temperature separation

In Figure 5.4 the new limits are compared to the data taken in the present work. All the data fall within the limits. The total temperature difference for the hot side is far from reaching the limit. This can be explained by the heat transferred along the tube walls. With a completely insulated tube build with a material having a low thermal conductivity, the temperature difference on the hot side would have been higher. It should also be pointed out that the inlet pressures in this work were not very high. In many researches (Stephan, 1982, Negm, 1988), the vortex tube was tested with pressure ratios p_{pl}/p_c going up to 5. For these experiments the temperature $T_{tc(min)}$ and $T_{th(max)}$ were -25 °C and 80 °C respectively. Since the maximum total temperature differences obtained in the present work were much lower (refer to Figure 3.2), the measured total temperatures could well be far from the limits.

It should be remembered again that the limits derived above may not be valid for every vortex tubes since empirical relations from the present experiments were used to derive them. However, to our knowledge, these limits are not exceeded by any experiments.

5.2.3 Cooling power efficiency

The limits derived above can give some descriptions of the operation of a vortex tube. If one wants to use the vortex tube in a cooling system, the cooling effect has to be described not only by a minimum temperature obtained but also by a cooling power efficiency, as shown in Figure 5.3b. From this figure, we can find that the maximum cooling power efficiency is for a flow rate ratio $j_c/j_o = 0.7$ and

$$\eta_{c(max)} = (j_c/j_o)\eta_{turb} = (0.7)(0.6) = 42\% \qquad (5.19)$$

This efficiency is much higher than what was calculated previously in the literature. For example, Hilsch (1948) measured a cooling efficiency of 24%. In the present calculation, the losses from the nozzle did not have to be taken into account since the inlet pressure used for calculating η_{turb} was the pressure measured after the nozzle. Having taken the inlet pressure before the nozzle as in many previous studies, the cooling efficiency would have been in the range of 25%. It can then be concluded that the cooling efficiency of the vortex tube itself is high, but the "approach" of the fluid in the nozzle is not very efficient. In the present work, the use of a plenum chamber decreased considerably the efficiency of the fluid "approach" due to the strong area variation. A more efficient nozzle would have a smooth and much slower area variation, minimizing pressure losses.

It will now be interesting to summarize the results from the paddle wheel model and to add some criticism. The paddle wheel model seen previously explains partly how the energy separation can be obtained in the vortex tube. With the turbine expansion, the model seems to adequately describe the cooling effect. However, the link between the heating and cooling processes is missing. In the paddle wheel model, the efficiency of the expansion process can be matched to obtain the right total temperature separation. However, there is no real similarities between the turbine-paddle wheel coupling and the frictional momentum transfer in the vortex tube. One can see how the cooling can be accomplished. However, it is not clear how the work extracted during the cooling expansion can be transferred to the outer fluid and can be dissipated there to generate heat. In a way, the explanation fails to correctly model the shaft connecting the turbine to the paddle wheel. Yet, by knowing the cooling process, one can at least estimate the net heating by invoking the conservation of energy. Therefore, the paddle wheel model help to understand the vortex tube effect and can be used for calculating total temperature separations, but fails to fully describe the physical process behind the energy separation effect.

5.3 Energy transfer by sound waves

So far in the thesis, nothing was said about the importance of sound waves. Takahama (1982) demonstrated the importance of sound waves in a modified vortex tube. By tuning an acoustic cavity which was replacing the standard tube, he was able to considerably reduce the temperature separation effect. He then proposed that strong sound waves were producing a tangential acoustic streaming close to the inlet, which was then driving a solid-body rotation. However, he just explained the cooling effect and nothing was said about the heating. Despite the lack of explanation of sound production and energy transfer processes, his discovery somehow pointed towards the importance of sound waves for temperature separation in vortex tubes. A model including sound waves in vortex tube could possibly explain how work extracted during the cooling expansion can be transferred to the outer fluid and can be dissipated there to generate heat. This process was unexplained by the paddle wheel model.

The vortex tube is not the only device where energy separation and sound waves are present. In 1954, Sprenger observed strong energy separation effects in a resonance tube. An example of its results are shown in Figure 5.5, which also contains a sketch of the set up. A jet of air with a total temperature close to 20 °C leaves the nozzle shown of the left-hand side of the sketch and impinges on a tube which is closed at the right end. The recovery temperature (temperature at the wall) T_r was varying strongly with the distance l and temperatures up to 440 °C were recorded when sound resonance was heard. Sound was produced by vortex rings created at the entrance.

The thermoacoustic effect, discovered by Wheatley in 1982 could explain the effect in the resonance tube and throw some light on the energy separation process in vortex tubes. For instance it is now known that in thermoacoustics devices, the maximum heat flux is not obtained at the point where the Carnot efficiency has a maximum but rather at a smaller efficiency (Ahlborn et Camiré, 1995). This agrees with the experimental evidence of the vortex tube (see Figures 5.3a and 5.3b), where the efficiency $\eta_{c(max)}$ is at a different location than $\eta_{turb(max)}$. In thermoacoustics, sound waves can pump heat against a temperature gradient. This effect seems to be present in the vortex tube. Further information about the thermoacoustic effect can be found in an excellent review by Swift, (1988).

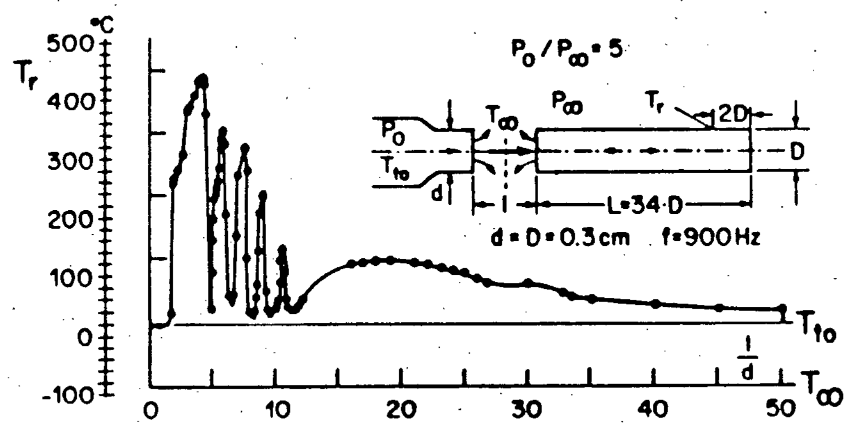

figure 5.5: The resonance tube

The examples discussed previously demonstrate the importance of sound waves in many flow fields where strong temperature gradients are present. The sound wave interaction could possibly explain the anomalous heat flux in a vortex tube. The presence of distinctive lines in the sound spectrum which were measured in this work and the variation of the spectral features with the flow ratio j_c/j_o indicate that sound waves play a significant role in the physics of the vortex tube. However, up to now no reliable intensity measurements have been done in the vortex tube. It is therefore premature to draw any quantitative conclusions on the importance of sound waves.

6 - Conclusion

The main objectives of this work was to develop a fully instrumented vortex tube allowing precise measurements of pressures, temperatures and flow rates. From the measurements obtained with this device, corrections to existing models were done in order to get a better understanding of the Ranque-Hilsch effect. To test the existing models, especially the two-streams model from Ahlborn et al. (1994), velocity profile measurements were performed. Furthermore, the vortex tube was tested at low inlet pressures to verify that the Ranque-Hilsch effect is still present when the tube works below atmospheric pressure, i.e. when air is sucked from the tube instead of being pushed through it.

6.1 Analysis of the two-streams model

It was found that the vortex tube used in the present work was behaving like a standard vortex tube, i.e. the total temperature separation was similar to commercial vortex tubes. When the data were analyzed and compared to the two-streams model from Ahlborn et al.(1994), it was found that the inlet conditions were playing a major role. The inlet velocity obtained from pressure measurements had been underestimated in the two-streams model. This was mainly due to an inaccurate inlet pressure measurement taken too far from the vortex tube. Since the pressure measurements in the present study were much more accurate, corrections to the two-streams model were performed. A new relation for the radial dynamics in the entrance plane was obtained.

The limit of temperature separation predicted by Ahlborn's model were violated by the new data. This was mainly due to some erroneous assumptions on the contribution of kinetic energy and on the heat transfer process occurring in the vortex tube. These assumptions were contradicted by the new experiments. In contradiction to Ahlborn's model, where the cold and hot streams have the same amount of energy, the vortex tube effect was explained in this work by a total temperature separation, in which the cold stream exits the tube with a lower energy than the hot stream.

6.2 Energy separation mechanisms

The Ranque-Hilsch effect was also compared to other types of flow where an energy separation is present. In a flow having a true solid-body rotation, it was found that a strong energy separation is occurring. Since a solid-body rotation is likely to occur in some parts of the vortex tube, the Ranque-Hilsch effect could be partly explained by its velocity field.

The pressure drop between the inlet and the cold exit in the vortex tube was also compared to a turbine expansion. A turbine also experiences a pressure drop and at the same time a temperature drop. The Ranque-Hilsch effect can then be compared to a paddle wheel model, where a turbine located in the cold core would experience an expansion, then generating work transferred to a paddle wheel located in the hot shell. The paddle wheel would dissipate the energy received from the cold core by friction. This model was used to estimate the vortex tube maximum cooling efficiency: $\eta_C = 42\%$. From the paddle wheel model and from the new experiments, new limits of total temperature separation were obtained:

Maximum cooling effect $$\left.\frac{T_{to} - T_{tc}}{T_o}\right|_{max} = 0.23 \qquad (6.1)$$

Maximum heating effect $$\left.\frac{T_{th} - T_{to}}{T_o}\right|_{max} = 0.63 \qquad (6.2)$$

Although these limits are realistic, i.e., we did not observed any data in the literature exceeding the limits, they were obtained with some empirical relations and therefore cannot be totally explained theoretically. Initially, it was hoped to find a model without empirical relations, where all the processes in the vortex tube could be explained. This proved to be impossible. Some of the relations, like the radial dynamics and the new total temperature separation limits were obtained from experimental results. Therefore, these limits could be slightly different for another vortex tube.

To confirm without any doubts the validity of the total temperature separation limits, the vortex tube needed to be tested at higher inlet pressure. However, due to the limitations of the compressor in the department of Physics at UBC, such experiments could not be performed.

6.3 Low pressure vortex tube

A low pressure vortex tube was tested. The pressures at the inlet and at the outlets were the following: $p_o = 0.93$ atm., $p_c = 0.3$ to 0.57 atm., $p_h = 0.3$ to 0.66 atm. With this vortex tube, a maximum cooling $T_{to} - T_{tc} = 16$ °C and a maximum heating $T_{th} - T_{to} = 7$ °C were obtained. The low pressure vortex tube was analyzed with the same model than the standard vortex tube, and it was found to behave like any other vortex tubes.

6.4 Sound waves in vortex tubes

In order to test the hypothesis of a heat transfer by sound waves in the vortex tubes, sound measurements for various inlet pressures and flow rate ratios were performed. These measurements demonstrated the presence of axial and rotational standing waves in the vortex tube. However, no calibrated spectrally resolved intensity measurements were obtained, and therefore no quantitative conclusion on the importance of sound waves were drawn.

6.5 Future research

To improve the vortex tube understanding and to confirm some of the results obtained in this work, several new experiments could be done.

1. Test the vortex tube with higher inlet pressure.

This would confirm the hypothesis of a Mach number always smaller than one. This would also confirm the total temperature separation limits.

2. Extend the flow field analysis to various locations in the vortex tube, especially to the cold end. In the present work some assumptions had to be done about the amount of kinetic energy at the cold end and on the velocity field. A more detailed flow field analysis would confirm or contradict these assumptions.

3. The low pressure vortex tube should be tested for different inlet and outlet pressures. In the present work, the vacuum pump system limited the testing to 0.3 atm. on the cold side. It would be interesting to test the tube to lower pressures.

4. In order to verify the possible cleaning of Diesel engine exhaust with the vortex tube, experiments on particulate trapping should be performed.

Nomenclature

Subscripts

c	cold
h	hot
n	nozzle
o	entrance
pl	plenum
r	radial
s	static
t	total
z	axial
ϕ	tangential

Symbols

a	sound speed
c_p	specific heat at constant pressure
D	tube inner diameter
d_n	nozzle holes diameter
d_c	cold end diameter
h	enthalpy
j	flowrate

j_c / j_o	flowrate ratio
Ma	Mach number
N	number of holes in nozzle
p	static pressure
Q	heat
r	radius
r*	radius separating free and forced vortex
R	gas constant and tube inner radius
R_c	cold end radius
T	temperature
t	time
X	pressure ratio $(p_o - p_c) / p_o$
u	velocity
γ	specific heat ratio
η_c	cooling power efficiency
η_{turb}	turbine energy efficiency
ρ	density
θ	angle between maximum velocity vector and z axis

References

Ahlborn, B. and Camiré, J., "Thermo acoustic heat pumps with maximum power transfer", American Journal of Physics, 63, (4), 1995, p.1-3.

Ahlborn, B., Keller, J.U., Staudt, R., Treitz, G. and Rebhan, E., "Limits of temperature separation in a vortex tube", Journal of Physics D: Applied Physics, 27, 1994, p.1-9.

Balmer, R.T., "Pressure-driven Ranque-Hilsch temperature separation in liquids", Journal of Fluids Engineering, vol.110, 1988, pp.161-4.

Baz, A. and Gilheany, J., "Vortex tube-assisted environmental control of hyperbaric chambers", Transactions of the ASME: Journal of energy ressources technology, Vol. 110, december 1988, p. 230-36.

Benedict, R.P., "Fundamentals of temperature, pressure and flowrate measurements", John-Wiley & Sons, 1984.

Bruun, H.H., "Experimental investigation of the energy separation in vortex tubes", Journal of Mechanincal Engineeirng science, Vol. 11, No. 6, 1969, p.567-82.

Bruno, T.J., "Vortex cooling for subambient temperature gas chromatography", Anal. Chem., 58, 1986, p.1595-6.

Bruno, T.J., "Laboratory applications of the vortex tube", Journal of chemical education, Vol. 64, No. 11, 1987, p.987-8.

Bruno, T.J., "A simple and efficient low-temperature sample cell for infrared spectrophotometry", Review of Scientific Instrument, V.63, October 1992, p. 4459-60.

Chanaud, R.C., "Experiments concerning the vortex whistle", The Journal of Acoustical Society of America, Vol. 35, No. 7, 1963, p.953-60.

Chanaud, R.C., "Observations of oscillatory motion in certain swirling flows", J. Fluid Mechanics, Vol.21, part 1, 1965, p.111-27.

Curzon, F.L. and Ahlborn, B., "Efficiency of a Carnot engine at maximum power output", Am. J. Phys., 43, 1975, pp.22-24.

Deissler, R.G. and Perlmutter, M., "Analysis of the flow and energy separation in a turbulent vortex", International Journal of heat and mass transfer, vol.1, 1960, pp.173-91.

Eckert, E.R.G., "Energy separation in fluid streams", Int. Comm. in Heat and Mass Transfer, vol.13, 1986, p.127-43.

Fekete, L.A., "Vortex tube has possibilities for high-pressure gas wells", The Oil and Gas Journal, August 7, 1967, p.143-4.

Fekete, L.A., "Vortex tube is intriguing separator", The Oil and Gas Journal, June 15, 1970, p.713.

Fekete, L.A., "Vortex tube separator may solve weigth/space limitations", Word Oil, July, 1986, pp.40-4.

Groves, Stuart, "The pitot tube and its application to the vortex tube", project report, Department of Physics, University of British Columbia, August 1994.

Hilsch, R., "Die Expansion von Gasen im Zentrifugalfed als Kälte prozess", Z. Naturf., 1, 1946, p.208-14.

Harnett, J.P. and Eckert, E.R.G., "Experimental study of the velocity and temperature distribution in a high-velocity vortex-type flow", Transaction of the ASME, May 1957, p.751-8.

Knoernschild, E., "Friction laws and energy transfer in circular flow, part II: Energy transfer in circular flow and possible applications (explaination of the Hilsch or Ranque effect), Tech. Rep. F-TR-2198-ND, GS-USAF, Wright Patterson Air orce Base no.78.

Kurosaka, M., "Acoustic streaming in swirling flow and the Ranque-Hilsch vortex tube effect", Journal of Fluid Mechanics, Vol.124, 1982, p. 139-72.

Lighthill, J., "Acoustic streaming", Journal of Sound and Vibration, Vol.61, No.3, 1978, p.391-418.

Linderstrøm-Lang, C.U., "Gas separation in the Ranque-Hilsch vortex tube", International Journal of heat and mass transfer, vol.7, 1964, p.1195-206.

Linderstrøm-Lang, C.U., "The three-dimensional distributions of tangential velocity and total-temperature in vortex tubes", Journal of Fluid Mechanics, vol. 45, part 1, 1971, p.161-87.

Marshall, J., "Effect of operating conditions, physical size and fluid characteristics on the gas separation performance of a Linderstrøm-Lang vortex tube", Int. J. Heat and Mass Transfer, Vol. 20, 1977, p. 227-31.

Munson, B.R., Young, D.F. and Okiichi, T.H., "Fundamentals of fluid mechanics", John Wiley and Sons, 1990.

Negm, M.I.M., Serag, A.Z. and Abdel, S.M., "Generalized correlations for the process of energy separation in vortex tubes", Modelling, Simulation & Control, B, ASME Press, vol. 14, 4, 1988, p.47-64.

Neill, W.R., "Investigation of intense sound waves in a Ranque-Hilsch vortex tube", University of British Columbia, August 1994.

Novikov, I.I., J.Nuclear Energy, II, (USSR), &, 125 (1958)

Ranque, G.H., "Expériences sur la détente giratoire avec productions simultanées d'un échappement d'air chaud et d'air froid", Journal de Physique et le Radium, IV, 1933, p.112-114.

Saad, M.A., "Compressible fluid flow", Prentice Hall, 1993.

Savino, J.M. and Ragsdale, R.G., "Some temperature and pressure measurements in confined vortex fields, Journal of Heat Transfer, February 1961, p.33-8.

Sibbertsen, W., "Vorrichtung zum Entfernen oxidierbarer bzw verbrennbarer Partikel aus Abgasen", German Patent Office, patent DE 3917888 A1, Dec.12, 1990 and private communication.

Sibulkin, M., "Unsteady, viscous, circular flow. Part 3. Application to the Ranque-Hilsch vortex tube", Journal of Fluid Mechanics, Vol.12, N.2, 1962, pp.269-93.

Sprenger, Z., angw. Math. Phys., 2, 1950, p.292.

Stephan, K., Lin, S., Durst, M., Huang, F. and Seher, D., "An investigation of energy separation in a vortex tube", International Journal of Heat and Mass Transfer, 26, 1983, p.341-8.

Swift, G.W., "Thermoacoustic engines", The Journal of Acoutical Society of America, Vol.84, No.4, 1988, p.1145-80.

Takahama, H., "Studies on vortex tubes", Bulletin of JSME, Vol.8, No.31, 1965, p.433-40.

Takahama, H. and Sogan, M., "Studies on vortex tubes (2nd report)", Bulletin of JSME, Vol.9, No.33, 1966, p.121-30.

Takahama, H. and Kawamura, H., "Performance characteristics of energy separation in a steam-operated vortex tube", International Journal of Engineering Science, vol.17,1979, pp.735-744.

Takahama, H., "Energy separation in vortex tubes with a divergent chamber", Transactions of the ASME: Journal of Heat Transfer, vol.103, 1981, pp.196-203.

Vonnegut, B., "Vortex thermometer for measuring true air temperatures and true air speeds in flight", The Review of Scientific Instrument, Vol. 21, No. 2, 1950, p.136-41.

Vonnegut, B., "A vortex whistle", The Journal of the Acoustical Society of America, Vol. 26, No.1, January 1954, p.18-20.

Appendix A - Data processing and vortex tube data

Some calculations were required to get the desired parameters from the raw data. Some of it was simple data conversion, which was converting data units in metric units. There was also calculations giving other parameters that were not measured directly (i.e. velocity, flow rate, etc.).This section shows the calculations done. The vortex tube averaged set of data is also presented.

A.1 Data processing

Unit conversion factors

$$p\,[\text{Pa}] = 6891.2 \cdot (p\,[\text{psig}] + 14.7) = 6891.2 \cdot p\,[\text{psia}] = 3377 \cdot (30 - p[\text{in. Hg.}])$$

$$T\,[\text{K}] = T\,[°\text{C}] + 273.15$$

Flow rate

The flow rate obtained by the orifice meters were calibrated with a rotameter Omega Fl 1413. This was allowing simple checks during the experiments since the reading on the computer screen was in the same units than the rotameter. However the rotameter was giving a reading in an "SCFM equivalent" flow rate, which is the flow rate that would be true if the fluid was at standard atmosphere. In the vortex tube experiments, the inlet conditions were different than standard atmosphere. A conversion formula given by Omega was used:

$$j\,[\text{CFM}] = 19.602 \cdot j\,[\text{SCFM eq.}] \cdot (p[\text{psig}] + 14.7) / (T\,[°\text{C}] + 273.15)$$

Then the simple gas law was used to get a mass flow rate from a volumetric flow rate:

$$j\ [kg/s] = 2.09 \times 10^{-3} \cdot j\ [SCFM\ eq.] \cdot (p[psig] + 14.7)^{1/2}\ /\ (T\ [°C] + 273.15)^{1/2}$$

Static and stagnation temperature

The temperature measurements in moving fluids are not as simple as pressure measurements. When a probe is inserted in a moving fluid, the measured temperature will not only indicate the fluid temperature but in addition a temperature equivalent to the kinetic energy of the fluid. Therefore, three temperature can be defined:

Static temperature T. This is the actual gas temperature, measured by a device that moves with the fluid and is hence in equilibrium with the fluid.

Dynamic temperature T_v. This is the thermal equivalent of the fluid kinetic energy.

Total temperature T_t. This temperature is the addition of the static and dynamic temperature. The three temperature can be related by the following relation (Benedict, 1984):

$$T_t = T + T_v = T + u^2 / 2c_p$$

for air, $c_p = 1.0035$ kJ/kg K ,

$$T_t = T + u^2 / 2007$$

An ideal probe will stagnate completely a moving gas and is totally isolated from the surroundings. Therefore, the probe will measure the total temperature. However, a real probe is subject to conductive heat transfer, and will not completely stop the moving fluid. A dynamic correction factor K may be defined so that

$$T_p = T + KT_v.$$

where T_p is the temperature measured by the probe. From Benedict (1984) , the dynamic correction factor for a bare Iron-Constantan thermocouples used in the experiments is K = 0.75. Then,

$$T = T_p - KT_v = T_p - 0.75T_v = T_p[K] - 0.75\ (u[m/s])^2/\ 2007$$

It is necessary to calculate the static temperature since it is the one used in thermodynamic relations. For fluid velocities < 50 m/s, the dynamic temperature is less than 1 K and the correction is not necessary. Therefore, no correction was done on the hot side of the tube and on the flowmeters calculations. However, the correction was necessary for measuring the nozzle and cold side temperature and velocity.

Pipe velocity

The pipe velocity was calculated using the flow rate, the pressure and the temperature:

$$u_{pipe} = j_o RTo/P_{plenum}A = 4.029 \times 10^6 \cdot j_o\ [kg/s] \cdot T_o\ /\ p_{plenum}\ [Pa]$$

Inlet velocity

Different techniques have been tried to calculate the inlet velocity. The difficulty here was to know the pressure in the nozzle. The pressure in the plenum chamber and inside the tube were known, and the plenum chamber pressure was generally exceeding the inside pressure by a factor 2.

A set of experiments was done with a pressure tap right in the center of one of the orifice. Then, this measured pressure was used to calculate the velocity from the flow rate formula:

$$u_o = j_o RT/(P_o A) = 14154 \times 10^3\ j_o[kg/s]\ T[K]\ /\ P_o[Pa]$$

Since the use of this formula requires the static temperature and vice versa, an iterative calculation was done to get both the static temperature and the velocity.

$$u_o = 14154 \times 10^3\, j_o[\text{kg/s}]\, (T_p - 0.75 u_o^2/2007) / P_o[\text{Pa}]$$

A.2 Vortex tube data

The next pages presents the averaged set used for all the calculations. The raw data taken directly from the computer are presented in the first columns and the calculated parameters are following.

	A	B	C	D	E	F	G	H	I	J	K	L	M	N
1	Ppl (Pa)	Ppl (psig)	Tin (C)	Po(tub)(psi	Po(n)(psig)	jo (SCFM)	Tc (C)	Pc (psig)	Th (C)	Ph(psig)	jc (SCFM)	Tin (K)	Po(tu) (Pa)	Po(n)(Pa)
2	170213	10	22.34	2.04	2.04	9.92	22.75	-0.01	23.28	0.40	0.18	295.49	115380	115380
3	170213	10	21.82	2.34	2.34	9.80	15.44	0.11	23.63	0.63	1.25	294.97	117395	117396
4	170213	10	21.74	2.58	2.58	9.81	14.08	0.19	23.97	0.76	2.16	294.89	119054	119055
5	170213	10	21.75	2.90	2.90	9.85	13.54	0.31	24.35	0.89	3.13	294.90	121308	121309
6	170213	10	21.77	3.16	3.16	9.95	12.86	0.43	24.84	1.10	3.89	294.92	123067	123067
7	170213	10	21.80	3.29	3.29	9.80	12.43	0.54	25.41	1.27	4.49	294.95	123948	123949
8	170213	10	21.98	3.54	3.54	9.79	12.11	0.76	25.67	1.55	4.98	295.13	125695	125695
9	170213	10	21.88	4.00	4.00	9.78	11.72	0.90	27.03	1.78	5.96	295.03	128876	128877
10	170213	10	22.07	4.34	4.34	9.61	12.03	1.20	27.30	2.20	6.67	295.22	131208	131208
11	170213	10	22.02	4.56	4.56	9.54	12.80	1.36	28.90	2.38	7.16	295.17	132689	132690
12	170213	10	22.05	4.83	4.83	9.35	13.79	1.63	29.15	2.73	7.69	295.20	134599	134600
13	170213	10	22.07	5.21	5.21	9.31	14.53	1.81	29.35	3.08	8.15	295.22	137228	137229
14	170213	10	22.10	5.61	5.61	9.11	16.08	2.28	28.97	3.56	8.71	295.25	139961	139962
15	170213	10	22.18	6.24	6.24	8.99	17.71	2.77	27.21	4.18	9.44	295.33	144271	144271
16	170213	10	22.19	6.24	6.24	8.87	17.49	2.78	27.13	4.22	9.46	295.34	144275	144276
17	239123	20	21.73	4.26	4.81	13.18	15.92	0.01	27.92	1.15	0.16	294.88	130680	134447
18	239123	20	21.57	4.37	4.84	13.16	12.35	0.06	27.59	1.27	0.72	294.72	131382	134654
19	239123	20	21.58	4.49	5.00	13.14	7.26	0.15	27.54	1.43	1.47	294.73	132261	135757
20	239123	20	21.66	4.61	5.10	13.07	6.28	0.22	27.86	1.54	2.16	294.81	133075	136446
21	239123	20	21.65	4.67	5.15	13.11	5.77	0.26	28.02	1.61	2.48	294.80	133455	136790
22	239123	20	21.71	4.78	5.20	13.11	5.21	0.32	28.40	1.72	2.90	294.86	134208	137135
23	239123	20	21.73	4.85	5.28	13.09	5.09	0.34	28.50	1.74	3.15	294.88	134698	137686
24	239123	20	21.76	4.88	5.30	13.08	4.96	0.39	28.95	1.81	3.42	294.91	134948	137824
25	239123	20	21.80	5.04	5.49	13.09	4.23	0.46	28.97	1.91	3.82	294.95	136017	139133
26	239123	20	21.77	5.07	5.50	13.03	3.78	0.49	29.14	1.96	4.12	294.92	136229	139202
27	239123	20	21.85	5.34	5.50	13.07	2.84	0.61	29.47	2.15	4.61	295.00	138071	139202
28	239123	20	21.90	5.38	5.64	13.05	3.36	0.64	29.97	2.25	4.91	295.05	138345	140167
29	239123	20	22.04	5.45	5.70	13.11	4.13	0.67	30.41	2.31	5.19	295.19	138830	140580
30	239123	20	21.91	5.55	5.80	13.03	3.32	0.83	31.18	2.54	5.62	295.06	139539	141270
31	239123	20	21.87	5.91	5.90	13.10	2.10	0.92	30.96	2.67	6.06	295.02	142000	141959
32	239123	20	21.85	5.92	6.10	13.00	2.79	1.03	32.20	2.87	6.43	295.00	142123	143337
33	239123	20	21.50	6.07	6.20	12.94	2.19	1.11	32.25	2.99	6.66	294.65	143155	144026
34	239123	20	21.70	6.31	6.40	13.03	1.19	1.27	32.69	3.19	7.00	294.85	144811	145404
35	239123	20	21.66	6.44	6.60	12.88	1.48	1.38	33.03	3.36	7.27	294.81	145707	146783
36	239123	20	21.62	6.61	6.70	12.77	1.18	1.53	34.17	3.58	7.56	294.77	146858	147472
37	239123	20	21.83	7.09	7.10	12.76	1.72	1.88	35.81	4.00	8.10	294.98	150125	150228
38	239123	20	21.85	7.18	7.20	12.68	1.85	1.98	36.40	4.19	8.25	295.00	150754	150917
39	239123	20	21.45	7.24	7.30	12.69	1.68	2.09	35.74	4.38	8.30	294.60	151220	151606
40	239123	20	21.59	7.26	7.38	12.66	1.68	2.08	36.27	4.34	8.46	294.74	151304	152158
41	239123	20	21.84	7.76	7.80	12.62	2.72	2.47	37.14	4.78	8.91	294.99	154772	155052
42	239123	20	21.75	7.71	7.80	12.49	2.86	2.50	37.36	4.83	9.05	294.90	154411	155052
43	239123	20	21.59	8.04	8.04	12.51	3.12	2.81	38.29	5.23	9.43	294.74	156734	156735

	A	B	C	D	E	F	G	H	I	J	K	L	M	N
44	239123	20	21.58	8.13	8.13	12.47	3.09	2.90	39.23	5.34	9.64	294.73	157320	157321
45	239123	20	21.86	8.46	8.46	12.31	4.77	3.25	39.64	5.70	10.08	295.01	159590	159591
46	239123	20	21.85	8.88	8.88	12.38	5.36	3.60	41.28	6.20	10.49	295.00	162526	162527
47	239123	20	22.11	9.34	9.34	12.30	6.46	3.94	40.70	6.53	10.88	295.26	165692	165693
48	239123	20	21.91	9.26	9.26	12.04	7.54	4.07	41.92	6.71	11.13	295.06	165086	165087
49	239123	20	22.09	9.37	9.37	11.96	8.14	4.17	41.58	6.80	11.26	295.24	165895	165896
50	239123	20	22.03	9.52	9.52	11.92	8.49	4.30	41.87	6.98	11.43	295.18	166910	166911
51	239123	20	21.96	9.89	9.89	12.03	9.07	4.59	42.27	7.36	11.71	295.11	169421	169422
52	239123	20	22.06	10.19	10.19	11.78	11.02	4.97	42.04	7.75	12.16	295.21	171519	171520
53	239123	20	22.24	10.73	10.73	11.81	12.82	5.52	38.75	8.45	12.72	295.39	175241	175242
54	239123	20	22.26	11.10	11.10	11.61	13.45	5.74	38.21	8.80	12.86	295.41	177784	177785
55	239123	20	22.21	11.53	11.53	11.46	14.44	6.17	39.66	9.26	13.30	295.36	180743	180745
56	239123	20	22.40	12.31	12.31	11.40	14.31	6.80	38.43	9.98	13.88	295.55	186157	186158
57	308035	30	21.1368	5.96986	7.5	14.7284	14.2402	-0.00868	23.7005	1.59387	-0.09688	294.29	142439	152985
58	308035	30	21.0848	6.01545	7.6	15.0532	10.0422	0.00647	24.1235	1.65054	0.33475	294.23	142753	153674
59	308035	30	21.0967	6.0869	7.65	14.9539	6.84286	0.04534	24.8807	1.747	0.65625	294.25	143246	154018
60	308035	30	21.0351	6.2562	7.7	14.8183	2.49118	0.10388	25.6181	1.85514	1.16334	294.19	144413	154363
61	308035	30	21.1553	6.41957	7.8	14.9134	0.95495	0.17024	26.3263	1.98537	1.91145	294.31	145538	155052
62	308035	30	21.1936	6.50847	7.85	14.8325	0.67236	0.22887	26.8402	2.07063	2.47737	294.34	146151	155397
63	308035	30	21.0894	6.5631	8	14.766	-0.82218	0.2964	27.3882	2.17162	2.9654	294.24	146527	156430
64	308035	30	20.966	6.82584	8.4	14.7801	-1.79902	0.43714	28.6011	2.40375	3.64121	294.12	148338	159187
65	308035	30	20.8867	7.08203	8.66	14.6701	-2.61553	0.57619	29.7221	2.64821	4.48672	294.04	150103	160978
66	308035	30	20.9022	7.43853	8.77	14.7046	-3.36184	0.78905	31.059	2.98236	5.37898	294.05	152560	161736
67	308035	30	21.2359	8.32065	9.4	14.6917	-3.76648	1.29939	33.8007	3.78013	7.03507	294.39	158639	166078
68	308035	30	21.1405	9.14129	9.6	14.6781	-4.22388	1.85041	37.2573	4.5465	8.13814	294.29	164294	167456
69	308035	30	21.0706	9.59972	9.8	14.5665	-4.58469	2.2829	38.5188	5.20401	8.79895	294.22	167453	168834
70	308035	30	21.1596	10.6032	10.6032	14.5261	-4.04404	3.09608	38.3712	6.29819	9.7975	294.31	174368	174369
71	308035	30	21.3889	13.291	13.291	14.0034	1.80898	5.59983	49.7065	9.33775	12.6731	294.54	192891	192892
72	308035	30	21.2771	13.5244	13.5244	14.1317	0.84709	5.79669	46.5439	9.58327	12.9152	294.43	194499	194500
73	308035	30	21.2441	13.6773	13.6773	14.0237	0.51468	5.90504	46.0424	9.73711	13.025	294.39	195553	195554
74	308035	30	21.2614	13.8732	13.8732	13.8212	2.30893	6.21036	46.7883	10.0602	13.3227	294.41	196903	196904
75	308035	30	21.3797	14.2733	14.2733	13.877	2.9987	6.49814	48.5989	10.4128	13.5903	294.53	199660	199661
76	308035	30	21.2398	15.3857	15.3857	13.8538	5.24579	7.42707	#DIV/0!	11.6205	14.1086	294.39	207326	207327
77	308035	30	21.217	15.1547	15.1547	13.7744	5.10146	7.36201	#DIV/0!	11.4206	14.4309	294.37	205734	205735
78	308035	30	21.3386	15.1709	15.1709	13.6554	5.97082	7.4506	51.5876	11.4793	14.4671	294.49	205845	205846
79	308035	30	21.4712	15.3786	15.3786	13.6156	6.39205	7.64903	51.4564	11.7297	14.6953	294.62	207276	207277
80	308035	30	21.4723	15.8752	15.8752	13.6365	8.13011	8.12666	50.1547	12.2894	15.0345	294.62	210699	210700
81	308035	30	21.5394	16.734	16.734	13.6737	9.11092	8.75604	#DIV/0!	13.1839	15.2039	294.69	216616	216618
82	308035	30	21.6513	16.6194	16.6194	13.4459	7.96693	8.74595	#DIV/0!	13.0721	15.3938	294.80	215827	215828
83	308035	30	21.3672	17.0973	17.0973	13.3128	12.162	9.29978	46.7999	13.7195	15.7613	294.52	219121	219122
84	308035	30	21.3582	17.192	17.192	13.0809	12.1147	9.33448	46.8816	13.8015	15.7931	294.51	219773	219774
85	308035	30	21.2969	17.8675	17.8675	13.2478	13.0787	10.127	42.3181	14.5986	16.3628	294.45	224428	224429
86	308035	30	21.2943	17.7872	17.7872	13.1282	13.0318	10.1226	42.4173	14.5618	16.4074	294.44	223874	223876

	A	B	C	D	E	F	G	H	I	J	K	L	M	N
87	308035	30	21.5215	18.4856	18.4856	12.9146	14.2309	10.8142	38.47	15.3672	16.8263	294.67	228687	228689
88	376946	40	22.16	7.72	10.29	16.31	9.14	0.04	27.80	2.10	0.13	295.31	154520	172211
89	376946	40	22.13	7.74	10.31	16.14	8.34	0.06	27.30	2.12	0.80	295.28	154609	172349
90	376946	40	22.17	7.77	10.42	16.02	6.63	0.07	27.05	2.17	1.04	295.32	154872	173107
91	376946	40	22.07	7.88	10.49	15.97	5.25	0.13	27.04	2.24	1.42	295.22	155611	173589
92	376946	40	22.09	7.99	10.54	16.08	2.54	0.16	27.08	2.32	1.73	295.24	156386	173934
93	376946	40	22.13	8.18	10.62	16.03	0.01	0.25	27.11	2.48	2.44	295.28	157644	174485
94	376946	40	22.05	8.52	10.68	16.13	-2.01	0.40	27.63	2.76	3.44	295.20	160023	174899
95	376946	40	22.11	8.55	10.72	16.08	-1.71	0.45	27.87	2.84	3.90	295.26	160224	175174
96	376946	40	21.99	8.70	10.77	16.01	-3.29	0.52	27.87	2.94	4.22	295.14	161268	175519
97	376946	40	22.09	8.82	10.84	16.05	-2.98	0.63	28.32	3.12	4.62	295.24	162065	176001
98	376946	40	22.08	8.86	10.87	16.06	-3.31	0.64	28.28	3.17	4.90	295.23	162380	176208
99	376946	40	22.22	8.99	10.99	16.05	-3.97	0.70	28.64	3.28	5.16	295.37	163285	177035
100	376946	40	22.10	9.35	11.17	16.00	-4.65	0.92	29.40	3.62	5.90	295.25	165756	178275
101	376946	40	22.07	10.10	11.30	15.98	-5.20	1.38	30.71	4.36	7.05	295.22	170868	179171
102	376946	40	22.20	10.86	11.75	15.95	-6.00	1.88	32.82	5.13	8.00	295.35	176170	182272
103	376946	40	22.12	12.03	12.21	15.87	-5.96	2.68	34.77	6.26	9.19	295.27	184183	185442
104	376946	40	22.28	12.95	12.95	15.78	-6.28	3.36	36.57	7.18	10.04	295.43	190567	190568
105	376946	40	22.29	14.24	14.24	15.76	-5.41	4.32	39.38	8.48	11.08	295.44	199438	199439
106	376946	40	22.33	14.74	14.74	15.54	-5.18	5.05	40.81	9.42	11.95	295.48	202857	202859
107	376946	40	22.36	15.61	15.61	15.56	-3.19	5.77	43.02	10.30	12.71	295.51	208838	208839
108	376946	40	22.41	16.32	16.32	15.52	-3.18	6.36	42.79	10.99	13.40	295.56	213783	213784
109	376946	40	22.44	17.52	17.52	15.42	-1.21	7.33	44.61	12.13	14.33	295.59	222021	222023
110	376946	40	22.50	19.06	19.06	15.40	0.41	8.66	45.41	13.66	15.40	295.65	232664	232665
111	91179	3	21.7371	19.4	17	8.12426	9.75795	20	26.8659	20	0.96139	294.89	35796.20	43901.00
112	91179	3	21.6606	19	16	8.15047	7.84722	19.7	26.6879	19.7	1.54833	294.81	37147.00	47278.00
113	91179	3	21.6236	18.7	15.8	8.09807	7.02995	19.6	26.6386	19.5	1.97026	294.77	38160.10	47953.40
114	91179	3	21.5893	18	15.6	8.05463	6.23139	19.4	26.7072	19	2.52964	294.74	40524.00	48628.80
115	91179	3	21.5816	17	15.4	7.9638	5.54321	19	27.0149	18	3.46655	294.73	43901.00	49304.20
116	91179	3	21.5875	16	15.2	7.97467	5.2897	18.5	27.3973	17.7	4.49604	294.74	47278.00	49979.60
117	91179	3	21.561	15.5	15.1	7.89226	5.47584	18	27.7103	17	5.25975	294.71	48966.50	50317.30
118	91179	3	21.5841	15	15	7.82244	6.30079	17.2	28.4887	16	5.93922	294.73	50655.00	50655.00
119	91516.7	2.9	21.5681	14	14	7.68563	7.7283	16.5	28.984	15	6.71597	294.72	54032.00	54032.00
120	91854.4	2.8	21.5228	13	13	7.65047	9.26955	15.8	28.8607	14	7.28037	294.67	57409.00	57409.00
121	92023.3	2.75	21.5019	12	12	7.46628	11.1648	14.9	28.5455	13	7.74567	294.65	60786.00	60786.00
122	93205.2	2.4	21.5186	12	12	7.10575	14.3866	14.4	27.3675	11.5	8.26472	294.67	60786.00	60786.00
123	94556	2	21.4734	9	9	6.695	16.5998	12.7	26.4848	10	8.31448	294.62	70917.00	70917.00
124														
125														
126														

	O	P	Q	R	S	T	U	V	W	X	Y	Z	AA	AB
1	jo (kg/s)	Tc (K)	Pc (Pa)	jc (kg/s)	Ph (Pa)	Th (K)	upipe(m/s)	To stat (K)	uo (m/s)	ucz (m/s)	uc (m/s)	Tc stat (K)	jc/jo	X
2	0.00599	295.90	101203	0.00008	104054	296.43	41.92	279.71	205.51	1.28	82.21	293.3707	0.0137	0.1229
3	0.00593	288.59	102043	0.00059	105625	296.78	41.40	279.99	200.21	9.00	80.59	286.1636	0.1001	0.1308
4	0.00593	287.23	102625	0.00103	106550	297.12	41.42	280.29	197.68	15.45	80.57	284.8037	0.1736	0.1380
5	0.00596	286.69	103415	0.00149	107456	297.50	41.58	280.65	195.24	22.21	81.19	284.2233	0.2510	0.1475
6	0.00602	286.01	104266	0.00187	108884	297.99	42.03	280.79	194.46	27.52	82.51	283.4612	0.3109	0.1528
7	0.00593	285.58	105005	0.00217	110062	298.56	41.37	281.38	190.57	31.60	82.52	283.0383	0.3659	0.1528
8	0.00592	285.26	106537	0.00242	111982	298.82	41.35	281.94	187.89	34.78	82.81	282.6972	0.4093	0.1524
9	0.00591	284.87	107499	0.00291	113557	300.18	41.29	282.48	183.33	41.40	84.21	282.2209	0.4930	0.1659
10	0.00581	285.18	109569	0.00329	116461	300.45	40.60	282.97	181.06	45.93	85.76	282.4317	0.5666	0.1649
11	0.00577	285.95	110653	0.00355	117671	302.05	40.29	283.78	174.56	49.14	85.38	283.2257	0.6151	0.1661
12	0.00565	286.94	112539	0.00383	120140	302.30	39.51	284.54	168.93	52.38	85.49	284.2061	0.6778	0.1639
13	0.00563	287.68	114486	0.00409	122544	302.50	39.32	285.00	165.37	55.14	86.11	284.9111	0.7275	0.1657
14	0.00551	289.23	116997	0.00441	125802	302.12	38.50	285.79	159.11	58.45	86.41	286.4348	0.8007	0.1641
15	0.00543	290.86	120377	0.00484	130124	300.36	37.97	286.63	152.52	62.63	87.43	288.0007	0.8903	0.1656
16	0.00536	290.64	120440	0.00485	130388	300.28	37.50	286.86	150.66	62.70	86.97	287.8171	0.9036	0.1652
17	0.00945	289.07	101351	0.00007	109234	301.07	46.93	268.25	266.98	1.13	106.80	284.8109	0.0078	0.2462
18	0.00944	285.50	101747	0.00034	110067	300.74	46.88	268.20	266.40	5.17	106.69	281.2420	0.0364	0.2444
19	0.00943	280.41	102333	0.00070	111153	300.69	46.81	268.62	264.36	10.35	106.25	276.1954	0.0748	0.2462
20	0.00937	279.43	102826	0.00104	111888	301.01	46.54	269.19	261.83	15.17	105.82	275.2461	0.1111	0.2464
21	0.00940	278.92	103058	0.00120	112377	301.17	46.69	269.16	261.98	17.41	106.23	274.7012	0.1277	0.2466
22	0.00940	278.36	103484	0.00141	113136	301.55	46.69	269.32	261.43	20.29	106.52	274.1247	0.1497	0.2454
23	0.00938	278.24	103654	0.00153	113304	301.65	46.62	269.60	260.08	22.01	106.34	274.0111	0.1630	0.2472
24	0.00937	278.11	103968	0.00166	113799	302.10	46.58	269.72	259.63	23.85	106.55	273.8691	0.1774	0.2456
25	0.00938	277.38	104471	0.00187	114465	302.12	46.64	270.11	257.80	26.58	106.49	273.1470	0.1990	0.2491
26	0.00934	276.93	104648	0.00202	114840	302.29	46.41	270.28	256.76	28.59	106.61	272.6811	0.2158	0.2482
27	0.00937	275.99	105532	0.00227	116116	302.62	46.58	270.23	257.46	31.80	107.78	271.6474	0.2420	0.2419
28	0.00935	276.51	105741	0.00242	116776	303.12	46.49	270.65	255.50	33.92	107.68	272.1778	0.2588	0.2456
29	0.00940	277.28	105901	0.00255	117189	303.56	46.74	270.70	256.01	35.82	108.49	272.8855	0.2716	0.2467
30	0.00934	276.47	106992	0.00278	118816	304.33	46.43	271.03	253.57	38.57	108.51	272.0737	0.2981	0.2426
31	0.00939	275.25	107625	0.00302	119669	304.11	46.66	270.98	253.67	41.39	109.59	270.7638	0.3217	0.2419
32	0.00931	275.94	108407	0.00321	121091	305.35	46.30	271.69	249.77	43.78	109.08	271.4945	0.3444	0.2437
33	0.00928	275.34	108917	0.00333	121935	305.40	46.08	271.66	248.00	45.16	109.00	270.9047	0.3591	0.2438
34	0.00934	274.34	110073	0.00353	123254	305.84	46.40	271.97	247.41	47.16	109.63	269.8532	0.3779	0.2430
35	0.00923	274.63	110842	0.00368	124469	306.18	45.87	272.76	242.93	48.85	108.76	270.2108	0.3983	0.2449
36	0.00916	274.33	111865	0.00384	125951	307.32	45.49	273.18	240.37	50.54	108.62	269.9223	0.4198	0.2414
37	0.00914	274.87	114288	0.00416	128864	308.96	45.45	274.15	236.10	53.60	108.59	270.4653	0.4547	0.2392
38	0.00909	275.00	114969	0.00425	130174	309.55	45.16	274.53	234.04	54.48	108.31	270.6179	0.4676	0.2382
39	0.00911	274.83	115718	0.00429	131456	308.89	45.19	274.21	233.56	54.62	108.22	270.4561	0.4712	0.2367
40	0.00908	274.83	115622	0.00437	131199	309.42	45.09	274.59	232.16	55.65	108.26	270.4518	0.4810	0.2401
41	0.00905	275.87	118308	0.00464	134232	310.29	44.97	275.62	227.70	58.05	108.01	271.5079	0.5133	0.2370
42	0.00896	276.01	118520	0.00472	134597	310.51	44.50	275.86	225.71	58.96	107.83	271.6662	0.5273	0.2356
43	0.00897	276.27	120644	0.00496	137309	311.44	44.55	276.03	223.80	60.91	108.28	271.8868	0.5532	0.2303

	O	P	Q	R	S	T	U	V	W	X	Y	Z	AA	AB
44	0.00894	276.24	121319	0.00508	138120	312.38	44.39	276.24	222.41	62.06	108.47	271.8421	0.5687	0.2288
45	0.00883	277.92	123729	0.00536	140578	312.79	43.87	277.38	217.21	64.48	108.20	273.5496	0.6068	0.2247
46	0.00887	278.51	126129	0.00562	144026	314.43	44.10	277.79	214.58	66.53	108.60	274.1011	0.6335	0.2239
47	0.00881	279.61	128448	0.00587	146294	313.85	43.85	278.83	209.65	68.50	108.28	275.2299	0.6660	0.2248
48	0.00863	280.69	129316	0.00601	147529	315.07	42.89	279.13	206.48	69.96	108.24	276.3096	0.6970	0.2167
49	0.00857	281.29	130056	0.00609	148162	314.73	42.63	279.64	204.29	70.65	108.02	276.9340	0.7109	0.2160
50	0.00854	281.64	130915	0.00621	149370	315.02	42.47	279.85	202.53	71.58	108.10	277.2739	0.7267	0.2157
51	0.00862	282.22	132926	0.00640	151994	315.42	42.88	279.94	201.51	72.83	108.63	277.8108	0.7420	0.2154
52	0.00844	284.17	135574	0.00669	154697	315.19	41.98	280.92	195.51	75.14	108.45	279.7755	0.7924	0.2096
53	0.00846	285.97	139358	0.00707	159517	311.90	42.11	281.59	192.15	77.75	109.33	281.5058	0.8354	0.2048
54	0.00832	286.60	140850	0.00718	161942	311.36	41.39	282.38	186.77	78.32	108.23	282.2241	0.8634	0.2078
55	0.00821	287.59	143847	0.00749	165108	312.81	40.87	283.02	181.73	80.24	108.27	283.2104	0.9117	0.2041
56	0.00816	287.46	148161	0.00793	170086	311.58	40.66	283.99	175.85	82.50	108.42	283.0692	0.9715	0.2041
57	0.01200	287.39	101240	-0.00005	112284	296.85	46.18	262.40	292.11	-0.70	116.85	282.2882	-0.0038	0.3382
58	0.01226	283.19	101345	0.00016	112675	297.27	47.19	261.47	296.11	2.39	118.47	277.9475	0.0130	0.3405
59	0.01218	279.99	101612	0.00031	113340	298.03	46.88	261.94	294.04	4.65	117.71	274.8153	0.0258	0.3403
60	0.01207	275.64	102016	0.00056	114085	298.77	46.45	262.46	291.37	8.16	116.83	270.5403	0.0467	0.3391
61	0.01215	274.10	102473	0.00093	114982	299.48	46.76	262.47	291.88	13.34	117.51	268.9446	0.0766	0.3391
62	0.01208	273.82	102877	0.00121	115570	299.99	46.51	262.92	290.00	17.25	117.28	268.6828	0.1001	0.3380
63	0.01203	272.33	103343	0.00145	116266	300.54	46.29	263.35	287.49	20.54	116.82	267.2283	0.1209	0.3394
64	0.01204	271.35	104312	0.00180	117865	301.75	46.33	264.06	283.62	25.06	116.18	266.3066	0.1493	0.3447
65	0.01195	270.53	105271	0.00223	119550	302.87	45.98	264.88	279.32	30.70	115.87	265.5175	0.1864	0.3461
66	0.01198	269.79	106738	0.00289	121853	304.21	46.09	265.00	278.82	36.50	117.35	264.6422	0.2248	0.3401
67	0.01197	269.38	110254	0.00358	127350	306.95	46.07	266.61	272.61	46.93	118.71	264.1170	0.2995	0.3361
68	0.01196	268.93	114052	0.00422	132631	310.41	46.02	266.94	270.56	53.33	120.65	263.4863	0.3529	0.3189
69	0.01187	268.57	117032	0.00462	137162	311.67	45.67	267.57	267.04	56.89	121.02	263.0923	0.3897	0.3068
70	0.01183	269.11	122636	0.00527	144703	311.52	45.54	269.21	259.18	61.94	120.77	263.6558	0.4451	0.2967
71	0.01140	274.96	139889	0.00720	165649	322.86	43.92	274.74	230.20	75.83	119.28	269.6418	0.6312	0.2748
72	0.01151	274.00	141246	0.00738	167341	319.69	44.32	274.58	230.47	76.77	119.97	268.6187	0.6415	0.2738
73	0.01142	273.66	141993	0.00747	168401	319.19	43.98	275.00	227.81	77.17	119.41	268.3361	0.6540	0.2739
74	0.01126	275.46	144097	0.00767	170628	319.94	43.34	275.72	223.64	78.62	119.09	270.1589	0.6816	0.2682
75	0.01130	276.15	146080	0.00787	173058	321.75	43.53	276.18	221.61	79.75	119.24	270.8357	0.6965	0.2684
76	0.01128	278.40	152481	0.00831	181380	#DIV/0!	43.44	277.28	213.99	81.36	118.10	273.1841	0.7368	0.2645
77	0.01122	278.25	152033	0.00849	180002	#DIV/0!	43.19	277.18	214.45	83.32	119.59	272.9074	0.7570	0.2610
78	0.01112	279.12	152643	0.00852	180407	324.74	42.83	277.59	212.64	83.49	119.19	273.8123	0.7660	0.2585
79	0.01108	279.54	154011	0.00868	182132	324.61	42.71	278.04	210.65	84.50	119.33	274.2209	0.7835	0.2570
80	0.01110	281.28	157302	0.00895	185989	323.30	42.78	278.47	207.92	85.80	119.50	275.9441	0.8063	0.2534
81	0.01113	282.26	161639	0.00916	192153	#DIV/0!	42.90	279.24	203.30	85.75	118.18	277.0421	0.8230	0.2538
82	0.01094	281.12	161570	0.00929	191383	#DIV/0!	42.19	279.73	200.83	86.66	118.17	275.8989	0.8491	0.2514
83	0.01084	285.31	165386	0.00955	195844	319.95	41.76	280.09	196.46	88.35	118.24	280.0872	0.8814	0.2452
84	0.01065	285.26	165625	0.00958	196410	320.03	41.03	280.62	192.81	88.46	117.36	280.1178	0.8995	0.2464
85	0.01079	286.23	171087	0.01007	201903	315.47	41.55	280.75	191.43	90.33	118.42	280.9887	0.9336	0.2377
86	0.01069	286.18	171057	0.01010	201649	315.57	41.17	280.92	190.23	90.57	118.30	280.9525	0.9447	0.2359

	O	P	Q	R	S	T	U	V	W	X	Y	Z	AA	AB
87	0.01051	287.38	175823	0.01048	207199	311.62	40.52	282.06	183.69	91.81	117.59	282.2135	0.9967	0.2312
88	0.01467	282.29	101603	0.00006	115756	300.95	46.30	258.97	311.87	0.95	124.75	276.4728	0.0043	0.4100
89	0.01452	281.49	101694	0.00038	115920	300.45	45.81	259.56	309.18	5.69	123.80	275.7646	0.0264	0.4100
90	0.01441	279.78	101790	0.00050	116242	300.20	45.50	260.27	306.28	7.36	122.73	274.1555	0.0346	0.4120
91	0.01437	278.40	102213	0.00069	116755	300.19	45.34	260.47	304.94	10.02	122.39	272.8039	0.0478	0.4112
92	0.01447	275.69	102400	0.00084	117257	300.23	45.65	260.22	306.13	12.10	123.05	270.0301	0.0580	0.4113
93	0.01442	273.16	102993	0.00119	118376	300.26	45.52	260.62	304.53	16.96	122.99	267.5069	0.0827	0.4097
94	0.01451	271.14	104058	0.00170	120307	300.78	45.77	260.33	305.46	23.68	124.46	265.3560	0.1169	0.4050
95	0.01447	271.44	104418	0.00193	120865	301.02	45.66	260.63	304.42	26.86	124.70	265.6285	0.1332	0.4039
96	0.01441	269.86	104866	0.00209	121592	301.02	45.45	260.84	302.95	28.87	124.57	264.0598	0.1453	0.4025
97	0.01444	270.17	105633	0.00230	122805	301.47	45.56	260.98	302.79	31.55	125.16	264.3210	0.1594	0.3998
98	0.01444	269.84	105731	0.00244	123130	301.43	45.58	261.03	302.51	33.38	125.52	263.9499	0.1689	0.4000
99	0.01444	269.18	106143	0.00258	123893	301.79	45.58	261.43	301.38	35.07	125.55	263.2933	0.1787	0.4004
100	0.01439	268.50	107631	0.00298	126267	302.55	45.42	261.87	298.89	39.79	126.00	262.5632	0.2067	0.3963
101	0.01437	267.95	110779	0.00361	131349	303.86	45.36	262.18	297.37	46.79	127.82	261.8460	0.2510	0.3817
102	0.01435	267.15	114286	0.00416	136659	305.97	45.30	263.27	292.98	52.17	128.28	260.9959	0.2901	0.3730
103	0.01427	267.19	119758	0.00490	144423	307.92	45.04	264.35	287.63	58.61	129.12	260.9637	0.3434	0.3542
104	0.01420	266.87	124434	0.00546	150801	309.72	44.83	266.09	280.19	62.74	128.44	260.7025	0.3844	0.3470
105	0.01417	267.74	131099	0.00617	159712	312.53	44.75	268.32	269.39	67.57	127.19	261.6974	0.4355	0.3427
106	0.01397	267.97	136114	0.00678	166224	313.96	44.12	269.74	262.45	71.55	127.05	261.9349	0.4853	0.3290
107	0.01399	269.96	141053	0.00731	172307	316.17	44.19	270.94	256.41	75.03	127.08	263.9302	0.5227	0.3246
108	0.01396	269.97	145146	0.00782	177021	315.94	44.09	272.03	250.91	78.00	127.11	263.9350	0.5605	0.3211
109	0.01386	271.94	151792	0.00852	184867	317.76	43.80	273.81	241.41	81.84	126.58	265.9490	0.6147	0.3163
110	0.01385	273.56	160976	0.00940	195413	318.56	43.76	275.59	231.66	85.67	126.20	267.6050	0.6791	0.3081
111	0.003595	282.91	33770.00	0.000264	33770.00	300.02	46.88	260.73	302.33	11.87	121.51	277.3902	0.0735	0.2308
112	0.003607	281.00	34783.10	0.000434	34783.10	299.84	47.03	264.32	285.63	18.77	115.78	275.9875	0.1202	0.2643
113	0.003584	280.18	35120.80	0.000555	35458.50	299.79	46.72	265.29	280.88	23.74	114.83	275.2522	0.1549	0.2676
114	0.003565	279.38	35796.20	0.000721	37147.00	299.86	46.47	266.18	276.47	30.15	114.62	274.4716	0.2021	0.2639
115	0.003525	278.69	37147.00	0.001007	39524.00	300.16	45.95	267.33	270.79	40.51	115.64	273.6957	0.2857	0.2466
116	0.003530	278.44	38835.50	0.001336	41537.10	300.55	46.01	267.89	268.06	51.36	118.89	273.1576	0.3786	0.2230
117	0.003494	278.63	40524.00	0.001596	43901.00	300.86	45.53	268.61	264.29	58.84	120.99	273.1558	0.4569	0.1946
118	0.003463	279.45	43225.60	0.001859	47278.00	301.64	45.13	269.31	260.85	64.43	122.63	273.8314	0.5369	0.1467
119	0.003408	280.88	45589.50	0.002153	50655.00	302.13	44.26	272.55	243.57	71.12	120.62	275.4411	0.6318	0.1563
120	0.003399	282.42	47953.40	0.002388	54032.00	302.01	43.97	274.81	230.57	75.38	119.11	277.1178	0.7023	0.1647
121	0.003321	284.31	50992.70	0.002611	57409.00	301.70	42.87	277.41	214.79	78.03	116.06	279.2813	0.7862	0.1611
122	0.003180	287.54	52681.20	0.002815	62474.50	300.52	40.54	278.71	206.62	82.37	116.69	282.4484	0.8852	0.1333
123	0.003019	289.75	58422.10	0.002971	67540.00	299.63	37.92	283.68	171.16	79.00	104.54	285.6662	0.9844	0.1762
124														
125														
126														

Appendix B - Heat transfer along the vortex tube walls and nozzle

This section presents some simple calculations to verify if the amount of heat Q_{out} calculated in chapter 4 could really be transferred by simple thermal conduction. The maximum amount of heat Q_{out} was about 100 Watts. Also, it was verified if any considerable heat transfer could be present in the nozzle.

B.1 Heat transfer along vortex tube walls

Three components of the vortex tube were analyzed separately: The tube, the hot end and the entrance block (see Figure B.1). All of them were modelled as cylinders: the hot end part was modelled as the combination of two cylinders. The heat conduction through the walls of a cylinder is represented by the following equation:

$$Q = (2\pi kL\,(T_1 - T_2)) \,/\, \ln\,(r_2 / r_1) \qquad \text{(B.1)}$$

Adding the heat transfer terms from the three components:

$$Q_{out}\,(\text{total}) = Q_{out}\,(\text{hot end}) + Q_{out}\,(\text{glass tube}) + Q_{out}\,(\text{entrance block}) \qquad \text{(B.2)}$$

Glass tube

$k = 0.76$ W/(m°C)

$r_1 = 1.27$ cm, $r_2 = 1.905$ cm

$L = 61$ cm

$$Q_{out}\,(\text{glass tube}) = 7.18(T_1 - T_2) \quad \text{(W/°C)}$$

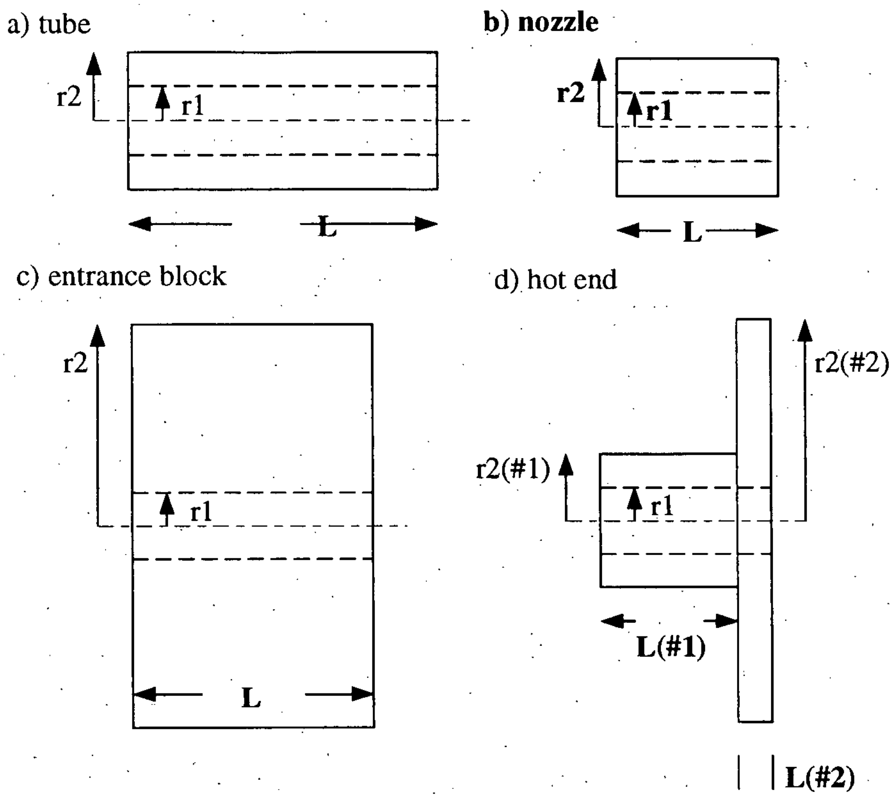

Figure B.1: Vortex tube parts used for heat transfer calculations: a) tube b) nozzle c) entrance block d) hot end

Hot end

$k = 111$ W/(m°C) (brass)

part 1: $r_1 = 1.27$ cm, $r_2 = 1.905$ cm

$L = 3.81$ cm

part 2: $r_1 = 1.27$ cm, $r_2 = 5.08$ cm

$L = 0.635$ cm

$$Q_{out} = Q_{out}\,(\text{part 1}) + Q_{out}\,(\text{part 2}) = 68.75(T_1 - T_2) \qquad (\text{W/°C})$$

Entrance block

$k = 111$ W/(m°C) (brass)

$r_1 = 1.27$ cm, $r_2 = 5.08$ cm

$L = 5.08$ cm

$$Q_{out}\text{ (entrance block)} = 25.56(T_1 - T_2) \qquad \text{(W/°C)}$$

By assuming the temperature difference $T_2 - T_1$ to be the same for each parts, we obtain

$$Q_{out} = 101.49\,(T_1 - T_2) \qquad \text{(W/°C)} \qquad \text{(B.3)}$$

With a temperature difference of about 1°C, an heat transfer of more than 100 Watts is possible. Therefore, even with the insulation around the tube, this heat transfer was possible.

B.2 Heat transfer along vortex tube nozzle

For simple calculation, one hole of the nozzle was modelled as a cylinder (see Figure B.1b). A maximum temperature difference was assumed to be 40 K. The temperature difference is overestimated since the maximum temperature difference in this work was around 25 K.

$k = 0.5$ W/m°C (Lucite)

$r_2 / r_1 = 4$

$L = 10$ cm

$T_2 - T_1 = 40$ K

$$Q_{nozzle} \approx 1\text{ W}$$

If Q_{nozzle} is represented as a possible increase of temperature, we get

$$T_{increase} = Q_{nozzle} / (c_p j_o/4) \approx 0.5\ °C$$

Therefore it was concluded that the heat transfer in the nozzle was negligible.

Appendix C - Design of a new vortex tube

After having build the vortex tube VT-01 and having analyzed the results, it was found that the vortex tube design could be improved. Some guidelines in the design of a better vortex tube are presented in this section.

Choice of the material

Although brass is a good material to work with (ease of machining, soldering), its heat conduction is so large that it can interfere with the energy separation effect in the vortex tube. In order to reduce considerably the possible heat transfer by the tube walls, Lucite should be used.

Entrance block design

The design of a plenum chamber allows rapid changes of the removable inlet nozzle. However, with that configuration the fluid experiences large variation in velocity and pressure from the air line to the inside of the vortex tube and therefore the inlet characteristics are difficult to measure. Ideally, the fluid should be brought to the tube in four separate lines having very smooth area variations. A new design respecting this condition would lead to more accurate velocity calculations.

Tube design

As discussed above, the use of Lucite would reduce the heat transfer along the walls. Moreover, it would be possible to drill pressure taps and therefore measure accurately the pressure variation along the tube. It would also be possible to have a more accurate inner diameter than with glass.

Appendix D - Computer program for data acquisition

```
#include "C:\LW\include\formatio.h"
#include "C:\LW\include\lwsystem.h"
#include "C:\LW\include\userint.h"
#include "vt.h"
#include "dt2805.h"
#define TRUE        1
#define FALSE       0

/********* functions declarations ********/
void VTRunAvg (int);
void Settings (void);
void VTRun (void);
int ad_imm();
void InitChannelHandleStrip (int []);
void InitGainHandleStrip (int[]);
void InitChannelNameHandleStrip (int[]);
void InitChannelNameHandleLabStrip (int[]);
void InitChannelNameSpace (char *[]);
void InitCalMHandleStrip (int []);
void InitCalBHandleStrip (int []);
int  MakeChannelList (int [], int[], int[], double[], double[], double[], double[], double[]);
void GetChannelName (int panel, int name_hndl[], char * CName[]);
void SetSelectableChannels (int, int[], int[], int[]);

double CalMVector[8], CalBVector[8], CalCVector[8], CalDVector[8], CalEVector[8],
   TCold, THot, TIn, PCold, PHot, PIn, FlowCold, FlowHot, FlowIn,
   AvgDataBuffer[8],FirstDataBuffer[8],data[8],test1;

int VTCtrlPanel, ChannelSelectPanel, SettingsPanel,
   TcoldGain, ThotGain, TinGain, PcoldGain, PhotGain, PinGain, FlowColdGain, FlowInGain,
   NumOfChannels,AvDaqAvg, panel, ctrl, i,
   ChannelList[8], ChannelHandle[8], GainHandle[8], CalBHandle[8], CalMHandle[8],
   ChannelVector[8], GainVector[8],GainIntVec[8], ChannelNameHandle[8], ChannelNameHandleLab[8],

   FileFormat, FileAppOver,SourceHandle;
char * ChannelName[8],  FileName[41] ;

/******* Main program ********/
void main()
{
/* initialization  */
InitChannelHandleStrip (ChannelHandle);
InitGainHandleStrip (GainHandle);
InitChannelNameHandleStrip (ChannelNameHandle);
InitChannelNameSpace (ChannelName);
InitCalMHandleStrip (CalMHandle);
InitCalBHandleStrip (CalBHandle);
ChannelSelectPanel = LoadPanel("VT.UIR", SELCHANS);
```

```
VTCtrlPanel = LoadPanel ("VT.UIR", VT_CTRL);
SettingsPanel = LoadPanel ("VT.UIR", SETTINGS);

/* Main screen initialization */
SetInputMode (VTCtrlPanel, VT_CTRL_STOP, 0);
SetInputMode (VTCtrlPanel, VT_CTRL_START, 1);
SetInputMode (VTCtrlPanel, VT_CTRL_QUIT, 1);
SetInputMode (VTCtrlPanel, VT_CTRL_SETTINGS, 1);


/* Display the main panel */
DisplayPanel (VTCtrlPanel);
SetActivePanel (VTCtrlPanel);
/* Get Ctrl Value */
GetCtrlVal (SettingsPanel, SETTINGS_AVDAQAVG, &AvDaqAvg);
GetChannelName (ChannelSelectPanel, ChannelNameHandle, ChannelName);
NumOfChannels = MakeChannelList (ChannelList, ChannelVector, GainVector, CalMVector,
CalBVector, CalCVector, CalDVector, CalEVector);
/* Then setup gain for interface */
for (i=0;i<NumOfChannels;i++) {
  switch (GainVector[i]){
  case 1:
    GainIntVec[i]=0;
    break;
  case 10:
    GainIntVec[i]=1;
    break;
  case 100:
    GainIntVec[i]=2;
    break;
  case 500:
    GainIntVec[i]=3;
    break;
  }
}
/* Then open temp.file and write date and time */
GetCtrlVal (SettingsPanel, SETTINGS_FILENAME, FileName);
SourceHandle=OpenFile (FileName,0,0,1);
FmtFile (SourceHandle,"date=%s\n",datestr());
FmtFile (SourceHandle,"time=%s\n",timestr());
FmtFile (SourceHandle,"tin\t pin\t fin\t tc\t pc\t th\t ph\t fc\n");
while(TRUE) {
  /* Wait for the user event */
  GetUserEvent (1, &panel, &ctrl);
  switch(ctrl) {
  case VT_CTRL_START:
    SetInputMode (VTCtrlPanel, VT_CTRL_STOP, 1);
    SetInputMode (VTCtrlPanel, VT_CTRL_START, 0);
    SetInputMode (VTCtrlPanel, VT_CTRL_QUIT, 0);
    SetInputMode (VTCtrlPanel, VT_CTRL_SETTINGS, 0);
    VTRunAvg (AvDaqAvg);
    break;
  case VT_CTRL_QUIT:
```

```
        UnloadPanel (VTCtrlPanel);
        CloseInterfaceManager ();
        exit (1);
        break;
    case VT_CTRL_SETTINGS:
        HidePanel (VTCtrlPanel);
        Settings ();
        break;
    case VT_CTRL_STOP:
        SetInputMode (VTCtrlPanel, VT_CTRL_STOP, 0);
        SetInputMode (VTCtrlPanel, VT_CTRL_START, 1);
        SetInputMode (VTCtrlPanel, VT_CTRL_QUIT, 1);
        SetInputMode (VTCtrlPanel, VT_CTRL_SETTINGS, 1);
        break;
    }
}
}

/*Function Settings*/
void Settings (void)
{
int i,loo1,loo2;
DisplayPanel (SettingsPanel);
SetActivePanel (SettingsPanel);
loo1=0;
while (loo1<1) {
    GetUserEvent (1, &panel, &ctrl);

    switch (ctrl) {
    case SETTINGS_SELCHANS:
        HidePanel (SettingsPanel);
        DisplayPanel (ChannelSelectPanel);
        loo2=0;
        while (loo2<1) {
            GetUserEvent (1,&panel,&ctrl);
            switch (ctrl) {
            case SELCHANS_OK:
                GetChannelName (ChannelSelectPanel, ChannelNameHandle, ChannelName);
                NumOfChannels = MakeChannelList (ChannelList, ChannelVector, GainVector,
                CalMVector, CalBVector, CalCVector, CalDVector, CalEVector);
                /* Then setup gain for interface */
                for (i=0;i<NumOfChannels;i++) {
                    switch (GainVector[i]){
                    case 1:
                        GainIntVec[i]=0;
                        break;
                    case 10:
                        GainIntVec[i]=1;
                        break;
                    case 100:
                        GainIntVec[i]=2;
                        break;
                    case 500:
```

```
                GainIntVec[i]=3;
                break;
              }
            }
            HidePanel (ChannelSelectPanel);
            DisplayPanel (SettingsPanel);
            loo2=1;
            break;
          case SELCHANS_CANCEL:
            HidePanel (ChannelSelectPanel);
            DisplayPanel (SettingsPanel);
            loo2=1;
            break;
          }
      }
    break;
    case SETTINGS_CANCEL:
      SetInputMode (VTCtrlPanel, VT_CTRL_START, 1);
      loo1=1;
      HidePanel (SettingsPanel);
      DisplayPanel (VTCtrlPanel);
      break;
    case SETTINGS_OK:
      GetCtrlVal (SettingsPanel, SETTINGS_AVDAQAVG, &AvDaqAvg);
      GetCtrlVal (SettingsPanel, SETTINGS_FILENAME, FileName);
      SourceHandle=OpenFile (FileName,0,FileAppOver,1);
      FmtFile (SourceHandle,"date=%s\n",datestr());
      FmtFile (SourceHandle,"time=%s\n",timestr());
      SetInputMode (VTCtrlPanel, VT_CTRL_START, 1);
      loo1=1;
      HidePanel (SettingsPanel);
      DisplayPanel (VTCtrlPanel);
      break;
    }
}
}


/* Function VTRunAvg: Continuous Data Acquistion */
void VTRunAvg (int Avg)
{
int j,i,loop1, cntr1,cntr2, Event,dumi,key,beeptest;
double test;
char dumstr [80];

/* Each channels will be scanned and data will be put in a buffer */
loop1=0;
Event=0;
test1=0;

/* Do a first run to take initial values */
/* Reinitialize buffer to 0 */
for (i=0; i < NumOfChannels; i++)
```

```
  FirstDataBuffer[i]=0.0;
for (j=0; j < Avg; j++){
  for (i=0; i < NumOfChannels; i++){
    data[i]=ad_imm (ChannelVector[i],GainIntVec[i]);
    FirstDataBuffer[i]=FirstDataBuffer[i] + (data[i]/Avg);
  }
}

/* Then average the buffer*/
for (i=0; i < NumOfChannels; i++)
  FirstDataBuffer[i]=(FirstDataBuffer[i]-2048)/(204.8*GainVector[i]);

/* Then scale the buffer with cal.factor */
FirstDataBuffer[1] = CalMVector[1]*FirstDataBuffer[1] +CalBVector[1];
FirstDataBuffer[2] = 0.08355-FirstDataBuffer[2];
FirstDataBuffer[4] = CalMVector[4]*FirstDataBuffer[4] +CalBVector[4];
FirstDataBuffer[6] = CalMVector[6]*FirstDataBuffer[6] +CalBVector[6];
FirstDataBuffer[7] = 0.08165-FirstDataBuffer[7];
while (loop1 <1) {
  Event = GetUserEvent (0, &panel, &ctrl);
  switch (ctrl){
  case VT_CTRL_STOP:
    SetInputMode (VTCtrlPanel, VT_CTRL_STOP, 0);
    SetInputMode (VTCtrlPanel, VT_CTRL_START, 1);
    SetInputMode (VTCtrlPanel, VT_CTRL_QUIT, 1);
    SetInputMode (VTCtrlPanel, VT_CTRL_SETTINGS, 1);
    loop1=1;
    break;
  }

/* Reinitialize buffer to 0 */
  for (i=0; i < NumOfChannels; i++)
    AvgDataBuffer[i]=0.0;
  for (j=0; j < Avg; j++){
    for (i=0; i < NumOfChannels; i++){
      data[i]=ad_imm (ChannelVector[i],GainIntVec[i]);
      AvgDataBuffer[i]=AvgDataBuffer[i] + (data[i]/Avg);
    }
  }

/* Then average the buffer*/
  for (i=0; i < NumOfChannels; i++) AvgDataBuffer[i]=(AvgDataBuffer[i]-2048)/(204.8*GainVector[i]);

/* Then scale the buffer with cal.factor*/
  AvgDataBuffer[0] = CalMVector[0]*AvgDataBuffer[0] +CalBVector[0];
  AvgDataBuffer[1] = CalMVector[1]*AvgDataBuffer[1] +CalBVector[1] -FirstDataBuffer[1];
  AvgDataBuffer[2] = CalMVector[2] +
CalBVector[2]*exp(CalCVector[2]*(AvgDataBuffer[2]+FirstDataBuffer[2]))
             +CalDVector[2]*exp(CalEVector[2]*pow((AvgDataBuffer[2]+FirstDataBuffer[2]),2)) ;
  AvgDataBuffer[3] = CalMVector[3]*AvgDataBuffer[3] +CalBVector[3];
  AvgDataBuffer[4] = CalMVector[4]*AvgDataBuffer[4] +CalBVector[4] -FirstDataBuffer[4];
  AvgDataBuffer[5] = CalMVector[5]*AvgDataBuffer[5] +CalBVector[5];
  AvgDataBuffer[6] = CalMVector[6]*AvgDataBuffer[6] +CalBVector[6] -FirstDataBuffer[6];
```

```
   AvgDataBuffer[7] = CalMVector[7] +
CalBVector[7]*exp(CalCVector[7]*(AvgDataBuffer[7]+FirstDataBuffer[7]))
               +CalDVector[7]*exp(CalEVector[7]*pow((AvgDataBuffer[7]+FirstDataBuffer[7]),2)) -
FirstDataBuffer[7];

/* Display values on screen */
   SetCtrlVal (VTCtrlPanel, VT_CTRL_TEMP_IN, AvgDataBuffer[0]);
   SetCtrlVal (VTCtrlPanel, VT_CTRL_PRES_IN, AvgDataBuffer[1]);
   SetCtrlVal (VTCtrlPanel, VT_CTRL_FLOW_IN, AvgDataBuffer[2]);
   SetCtrlVal (VTCtrlPanel, VT_CTRL_TEMP_C, AvgDataBuffer[3]);
   SetCtrlVal (VTCtrlPanel, VT_CTRL_PRES_C, AvgDataBuffer[4]);
   SetCtrlVal (VTCtrlPanel, VT_CTRL_TEMP_H, AvgDataBuffer[5]);
   SetCtrlVal (VTCtrlPanel, VT_CTRL_PRES_H, AvgDataBuffer[6]);
   SetCtrlVal (VTCtrlPanel, VT_CTRL_FLOW_C, AvgDataBuffer[7]);
   SetCtrlVal (VTCtrlPanel, VT_CTRL_FLOW_H, AvgDataBuffer[2]-AvgDataBuffer[7]);
   SetCtrlVal (VTCtrlPanel, VT_CTRL_H_T, (AvgDataBuffer[2]-AvgDataBuffer[7])/AvgDataBuffer[2]);
   SetCtrlVal (VTCtrlPanel, VT_CTRL_C_T,AvgDataBuffer[7]/AvgDataBuffer[2]);
   SetCtrlVal (VTCtrlPanel, VT_CTRL_delta_Th, (AvgDataBuffer[5]-AvgDataBuffer[0]));
   SetCtrlVal (VTCtrlPanel, VT_CTRL_delta_Tc, (AvgDataBuffer[3]-AvgDataBuffer[0]));

   key= keyhit();
   SetCtrlVal(VTCtrlPanel, VT_CTRL_SAVING, 0);
   if (key == 1) {
      beep ();
      SetCtrlVal(VTCtrlPanel, VT_CTRL_SAVING, 1);
      FmtFile(SourceHandle,"%f\t %f\t %f\t %f\t %f\t %f\t %f\t %f\t %f\n",
      AvgDataBuffer[0], AvgDataBuffer[1], AvgDataBuffer[2], AvgDataBuffer[3],
      AvgDataBuffer[4], AvgDataBuffer[5], AvgDataBuffer[6], AvgDataBuffer[7], timer());
   }
}
}
/* RealTime Data Acquisition function */
int ad_imm(int chan,int gain)
{
int value, dummy, l1, testloop;
l1=0;
while (l1==0) {
   l1=1;
   outp(COMMAND_PORT,STOP);
   dummy = inp(DATA_PORT);
   for (i=0; ((inp(STATUS_PORT)&READY)==0) && (i<10000);i++);
      if (i==10000) l1=0;
   outp(COMMAND_PORT,CLEAR_ERROR);
   for (i=0;((inp(STATUS_PORT)&READY)==0) && (i<10000);i++);
      if (i==10000) l1=0;
   outp(COMMAND_PORT,READ_AD_IMM);
   for (i=0;((inp(STATUS_PORT)&DATA_IN_FULL)!=0) && (i<10000);i++);
      if (i==10000) l1=0;
   outp(DATA_PORT,gain);
   for (i=0;((inp(STATUS_PORT)&DATA_IN_FULL)!=0) && (i<10000);i++);
      if (i==10000) l1=0;
   outp(DATA_PORT,chan);
   for (i=0;((inp(STATUS_PORT)&DATA_IN_FULL)!=0)&& (i<10000);i++);
```

```
    if (i==10000) l1=0;
  for (i=0;((inp(STATUS_PORT)&DATA_OUT_READY)==0) && (i<10000);i++);
    if (i==10000) l1=0;
  value = inp(DATA_PORT);
  for (i=0;((inp(STATUS_PORT)&DATA_OUT_READY)==0) && (i<10000);i++);
    if (i==10000) l1=0;
  }
value = value+(inp(DATA_PORT)<<8);
return(value);
}

/******************************************************************************/
/* functions for initialization of handle arrays:                    */
/* The controls on LabWindows user interface panels have constant values. */
/* These values may be assigned to elements of an array, so that          */
/* GetCtrlVal, SetCtrlVal, SetInputMode, etc. functions can be called in  */
/* a loop.                                                                */
/******************************************************************************/
void InitChannelHandleStrip(int HandleArray[])
{
HandleArray[0] = SELCHANS_CHAN0;
HandleArray[1] = SELCHANS_CHAN1;
HandleArray[2] = SELCHANS_CHAN2;
HandleArray[3] = SELCHANS_CHAN3;
HandleArray[4] = SELCHANS_CHAN4;

HandleArray[5] = SELCHANS_CHAN5;
HandleArray[6] = SELCHANS_CHAN6;
HandleArray[7] = SELCHANS_CHAN7;
}

void InitGainHandleStrip(int HandleArray[])
{
HandleArray[0] = SELCHANS_GAIN0;
HandleArray[1] = SELCHANS_GAIN1;
HandleArray[2] = SELCHANS_GAIN2;
HandleArray[3] = SELCHANS_GAIN3;
HandleArray[4] = SELCHANS_GAIN4;
HandleArray[5] = SELCHANS_GAIN5;
HandleArray[6] = SELCHANS_GAIN6;
HandleArray[7] = SELCHANS_GAIN7;
}

void InitCalMHandleStrip( int HandleArray[])
{
HandleArray[0] = SELCHANS_m0;
HandleArray[1] = SELCHANS_m1;
HandleArray[2] = SELCHANS_m2;
HandleArray[3] = SELCHANS_m3;
HandleArray[4] = SELCHANS_m4;
HandleArray[5] = SELCHANS_m5;
HandleArray[6] = SELCHANS_m6;
HandleArray[7] = SELCHANS_m7;
```

```
}

void InitCalBHandleStrip( int HandleArray[])
{
HandleArray[0] = SELCHANS_b0;
HandleArray[1] = SELCHANS_b1;
HandleArray[2] = SELCHANS_b2;
HandleArray[3] = SELCHANS_b3;
HandleArray[4] = SELCHANS_b4;
HandleArray[5] = SELCHANS_b5;
HandleArray[6] = SELCHANS_b6;
HandleArray[7] = SELCHANS_b7;
}

void InitChannelNameHandleStrip(int HandleArray[])
{
HandleArray[0] = SELCHANS_NAME0;
HandleArray[1] = SELCHANS_NAME1;
HandleArray[2] = SELCHANS_NAME2;
HandleArray[3] = SELCHANS_NAME3;
HandleArray[4] = SELCHANS_NAME4;
HandleArray[5] = SELCHANS_NAME5;
HandleArray[6] = SELCHANS_NAME6;
HandleArray[7] = SELCHANS_NAME7;
}

/**************************************************************************/
/* function: MakeChannelList                                    */
/* This function gets the values of channel selection controls, and assign */
/* the the values to ChnlVector, GVector and CalVector.                   */
/* The total number of channels that are ON, is returned by the function. */
/**************************************************************************/
int MakeChannelList(int channel_list[], int ChnlVector[], int GVector[], double CalMVector[],
double CalBVector[], double CalCVector[], double CalDVector[], double CalEVector[])
{
int i, num_channels, chans_configed, index;
chans_configed = 0;
num_channels = 8;
index = 0;
/* initialize */
for (i=0; i<8; i++) {

   channel_list[i] = 0; /* reset */
   ChnlVector[i] = -1;
}
for (i=0; i<num_channels; i++) {
   GetCtrlVal(ChannelSelectPanel, ChannelHandle[i], &channel_list[i]);
   if (channel_list[i]) {
      ChnlVector[index] = i;
      GetCtrlVal (ChannelSelectPanel, GainHandle[i], &GVector[index]);
      GetCtrlVal (ChannelSelectPanel, CalMHandle[i], &CalMVector[index]);
      GetCtrlVal (ChannelSelectPanel, CalBHandle[i], &CalBVector[index]);
      index++;
```

```
    }
    /* Flowmeter calibration */
    GetCtrlVal (ChannelSelectPanel, SELCHANS_c2, &CalCVector[2]);
    GetCtrlVal (ChannelSelectPanel, SELCHANS_d2, &CalDVector[2]);
    GetCtrlVal (ChannelSelectPanel, SELCHANS_e2, &CalEVector[2]);
    GetCtrlVal (ChannelSelectPanel, SELCHANS_c7, &CalCVector[7]);
    GetCtrlVal (ChannelSelectPanel, SELCHANS_d7, &CalDVector[7]);
    GetCtrlVal (ChannelSelectPanel, SELCHANS_e7, &CalEVector[7]);
    chans_configed = channel_list[i] + chans_configed;
}
return (chans_configed);
}

/***************************************************************************/
/* function:  InitChannelNameSpace                              */
/* This function initialize the character pointers to default names. of   */
/* analog input channels.                               */
/***************************************************************************/
void InitChannelNameSpace (char * CName[])
{
CName[0] = "Channel 0    ";
CName[1] = "Channel 1    ";
CName[2] = "Channel 2    ";
CName[3] = "Channel 3    ";
CName[4] = "Channel 4    ";
CName[5] = "Channel 5    ";
CName[6] = "Channel 6    ";
CName[7] = "Channel 7    ";
}

/***************************************************************************/
/* function: GetChannelName                              */
/* This function gets name from the user interface panel, and stores them */
/* character array.                               */
/***************************************************************************/
void GetChannelName (int panel, int name_hndl[], char * CName[])
{
int i, num_channels;
num_channels = 8;
for (i=0; i<num_channels; i++)
    GetCtrlVal (panel, name_hndl[i], CName[i]);
}
```